Simulation of High Resolution Winds Over the Southern Benguela Upwelling System with Potential Application to Harmful Algal Blooms

Natalie Burls

Supervisor:
Chris Reason

Department of Oceanography
University of Cape Town
Rondebosch, South Africa

submitted to the Faculty of Science, University of Cape Town
in fulfilment of the academic requirements for the degree of Master of Science

August 2006

Abstract

The southern Benguela upwelling system is particularly susceptible to Harmful Algal Blooms (HABs), most of which are attributed to dinoflagellate species. Dinoflagellates are favoured by stratified conditions. Consequently, temporal and spatial variations in ocean and atmospheric conditions that favour stratification will encourage HAB development. Temporally, prolonged relaxation of the dominant equatorward winds during late summer typically results in quiescent phases in upwelling which promote stratification and bloom development. This was the case in March 2001 where persistent west coast trough conditions in the atmosphere over western South Africa caused a prolonged period of weak across-shore pressure gradients and light variable winds which resulted in a bloom event north of Cape Columbine. This March 2001 HAB event has been selected as a case study to examine the atmospheric forcing conducive to HABs in the southern Benguela. Primarily the role of mesoscale (10-100km) spatial variability in wind stress forcing in controlling mixed layer characteristics and hence phytoplankton species distribution is investigated.

Since understanding of the spatial variability in the local wind field which results from the adjustment of the large scale flow to regional topography and thermal gradients is limited by lack of observations, an attempt is made in this thesis to utilise regional atmospheric modeling to resolve mesoscale spatial variations in wind stress forcing over the southern Benguela. A regional atmospheric model has been used to simulate low-level coastal winds at high resolution (3km) over the southern Benguela upwelling system for the March 2001 period and to assess the sensitivity to different resolution sea surface temperature forcing. The ability of a regional atmospheric model to resolve the mesoscale spatial variability in wind stress forcing over the southern Benguela is demonstrated. The model output has been validated quantitatively through comparison with limited observations and qualitatively through comparison with wind fields observed in aircraft surveys conducted during previous summers. The regional model was capable of reproducing the qualitative effect of topographic forcing and thermal gradients on the equatorward flow. Local enhancement of low-level wind speed due to the interaction of the synoptic equatorward flow with both the Cape Peninsula and Cape Columbine was reproduced with associated bands of wind maxima, while lighter winds were seen in the lee of these capes.

Spatial variability in the low-level wind field north of Cape Columbine is suggested as being favourable for the development of HABs which are prone to the greater St Helena Bay region. Shallower average mixed layer depths due to strong solar heating and lower

wind conditions in the sheltered wind wake which resides in the lee of Cape Columbine appears to be important for the enhanced surface water stratification and phytoplankton species distribution typically observed north of Cape Columbine. Enhanced cyclonic curl at in-shore stations due to land-sea contrasts in surface friction may be responsible for the gradual rise of the base of the thermocline in-shore as Ekman pumping increases. These stratified surface waters together with the availability of nutrient rich sub-thermocline water near the surface in turn promote dinoflagellate growth during upwelling favourable winds, hence pre-conditioning the region prior to HAB events which develop during prolonged quiescent phases. A significant onshore wind stress component during quiescent phases in upwelling is needed to advect these high biomass blooms into the near-shore environment where they have the greatest impact upon coastal communities. During periods of weak synoptic across-shore pressure gradients, seabreezes which develop in the region further help in promoting an enhanced on-shore component in wind stress north of Cape Columbine, which is favourable for the on-shore advection of HABs.

Acknowledgements

I would like to express my gratitude to the following individuals and organisations:

My supervisor Prof. Chris Reason for his supervision, advice and guidance.

Grant Pitcher, Kabumbwe Hansingo and Steward Bernard, to whom I am grateful for their guidance and constructive feedback.

Partial funding for this study from the South African National Research Foundation (NRF) and UCT Postgraduate Funding Office is gratefully acknowledged.

The following individuals and organisations need to be thanked and acknowledged for providing data used in this thesis:

Grant Pitcher from MCM for March 2001 hydrographic and biological data, as well as those who contributed to the data collection and analysis - S. Bernard, D. Calder, A. du Randt, S. Etheridge, T. Probyn and C. Roesler.

Cersat Infermer for QuikScat Mean Wind Fields (MWF) and Jet Propulsion Laboratory / Physical Oceanography Distributed Active Archive Centre (JPL/PO.DAAC) for SeaWinds level 2B data used in creating MWF (http://www.ifremer.fr/cersat).

European Centre for Medium-Range Weather Forecasts (ECMWF) for 40 Years Re-Analysis (ERA-40) data (http://www.ecmwf.int).

The Master Environmental Library (MEL) for providing Navy Operational Global Atmospheric Prediction System (NOGAPS) data (https://mel.dmso.mil).

The National Centre for Environmental Prediction (NCEP) for re-analysis data produced in collaboration with the National Centre for Atmospheric Research (NCAR) obtained from the National Oceanic and Atmospheric Administration/Climate Diagnostics Centre (NOAA/CDC) (http://www.cdc.noaa.gov/cdc/data.ncep.reanalysis.html).

Remote Sensing Systems and the NASA Ocean Vector Winds Science Team for QuikSCAT data are available at www.remss.com.

The South African Weather Service for observational data and synoptic charts used, particularly Tracey Gill and Kevin Winter.

United States Geological Survey (USGS) for topographic and land-use data used in MM5.

The National Oceanic and Atmospheric Administration (NOAA) for the NOAA Optimum Interpolation (OI) SST version 2 (v2) data and the Climate Diagnostics Centre who has collected and made available weekly NOAA OI SST v2 data (http://www.cdc.noaa.gov/cdc/data.noaa.oisst.v2.html).

Herve Demarcq and Kobus Agenbag for providing the Meteosat SST images used.

Contents

List of Figures

Chapter 1

Introduction

The southern Benguela region, situated off the west coast of southern Africa is dominated by upwelling during austral summer. This upwelling is forced by an equatorward alongshore wind stress field associated with the South Atlantic High, which shifts southwards during the summer. Coastal winds are the dominant forcing for the southern Benguela current system, with stress and wind stress curl playing an important role in driving upwelling and coastal circulation. Dictated by wind forcing, the upwelling structure and coastal currents control the physical environment of a vast number of living organisms in the southern Benguela.

Phytoplankton are one such group of organisms that are strongly influenced by the physical environment characteristic of an upwelling system. Under specific physical conditions, phytoplankton growth in the southern Benguela can become harmful in nature. The southern Benguela is particularly susceptible to Harmful Algal Blooms (HABs), with most of these being attributed to toxic and non-toxic dinoflagellate species (Hortsman, 1981; Pitcher and Calder, 2000). Algal blooms in the southern Benguela become harmful as a result of either their high biomass or the presence of toxic species. The focus here falls more towards high biomass flagellate blooms as the physical factors leading to high biomass bloom formation are more readily identifiable than those favouring toxic species.

It has been established that dinoflagellate species are generally responsible for high biomass harmful blooms in the southern Benguela. Dinoflagellates require a stratified water column in order to dominate and flourish (Pitcher and Calder, 2000). As a result, temporal and spatial variations within the upwelling system favouring upper ocean stratification are responsible for harmful bloom formation.

A primary region of HAB occurrence within the southern Benguela upwelling system has been identified along the Namaqua shelf north of Cape Columbine between 32° and 33°S. This region is referred to as the greater St Helena Bay region (Figure 2.1) (Pitcher and Calder, 2000; Shannon and Nelson, 1996). The topographical influence of the Cape Columbine peninsula on shelf circulation, upwelling and stratification, may offer some explanation as to why this region favours HAB formation (Penven, 2000a; Penven et al., 2000b; Gan and Allen, 2002a,b; Graham and Largier, 1997). Wind stress and wind stress curl also play an important role in driving coastal circulation in this region. A key question this thesis hopes to address is how the local topography and land-sea distribution of the greater St Helena Bay region influences local wind forcing conducive to HAB development.

The synoptic weather patterns responsible for quiescent phases in upwelling, which favour bloom development and the on-shore advection of HABs, are fairly well understood (Pitcher et al., 1995). What is less understood is the adjustment of the large scale atmospheric flow to regional topography and thermal gradients. Previous studies at Cape Columbine have indicated that the summer synoptic wind field is influenced by the cape (Kamstra, 1985; Jury, 1985a,b), however an understanding of the spatial variability is limited by few observations. Although satellite scatterometers produce surface wind estimates at 25km resolution, pixels in the primary region of interest near the coast are contaminated. An alternative is to utilise mesoscale atmospheric modelling. Advances in computational power enable high resolution winds to be simulated. An attempt is made in this thesis to utilise regional atmospheric modeling to resolve mesoscale spatial variations in wind stress forcing. The fifth-generation Pennsylvania State University / National Centre for Atmospheric Research (PSU/NCAR) Mesoscale Model (MM5) has been used to simulate low-level coastal winds at high resolution (3km) over the southern Benguela upwelling system.

The HAB division of Marine and Coastal Management (MCM) have in recent years conducted annual observations of algal bloom development, during the late summer period when the incidence of HABs is known to be high. These have taken place off-shore of Lambert's Bay approximately 100km north of Cape Columbine - a region prone to bloom development. Based on the MCM hydrographic and biological data provided, a case study event has been selected as the focus of this study. A HAB event in March 2001 was chosen as a case study for assessing the role of temporal and spatial wind stress variability in forcing physical mechanisms which in turn dictate HAB development and advection.

This thesis is aimed at improving the understanding of mesoscale (10-100km) variability in

wind stress forcing over the southern Benguela and its influence on the development and advection of HABs. Particular focus falls on the role of wind stress in creating a physical environment conducive to the formation of high biomass HABs. Ultimately an enhanced understanding of the processes involved will improve the ability to forecast regional HAB events.

This introductory chapter is followed by a review of the literature on the southern Benguela upwelling system and the development of HABs within it. The third chapter describes the configuration of the MM5 regional atmospheric model as well as the data and analytical techniques used in this thesis. In the fourth chapter, an assessment of the temporal variability in along-shore wind stress forcing within the region of interest has been conducted using Continuous Wavelet Analysis and the chosen event described and categorised in terms of the observed temporal variability in along-shore wind forcing. The model output from the two simulations conducted has been validated in the fifth chapter and analysed in the sixth chapter. In the seventh chapter, the implications of spatial variability in the wind stress fields derived from the simulated low-level winds on HAB development and advection are discussed. Chapter eight presents the conclusions of the study.

Chapter 2

Literature Review

2.1 The Southern Benguela Upwelling System

The Benguela current system is situated along the west coast of southern Africa bordered by the Angola Current system to the north and the Agulhas current system to the south. As one of four major eastern boundary current systems, the Benguela region like those west of Peru, California and North West Africa, is dominated by upwelling. Stretching from the Angola-Benguela front to the southern tip of Africa, upwelling is forced by an equatorward along-shore wind stress field associated with the South Atlantic High (SAH) pressure system (Shannon, 1985). Upwelling within the Benguela system varies both temporally and spatially. Centres of upwelling occur where upwelling is enhanced by factors such as the orientation of the coastline, a narrowing of the continental shelf, an enhanced average along-shore wind stress, or cyclonic wind-stress curl (Shannon, 1985; Shannon and Nelson, 1996; Hardman-Mountford et al., 2003). Temporal variability in Benguela upwelling activity is directly related to variability in the along-shore wind stress forcing which occurs at time scales ranging from diurnal to inter-annual and longer.

2.1.1 Atmospheric Forcing

Synoptic pressure gradient fields along the west coast of southern Africa are established between the SAH and the Inter-Tropical Convergence Zone (ITCZ) to the north and continental heat lows to the east. These pressure gradients control the south-easterly trade winds responsible for upwelling within the Benguela. South of the continent the pressure

gradients between the SAH and the circumpolar trough force predominantly westerly flow, with modulations in wind direction occurring due to the eastward passage of mid-latitude cyclones (Hardman-Mountford et al., 2003; Shillington et al., 2006).

Seasonal variability in upwelling activity differs between the southern and northern Benguela due to differing seasonal wind regimes. A seasonal shift in the latitudinal position of the SAH and ITCZ causes the trade winds to migrate meridionally. North of 31°S, along-shore wind stress associated with the trade winds is experienced all year round, resulting in perennial upwelling in the central and northern Benguela (Hardman-Mountford et al., 2003; Shannon and Nelson, 1996). South of 31°S, winds favourable for upwelling are highly seasonal, with upwelling activity peaking during austral summer when the trade winds are at their furthest south (Shannon and Nelson, 1996). During summer, the SAH shifts southwards and a continental heat low develops over western South Africa enhancing the across-shore pressure gradient field which drives equatorward along-shore winds. During winter, the SAH shifts northwards and the southern Benguela is dominated by north-westerly and south-westerly wind events due to the passage of mid-latitude fronts. This cycle results in seasonal wind induced upwelling in the southern Benguela region, with upwelling reaching a maximum in austral spring and summer (Andrews and Hutchings, 1980).

Within this seasonal variability, considerable synoptic and mesoscale variability is experienced in the coastal winds of the southern Benguela. The dominant upwelling favourable wind regime during summer months is modulated by the passage of mid-latitude cyclones moving eastward, south of the continent (Nelson and Hutchings, 1983; Shannon and Nelson, 1996). Preston-Whyte and Tyson (2000) suggests that this modulation is a result of a synoptic cycle with a period of 2-8 days. A pulsing in southern Benguela upwelling activity occurs as upwelling subsides in response to equatorward wind relaxation or reversal.

This pulsing can be described in terms of active and quiescent phases of upwelling. Periods of strong active upwelling are synoptically forced by a ridging of the SAH south of the continent. Quiescent phases of equatorward wind relaxation or reversal are typically associated with the passage of mid-latitude cyclones south of the continent, coastal lows tracking down the west coast along the escarpment or the development of a west coast trough. During spring and autumn, the frequency of cut off lows increases substantially (Singleton and Reason, 2006) and these systems may also be responsible for the perturbation of the equatorward flow. During summer, prolonged quiescent phases may be attributed to west coast troughs. Most common in the southern Benguela during summer, west coast troughs

relax the across-shore surface pressure gradient and hence the along-shore equatorward flow, as the linking of continental and marine low pressure cells displace the SAH westwards (Pitcher et al., 1995; Shillington et al., 2006). Mesoscale systems responsible for the modulation of upwelling in the southern Benguela during the summer are seabreezes and coastal lows (Preston-Whyte and Tyson, 1988; Reason and Jury, 1990).

Jury et al. (1990a) attributes an enhanced response in fluctuations in sea temperature, sea level and along-shore current to the generation of coastally trapped waves in both the atmosphere and the ocean by the passage of westerly waves in the mid-latitude atmosphere (Schumann and Brink, 1990; Jury et al., 1990a,b). In the atmosphere, coastally trapped disturbances known as coastal lows are generated by the interaction of the ridging SAH with the southern African escarpment, sometimes with a trailing cold front to the southwest (Reason and Jury, 1990). Forming near 25°S, coastal lows propagate southwards along the west coast and then northward along the east coast. Jury et al. (1990b) suggests that barotropic coastally trapped waves in the ocean may propagate in phase with along-shore wind reversal caused by propagating coastal lows.

Pulsing in upwelling within the southern Benguela during the summer upwelling season generally has a period of 3-10 days due to wind relaxation or reversal (Shannon and Nelson, 1996). This period is consistent with the 2-8 day period of the synoptic cycle suggested by Preston-Whyte and Tyson (2000). More recently, Risien et al. (2004) assessed the temporal variability in along-shore wind stress between 24 and 35°S on timescales between four and sixty four days by performing wavelet analysis on sixteen months of QuikSCAT satellite wind stress data. A bimodal distribution was found to occur with peaks at 4-12 days and 25-50 days and with the majority of the power occurring during the summer months. The the higher frequency oscillations in along-shore wind stress are attributed to the passage of mid-latitude cyclones in winter and coastal lows in summer. Risien et al. (2004) identified this short-period peak in along-shore wind stress variability off the coast of southern Africa to be similar to findings of short-period fluctuations in sea level pressure and sea level data by Kamstra (1987), Preston-Whyte and Tyson (1973) and Jury et al. (1990a). Risien et al. (2004) suggested that the low frequency oscillations with a period of 25-50 days were related to eastward propagating wind events originating over eastern South America.

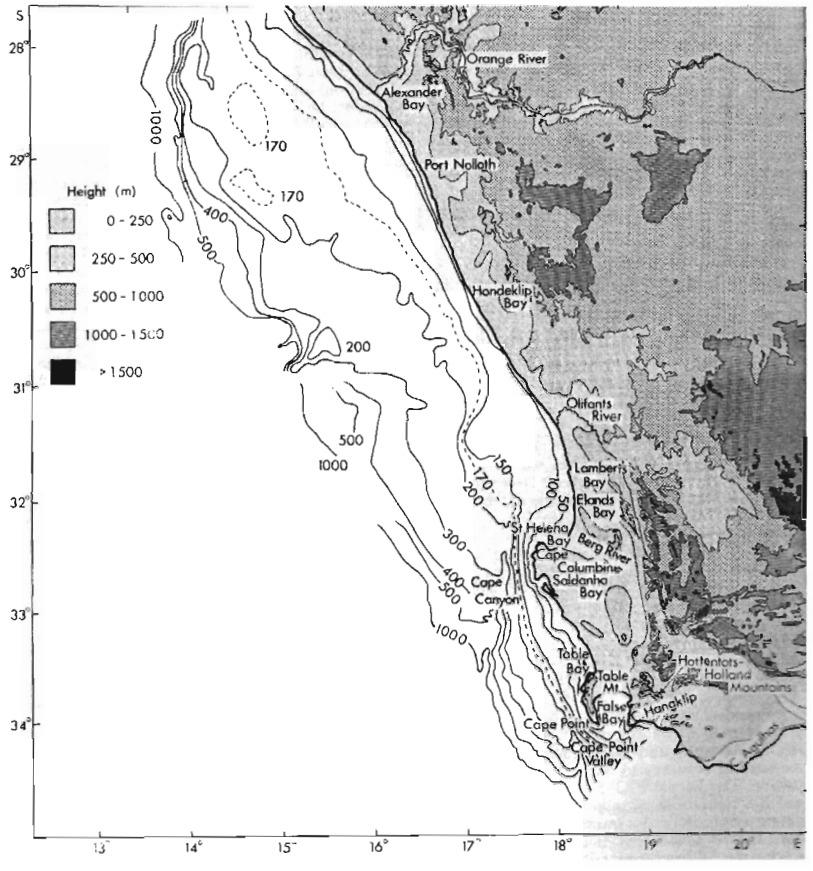

Figure 2.1: Bathymetry and Topography of the southern Benguela adapted from Taunton-Clark, 1985.

2.1.2 Bathymetry and Topography

The southern Benguela can be divided into three main upwelling cells. They are the Namaqua (30°S), the Cape Columbine (33°S), and the Cape Peninsula (34°S) cells as depicted in Figure 2.2 (Shannon, 1985; Lutjeharms and Meeuwis, 1987) which shows the upwelling cells as local SST minima. In terms of bathymetry (Figure 2.1), the shelf is relatively narrow at both the Cape Columbine headland and the Cape Peninsula with a width of roughly 40km. Between 31 and 33°S, there is an inner and an outer shelf break (220-380m and 500m) which merge at 33°S to form a single deep shelf (Shannon and Nelson, 1996). Further to the north, the shelf widens to 180km west of the Orange River. Several submarine canyons exist between 31 and 35°S with the biggest being the Cape Canyon, the head of which lies 60km west of Cape Columbine (Shannon and Nelson, 1996).

Also important in influencing the shelf circulation, is the topography of the land which lies adjacent to the southern Benguela shelf (Figure 2.1). The coastal wind field is the dominant forcing behind shelf circulation in the southern Benguela, the behaviour of which is in turn influenced by coastal topography. The west coast of southern Africa consists of a narrow coastal plain of between 50-75km backed by coastal mountains which rise to the main continental escarpment of 1 to 1.5km in altitude (Reason, 1996). North of 32°S, the coastline is fairly regular but several headlands exist south of 32°S. Granitic outcrops at Cape Columbine and the Cape Peninsula are responsible for the formation of exposed bays to the north of them (St Helena Bay and Table Bay) and enclosed bays to the south of them (Saldanha Bay and False Bay) (Shannon and Nelson, 1996). The Cape Columbine headland, which is situated at roughly 32.8°S 18°E extends seawards by approximately 40km, and consists of smooth low level hills. Topography on the Cape Columbine headland reaches a maximum height of 250m (Jury, 1985a). To the north, the coastline bends away forming St Helena Bay. Along the coastline to the north, there are two river valleys - the Berg River (which enters the ocean at the southern arc of St Helena Bay) and the Olifants River further north. South of Cape Columbine lies the Cape Peninsula along which mountains reach a height of almost 1100m (Shannon and Nelson, 1996).

2.2 Harmful Algal Blooms in the Southern Benguela

In the above section, the main aspects governing upwelling and shelf circulation in the southern Benguela have been discussed. Influenced by meteorological and topographical forcing, upwelling varies not only spatially, but temporally between active and quiescent phases. Coastal winds are the dominant forcing for the southern Benguela current system, with stress and wind stress curl playing an important role in driving upwelling and coastal circulation. Governed by wind forcing, the upwelling structure and coastal currents control the physical environment of a vast number of living organisms in the southern Benguela including the phytoplankton. The Benguela upwelling system creates a dynamic and unique environment for phytoplankton growth. The two most important controls of phytoplankton growth are light and nutrients. Therefore, the availability of nutrients in the euphotic zone is essential for growth. During active upwelling, nutrients are brought to the surface. Phytoplankton growth is however limited by the turbulent mixing of the water column during this phase, which prevents confinement within the euphotic zone (Pitcher and Calder, 2000).

The southern Benguela is particularly susceptible to HABs, most of which are attributed to toxic and non-toxic dinoflagellate species (Hortsman, 1981; Pitcher and Calder, 2000). Algal blooms in the southern Benguela become harmful as a result of either their high biomass or the presence of toxic species, or a combination of both. Although the factors responsible for shifts in the phytoplankton community structure to that where flagellate taxa dominate are not as yet fully understood (Smayda and Reynolds, 2001; Pitcher and Nelson, 2006), dinoflagellates are considered as being susceptible to turbulence and better adapted to lower energy, stratified conditions (Cullen and MacIntyre, 1998; Estrada and Berdalet, 1998; Margalef, 1978; Probyn et al., 2000).

Pitcher and Nelson (2006) have investigated how ocean surface boundary layer dynamics favour the development of HABs in the southern Benguela by relating phytoplankton species composition to the degree of stratification of the surface layer. They have found a strong relationship to exist between stratification and the phytoplankton species composition. Typically the succession of a diatom dominated phytoplankton species composition to a dinoflagellate dominated species composition is driven by changes leading from a well mixed, nutrient-rich water column to a nutrient-poor stratified environment (Pitcher and Nelson, 2006).

Diatoms thrive in high-nutrient, high-turbulence environments (Margalef, 1978) and therefore typically dominate turbulent, nutrient-rich newly upwelled water in the southern Benguela. Diatoms have silicate structures and cannot swim so they depend both on high concentrations of silicate and turbulent mixing to maintain their presence in the euphotic zone. As the water column becomes stratified, the availability of nutrients in the euphotic zone is reduced, and diatoms are succeeded by dinoflagellates. Their ability to swim allows dinoflagellates to migrate vertically to retrieve nutrients in stratified, low nutrient conditions (Smayda, 1997). The phytoplankton community structure is therefore strongly related to the extent of stratification, with the diatoms dominating a turbulent well-mixed water column and the presence of dinoflagellates increasing relative to stratification.

Prolonged stratified, stable conditions provide the opportunity for dinoflagellates to flourish resulting in high biomass blooms. Greater insight into the physical mechanisms resulting in stratification of the mixed layer will assist in predicting the development of HAB events. Although certain aspects of bloom development and advection within southern Benguela are understood, there are still gaps in our understanding. In the sections to follow, previous research and literature on the topic is reviewed, highlighting the remaining questions which demand further investigation. Particular consideration is given to the mechanisms that

create a physical environment which favours the development of HABs, and control the advection of waters containing HABs.

While the switch in dominant phytoplankton species from diatom to dinoflagellate species can be predicted based on the the physical environment (turbidity of the water column), it is unfortunately not as easy to predict the type of dinoflagellate species (i.e. toxic or non-toxic) based purely on such knowledge (Pitcher and Nelson, 2006). As a result, the focus turns more towards the mechanisms behind the formation of high biomass dinoflagellate blooms rather than toxic species content.

2.3 High Biomass Bloom Development and Advection

2.3.1 Bloom Development

Research has established that the presence of the dinoflagellate species responsible for harmful blooms in the southern Benguela is favoured by a stratified water column (Pitcher and Boyd, 1996; Pitcher et al., 1998; Pitcher and Calder, 2000; Probyn et al., 2000; Pitcher and Nelson, 2006). As a result, temporal and spatial variations within the upwelling system favouring stratification are responsible for HAB formation.

Temporally, stratification is enhanced towards the end of the upwelling season as the prevailing upwelling favourable winds weaken and insolation remains high. The frequency of upwelling events reduces due to the decreasing thermal gradient between the landmass and the ocean, as well as the north-westward movement of the South Atlantic subtropical anticyclone associated with the transition from summer to winter synoptic weather patterns (Pitcher et al., 1995, 1998). Prolonged quiescent phases associated with HAB events have been identified as being predominantly due to the development of West Coast troughs (Pitcher et al., 1995). The development of a west coast trough is associated with periods of active continental convection over Namibia, together with an upper air westerly wave trough to the south-west of the continent (Preston-Whyte and Tyson, 1988). This results in a surface low pressure trough over the west coast linking continental tropical and marine mid-latitude low pressure systems and displacing the South Atlantic High pressure system westwards. During such a west coast trough event, weak surface pressure gradients and light winds favour the development of the thermocline in the southern Benguela, thereby increasing stratification (Pitcher et al., 1995).

Spatially, a primary region of HAB occurrence within the southern Benguela upwelling system has been identified along the Namaqua shelf, north of Cape Columbine between 32° and 33°S. This area is referred to as the greater St Helena Bay region (Shannon and Nelson, 1996; Pitcher and Calder, 2000). Here the shelf is relatively broad, favouring stability of the water column and stratification (Probyn et al., 2000; Pitcher and Nelson, 2006). It has also been suggested that stratification is intensified in this region by exceptionally cold bottom water. This very cold bottom water floods the southern Orange-Namaqua shelf through a valley at approximately 31.5°S, and is advected southward by the poleward undercurrent (Probyn et al., 2000).

During upwelling conditions, a cool plume of newly upwelled water typically extends northwards from the Cape Columbine peninsula across St Helena Bay. Warmer waters are found on the inshore of this cold plume within the bay. Along the coastline north of the Cape Columbine peninsula, a narrow band of coastal upwelling is forced by coastal Ekman divergence, separating warmer water from the coast (Taunton-Clark, 1985). Typical sea surface temperatures (SSTs) resulting from upwelling circulation on the broad shelf region north of Cape Columbine are depicted in Figure 2.2.

Inshore of the coastal upwelling front associated with this narrow band of Ekman upwelling, the water column is turbulent and well-mixed as cool, nutrient rich water is brought to the surface. This water is dominated by diatoms, due to its turbulent nutrient-rich nature. Warmer more stratified water exists offshore of the coastal upwelling front. Here dinoflagellate populations occur in a subsurface stratum associated with the thermocline where a balance is obtained between their nutrient and light requirements (Pitcher et al., 1998). During active upwelling, subsurface populations associated with the thermocline are brought to the surface by the uplifted thermocline at the upwelling front. With increased light levels near the surface, production increases, resulting in increased dinoflagellate concentrations and the development of a bloom.

More recent evidence revealed by transects conducted offshore of Lambert's Bay (32°S), has indicated that the spatial distribution is more complicated than simply the succession from diatom-dominated turbulent surface waters inshore of the coastal upwelling front to more stratified dinoflagellate-dominated surface water offshore of the front (Pitcher and Nelson, 2006). Diatom dominated turbulent water has been found to occur yet again offshore of the stratified dinoflagellate waters (Pitcher and Nelson, 2006). Pitcher and Nelson (2006) attribute this unexpected spatial pattern in phytoplankton species distribution to changes in the upper mixed layer characteristics resulting from regional anomalies in the coastal

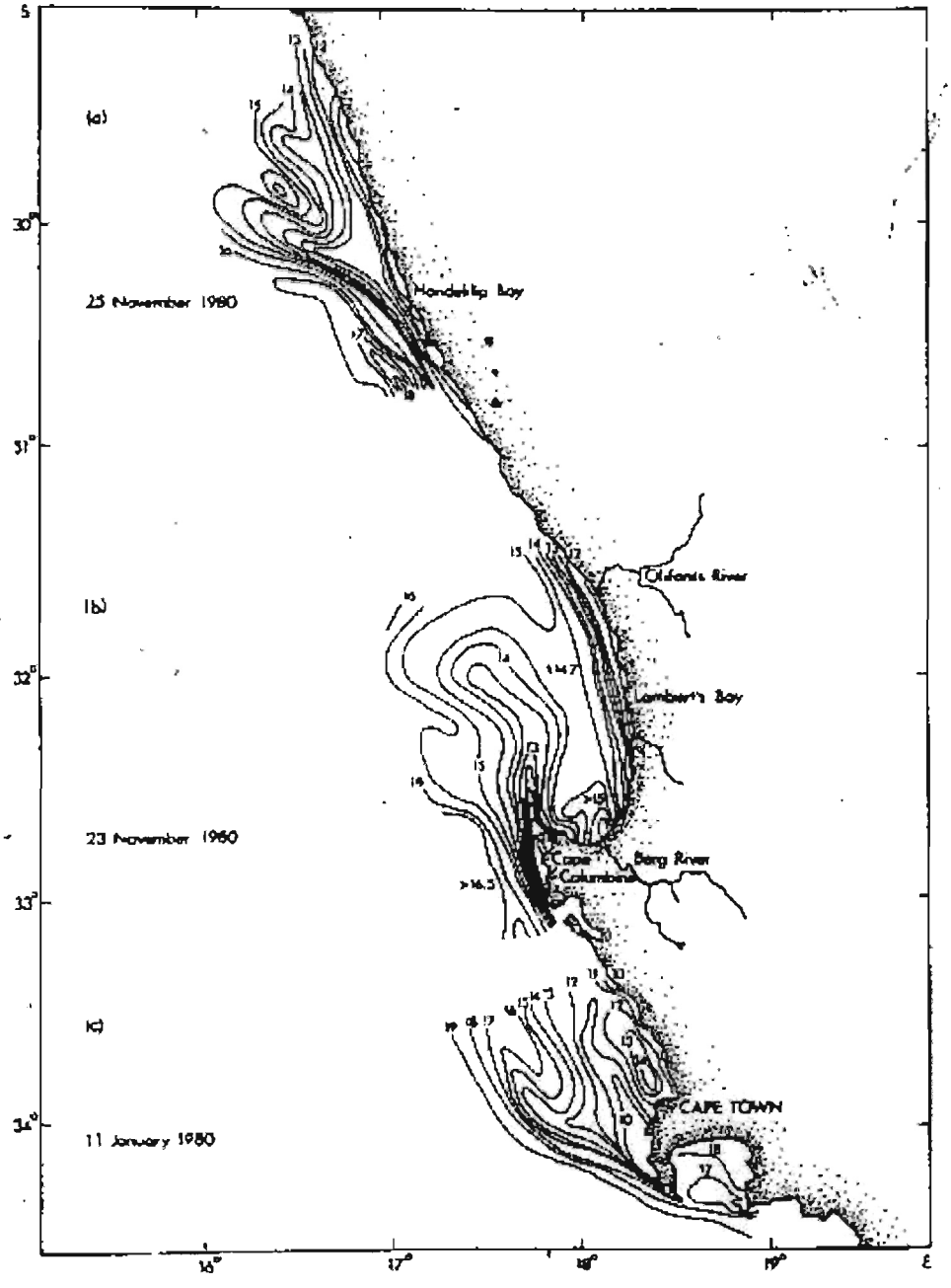

Figure 2.2: A montage of the Cape Peninsula, Cape Columbine and Hondeklip upwelling sites defined by aerial radiation thermometry taken from Nelson and Hutching, 1983.

current and wind structures induced by Cape Columbine. The turbulent diatom dominated water found offshore of the stratified dinoflagellate waters is believed to originate from the Cape Columbine upwelling plume having been advected downstream by northward flow. Pitcher and Nelson suggest two physical mechanisms which may be responsible for the deepening of the mixed layer depth and subsequently the change in phytoplankton species composition offshore. Firstly, the offshore deepening of the mixed layer could be driven by wind stress shear resulting in increased wind mixing off-shore. Secondly, greater shear instabilities at the base of the mixed layer, due to stronger surface currents offshore could enhance entrainment and deepen the mixed layer.

Equally as important as understanding the physical mechanisms which favour dinoflagellate species dominance, is an understanding of the physical processes that transport, concentrate and dissipate dinoflagellate blooms. Shelf circulation, driven by meteorological forcing, can cause rapid shifts in the biomass and species composition of the inshore phytoplankton community in the southern Benguela (Pitcher and Boyd, 1996; Pitcher et al., 1998; Pitcher and Nelson, 2006).

2.3.2 Observed Coastal Circulation Downstream of Cape Columbine

South of St Helena Bay, the along-shore flow between the Cape Columbine peninsula and the shelf break has been identified as being predominantly northwards (Duncan and Nell, 1969; Holden, 1985). Adjacent to the peninsula, the shelf is steep and narrow, preventing cross topographic currents and topographically constraining the along-shore flow. As a result, velocities here are higher than elsewhere on the shelf (Penven, 2000a; Penven et al., 2000b; Holden, 1985). Rounding the Cape Columbine peninsula, the shelf broadens significantly and slopes gently, reducing the topographical control on the flow. This results in the across-shelf flow and the tidal and inertial motions observed in this region (Holden, 1985; Boyd et al., 1992).

An early drift card study carried out by Duncan and Nell (1969) revealed a near-shore southward counter current just north of Cape Columbine which was present even during upwelling favourable winds. This was hypothesised as belonging to the coastal leg of a local cyclonic gyre. Using radio-tracked drifters, Holden (1985) was able to confirm the existence of a large cyclonic coastal gyre north of Cape Columbine in St Helena Bay.

Using all available data collected by the F.R.S. Africana between November 1989 and January 1994, Boyd and Oberholster (1994) assessed the average flow pattern north of St

Helena Bay. They found currents inshore of the 200m isobath to be weak with a mean onshore curvature in the flow towards Hondeklip Bay. Although it was stated that higher resolution current data was needed, the flow pattern on the outer shelf was found to be variable yet generally northwards. Subsurface flow along the continental shelf between Cape Columbine and Namaqua upwelling cells is dominated by the presence of a poleward counter-current (De Decker, 1970; Holden, 1987). A surface counter current forms inshore in winter and also in summer when there is no active upwelling. Its presence has been attributed to barotropic reversals in the along-shore direction (Shannon and Nelson, 1996; Holden, 1987). These reversals are believed to be the result of barotropic coastally trapped waves generated by along-shore wind relaxation and reversal (Shannon and Nelson, 1996; Holden, 1987).

2.3.3 Retention and Advection

A retentive region of high phytoplankton biomass along the broad shelf region north of Cape Columbine is identifiable in seasonal composites of remotely sensed SST and ocean colour (Pitcher and Weeks, 2006; Weeks et al., 2004). Phytoplankton concentrations higher than can be explained by local growth have been observed here (Pitcher et al., 1998).

A cyclonic gyre north of Cape Columbine (Holden, 1985; Penven, 2000a; Penven et al., 2000b) is thought to be responsible for retentive near-surface circulation within the St Helena Bay. As mentioned, transects conducted further north offshore of Lambert's Bay revealed that stratified dinoflagellate dominated water exists in a region of convergence between the turbulent diatom dominated waters inshore and offshore (Pitcher and Nelson, 2006). During active upwelling, the surface flow along the shelf is predominantly northwards. Dinoflagellates accumulate in a region of convergence created between the narrow belt of coastal upwelling and the core northward flow which has an onshore curvature (Boyd and Oberholster, 1994; Pitcher and Boyd, 1996; Pitcher and Nelson, 2006).

An important element of HABs in the southern Benguela are the advective regimes responsible for the shoreward accumulation of HABs (Pitcher and Nelson, 2006). Hydrodynamic processes on the shelf are primarily driven by coastal winds. It is during quiescent phases, when equatorward coastal winds relax, that blooms are advected onshore, accumulating and impacting upon the coast. Across-shelf currents are observed as becoming weak - even reversing to onshore. The upwelling front moves inshore, together with its associated surface blooms (Pitcher and Boyd, 1996; Pitcher et al., 1998; Pitcher and Nelson, 2006).

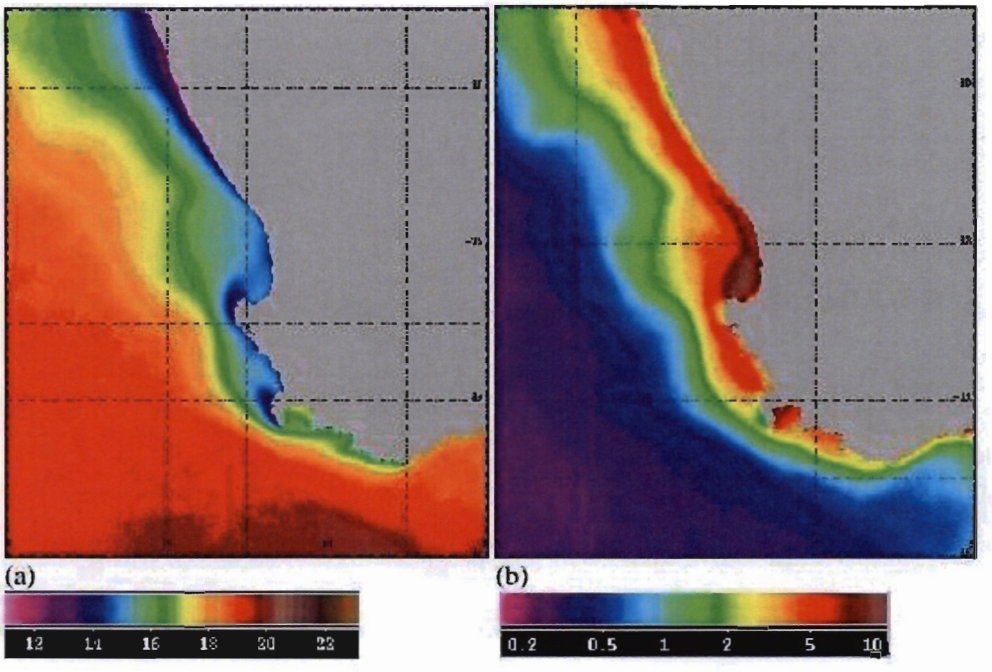

Figure 2.3: Five year (July 1998 - July 2003) composites of (a) NOAA AVHRR 1km resolution SST and (b) SeaWiFs chlorophyll, adopted from Pitcher and Weeks, 2006.

During prolonged quiescent periods this accumulation inshore results in dense harmful blooms.

Onshore movement during the quiescent phase is often accompanied by the southward flow of surface water, which results in the southward propagation of these blooms along the coast (Pitcher et al., 1998). This southward surface flow is thought to be associated with a barotropic shelf flow forced by coastally trapped waves generated over the southern Namaqua shelf by along-shore wind relaxation and reversal (Holden, 1987; Lambeth and Nelson, 1987; Schumann and Brink, 1990; Probyn et al., 2000). Based on current data from a mooring approximately 2 nautical miles off-shore of Lambert's Bay, Fawcett (2006) found along-shore reversals in the near-surface current to be highly correlated with reversals in the local wind field, with the current lagging the wind by 12 hours. Fawcett (2006) suggests the high correlation between the poleward flow observed in the mooring data and the relaxation of equatorward winds may be due to a negative along-shore pressure gradient set up by the presence of a cape downstream as demonstrated by Gan and Allen (2002a; 2002b). In the southern Benguela system, blooms are generally observed first in this broad shelf region north of Cape Columbine during March, at which time blooms are generally absent south of Cape Columbine. They are later advected southward during a prolonged quiescent phase by southward surface flow. Thus HABs are most common in Cape Town during April and May (Probyn et al., 2000; Pitcher and Calder, 2000).

While typical characteristics of bloom distribution and advection along the Namaqua shelf have been observed during both active and quiescent upwelling activity and are fairly well understood, a more in-depth understanding is required of the mechanisms forcing the resultant bloom distribution and advection. To predict HAB events, the primary physical mechanisms behind HAB development and advection need to be identified and quantified. Meteorological and topographical forcing present physical mechanisms that could help determine the mixed layer characteristics and flow patterns which control the introduction, concentration and dissipation of blooms. The role that coastal topography together with temporally fluctuating and spatially variable winds might play in HAB dynamics is discussed in the next section.

2.4 Physical Mechanisms Favouring HAB Development and Advection

2.4.1 Influence of the Cape Columbine Peninsula

The topographical influence of the Cape Columbine peninsula on shelf circulation and upwelling structure may offer some explanation as to why the broad shelf region north of Cape Columbine favours HAB formation (Gan and Allen, 2002a,b; Graham and Largier, 1997; Penven, 2000a; Penven et al., 2000b).

Penven (2000a; 2000b) explored the influence of the Cape Columbine Peninsula and the downstream broadening of the shelf on coastal circulation induced by idealised upwelling favourable winds. He used a numerical model in which he made the assumption that the shelf circulation was essentially barotropic and that bottom friction is linear. Coastal geometry and bottom topography were also simplified. Despite these simplifications, flow detachment occurred from Cape Columbine and a cyclonic eddy was produced in the bay. The presence of this stationary attached-cyclonic-eddy is in qualitative agreement with the in-situ measurements of Holden (1985).

Analysis of the momentum equation terms indicated that at zero order, the recirculation was controlled predominantly by a geostrophic balance. As Coriolis acceleration forces the flow away from the coast downstream of the cape, conservation of mass generates a pressure gradient in balance with Coriolis acceleration. This results in a down-slope, low pressure towards the coast just downstream of the cape (Csanady, 1982; Penven, 2000a). The balance between forces was assessed at first order by adding the pressure gradient and Coriolis acceleration terms to find the ageostrophic pressure gradient. Cyclo-geostrophic dynamics were observed towards the edge of the cyclonic recirculation pattern where a relatively high ageostrophic pressure gradient was found. Here the advection term, comparable to the centrifugal force term based on the local radius of curvature, was found to compete with the ageostrophic pressure gradient. Penven (2000a) suggests that the advective term, forcing water particles away from the cape appeared to be responsible for the detachment of flow around the cape. The along-shore extension of this attached cyclonic eddy regime (Boyer and Tao, 1987) was found to be controlled by the wind stress and bottom friction values, with the size of the eddy being positively related to the intensity of the wind forcing.

Penven (2000a) indicated that the flow pattern in the bay could be explained in terms of a standing coastal-trapped wave in equilibrium with the along-shore equatorward current. Penven (2000a) illustrated that development of the upwelling plume observed north of Cape Columbine (Taunton-Clark, 1985) could be attributed to the horizontal advection of water, upwelled south of Cape Columbine around the attached cyclonic eddy. Similar findings of divergence and increased upwelling around capes, have been identified in model studies of circulation around capes in the Californian upwelling system (Gan et al., 2005; Roughan et al., 2005). The upwelling plume, and the associated circulation patterns, appear to serve as a retentive mechanism which limits across-shelf exchange. Penven (2000a; 2000b) quantified retention using a tracer and found the relationship between the intensity of retention and wind forcing to be a positive one with stronger upwelling favourable winds enhancing recirculation and retention within the near-shore region to the lee of the cape. As a result of this topographically induced circulation, stronger upwelling favourable winds could in fact enhance retention within the near-shore area north of Cape Columbine despite the intensification of the offshore flow due to coastal upwelling.

As mentioned, a surface counter-current is observed inshore along the Namaqua shelf north of Cape Columbine in the absence of upwelling favourable winds (Shannon, 1985). This phenomena has been observed to occur along most of the southern Benguela shelf and has been attributed to barotropic reversals in the along-shore direction (Shannon, 1985; Holden, 1987). These reversals are believed to be the result of barotropic coastally trapped waves propagating in response to along-shore wind relaxation and reversal (Schumann and Brink, 1990; Holden, 1987). Another possible mechanism, responsible for the generation of a coastal counter-current north of Cape Columbine during upwelling favourable wind relaxation, has been demonstrated by Gan and Allen (2002a; 2002b). Like Penven, they use a numerical model to quantitatively assess the interaction of wind forced circulation with along-shore variations in shelf topography. Their study, however, observes flow under upwelling favourable wind as well as the flow subsequent to wind relaxation.

Gan and Allen (2002a; 2002b) studied the wind forced circulation on the northern Californian shelf between 37°- 40°N. Their first study was an idealised experiment aimed at looking at the basic process taking place using the Princeton Ocean model (POM). With a realistic high grid resolution, coast line and bottom topography, the effects of the capes at Pt Reyes (38°N) and Pt Arena (39°N) were examined. The model ocean, initially at rest, was forced with upwelling favourable winds for 10 days at which point this wind stress is decreased to zero over three days. In agreement with Penven's (2000a) study, the along-

shore current that developed in response to the upwelling favourable wind forcing, was observed to increase in magnitude as it flowed around the capes separating from the coast downstream of the capes, with the coldest surface water observed in those locations. Unlike the Columbine example, no attached cyclonic eddy recirculation pattern was observed during upwelling favourable wind stress forcing. However similarly geostrophic balance and cyclo-geostrophic dynamics were identified as the two mechanisms controlling flow in the vicinity of the capes causing a low pressure to develop at the coast near the cape. Cyclo-geostrophic dynamics are referred to as a gradient wind-like balance (Holton, 1992) by Gan and Allen (2002a). The local low pressure caused an along-shore pressure gradient that forced a counter-current during the relaxation of upwelling favourable winds.

Gan and Allen's (2002b) second study was aimed at modeling the response of shelf circulation to the time varying wind stress observed. The nature of the coastal ocean response is more complex than that of the first idealised experiment, but nevertheless similar dynamics are found. Overall their model output compared well with oceanographic observations. Both experiments demonstrated that coastal capes significantly influence circulation during upwelling favourable winds by causing along-shore variability in upwelling intensity and flow. In addition, the presence of the cape leads to the formation of an along-shore pressure gradient, which forces a counter-current during the relaxation of upwelling favourable winds. Similarly an along-shore pressure gradient may be induced north of Cape Columbine driving southward flow during the relaxation of upwelling favourable winds which contributing to the retentive nature of circulation within the region and to the southward transport of blooms (Pitcher and Nelson, 2006; Fawcett, 2006).

2.4.2 Influence of Spatially and Temporally Varying Wind Stress

Penven's (2000b; 2000a) idealised numerical study established that both the observed cyclonic recirculation pattern north of Cape Columbine, and the development of an upwelling plume can be explained in terms of the barotropic response of an equatorward current to the Cape Columbine Peninsula and the downstream broadening of the shelf. Gan and Allen's (2002a; 2002b) experiments provide an idea of the role capes may play in the shelf circulation response to the relaxation of upwelling favourable winds. However, no model investigations have taken place to quantify the effects of spatial variations in wind stress on upwelling, stratification and shelf circulation north of Cape Columbine. Observational evidence of the effects have been offered by various authors (Jury, 1988, 1985b,a; Kam-

stra, 1985; Taunton-Clark, 1985). Other comparable studies in the Californian upwelling region have revealed that mesoscale wind features caused by the interaction of the synoptic wind field with the capes result in spatial variability in upwelling circulation (Enriquez and Friehe, 1995; Capet et al., 2004; Gan et al., 2005; Marchesiello et al., 2003; Pickett and Paduan, 2003; Samelson et al., 2002).

2.4.2.1 The Influence of Mesoscale Coastal Wind Features on Upwelling Circulation and its Associated Temperature Structure

Enriquez and Friehe (1995) and Pickett and Paduan (2003) argued that large wind stress curl values can result in upward Ekman pumping in coastal upwelling systems with magnitudes of upwelling comparable to that due to coastal Ekman divergence. In their numerical model study, Enriquez and Friehe (1995) established that non-zero wind stress curl does in fact affect wind driven transport in coastal upwelling systems thereby changing the thickness of the upper layer. Enriquez and Friehe used a two-layer vertically integrated numerical model to assess the relative importance of upwelling due to Ekman pumping to coastal Ekman divergence. Using the numerical model forced by wind curl values consistent with aircraft observations over the northern Californian coast, they investigated the effect of wind stress and wind stress curl on the time evolution of the upper layer depth model. They found non-zero curl altered the thickness of the upper layer, expanding the horizontal extent of upwelling. The presence of the coast was however found to diminish Ekman pumping compared to offshore values (Enriquez and Friehe, 1995).

Mesoscale atmospheric models are able to qualitatively capture cape induced wind anomalies as well as the across-shore decrease in along-shore wind speed towards the coast (Capet et al., 2004). This decrease in wind speed within the narrow coastal strip is due to the change in surface drag and the depth of the atmospheric boundary layer from the sea to the land. However, the structure of the across-shore wind profile produced by the U.S navy model COAMPS differs significantly with differing resolution (Capet et al., 2004). The higher the resolution, the smaller the region over which the decline in wind speed occurs and the higher the related wind stress curl. This indicates that the mesoscale atmospheric model could not quantitatively determine the true structure of the coastal wind. Capet et al. (2004) investigated the impacts on upwelling of this exaggerated decrease in along-shore wind stress and the associated increase in wind stress curl, compared to that of realistic decreases in observed moored wind measurements. Their comparative

investigation illustrates the effect of increase cyclonic wind stress curl and its associated Ekman pumping on upwelling circulation. Capet et al. investigated how differing coastal wind profiles affect upwelling circulation and the associated temperature structure along the Californian coast using the Regional Oceanic Model System (ROMS). Both the effects of upwelling due to coastal Ekman divergence and upwelling due to Ekman pumping are considered.

The coastal wind structure significantly influences the along-shore current structure. Large cyclonic curls favour depth-averaged poleward currents through Sverdrup balance (although eddy Reynolds stress acts to further redistribute the wind-curl input) (Capet et al., 2004). Capet et al (2004) found the poleward current to almost surface at the shore when ROMS was forced by the wind profile with large positive curl and weak coastal winds. When ROMS was forced by a wind profile with lower wind stress curl values and stronger winds near the coast, the under-current was confined to below 40m and velocities were weaker. The different wind profiles also lead to different across-shore temperature structures, suggesting that the Ekman divergence and Ekman pumping lead to different upwelling structures. Upwelling forced by wind stress curl resulted in a gradual rise and doming of the thermocline in a strip 10-30km off the coast, where the wind stress curl reaches a maximum. Ekman divergence forced by strong along-shore winds causes the thermocline to rise sharply at the coast (Capet et al., 2004).

Penven et al. (2001) conducted a regional simulation of the Benguela upwelling system using ROMS. With a horizontal resolution of 9km, most of the mesoscale dynamics of the Benguela upwelling system were reproduced. The model was forced by wind, heat and salinity fluxes extracted from COADS monthly climatology. Reasonable agreement was found between simulated and observed mesoscale circulation structures at the surface and deeper levels. The main discrepancy between the model outputs and observed data appeared off the west coast region during summer with simulated SSTs being significantly lower then those observed from satellites. This can be attributed to the use of poorly temporal and spatially resolved wind data from a monthly climatology to force the ocean model. The high-frequency variability of pulsing equatorward wind stress forcing is smoothed out, resulting in persistent upwelling favourable wind forcing during the whole summer season. In addition, the decrease of wind stress toward the coast is not resolved and so a greater coastal wind stress magnitude than those which occur in reality was used in the model. As a result, enhanced coastal Ekman divergence leads to greater upwelling velocities and cooler SSTs at the coast. Therefore in order to more accurately represent the

upwelling structure and associated circulation, regional oceanic models need to be forced with winds which adequately resolve spatial variability in wind stress forcing.

A number of studies have found that irregularities in coastline or coastal topography induce cyclonic wind stress curl patterns which lead to corresponding regions of increased Ekman transport divergence and Ekman pumping (Dorman et al., 2000; Koracin and Dorman, 2001). Pickett and Paduan (2003) established the significance of capes along the Californian coast and their associated wind stress curl patterns in influencing currents and biological productivity. Chelton (1982) has related wind stress curl along the Californian coast to seasonal distributions of zooplankton, suggesting that Ekman pumping is an important source of nutrients. Curl patterns induced by Cape Columbine may result in Ekman pumping which acts to lift the thermocline and increase stratification along the broad shelf region north of the Cape. Ekman pumping may play an important role in supporting dinoflagellate growth during upwelling favourable wind. Growth in dinoflagellate populations which occur in a subsurface stratum associated with the thermocline maybe enhanced due to increased light levels as the thermocline is uplifted through Ekman pumping.

2.4.2.2 The Influence of Spatially Varying Coastal Winds on Upper Mixed Layer Characteristics

Although Ekman pumping may act to uplift the thermocline and increase stratification through upward vertical velocities induced by Ekman divergence, the depth of the upper mixed layer is largely determined by vertical mixing due to wind stress. Horizontal variations in mixed layer depth may be induced by horizontal variations in wind stress intensity. While wind stress induces turbulent vertical velocities which mix surface waters and deepen the mixed layer, a positive buoyancy flux acts to stratify and stabilise surface waters, reducing turbulent mixing within the mixed layer. Caldeira and Marchesiello (2002) investigated the effects of wind sheltering in the southern Californian Bight using simulated wind from the COAMPS regional atmospheric model and surface heat and salinity flux forcing from the COADs climatology to derive Ekman and Monin-Obukhov depth scales. They found a strong correlation between observed SSTs, stratification and wind stress, with low turbulent mixing rates associated with wind sheltering. A warm island wake was characterised by sharp stratification over the first few meters during the day, due to strong solar heating and low wind conditions. Wind sheltering in the lee of Cape Columbine might well be responsible the increased stratification observed on the broad

shelf region north of the cape.

2.4.2.3 The Influence of Across-Shelf Winds on Onshore Advection

Process oriented two dimensional modeling studies, ignoring along-shore variability, have shown that the dynamics governing across-shelf transport in the surface layer differ between the inner-shelf and outer-shelf regions (Austin and Lentz, 2002; Tilburg, 2003). During both upwelling and downwelling, a front forms, and is displaced offshore where the pycnocline intersects the surface or bottom respectively. A large across-shelf horizontal density gradient is associated with this front which divides the shelf into the inner and outer shelf regions with differing stratification (Austin and Lentz, 2002). Inshore of the front, the water column is turbulent and well mixed, and the bottom and surface Ekman layers merge. Offshore of the front, the water column is stratified helping to separate the surface and the bottom Ekman layers by preventing vertical mixing. Here, full across-shore Ekman transport occurs in the surface Ekman layer with a compensating flow below (Austin and Lentz, 2002). Inshore of the front, the interaction of the surface and bottom layer significantly reduces the Ekman across-shelf transport force by along-shore winds. Instead the transfer of wind stress through the water column is direct, with advection occurring in the same direction as the wind (Ekman, 1905; Tilburg, 2003). Within the inner-shelf region, the physical mechanism responsible for across-shelf transport has been attributed to across-shelf winds (Austin and Lentz, 2002; Tilburg, 2003). Although the vertically integrated transport of across-shelf winds in the inner-shelf region is zero, they can generate significant surface across-shelf velocities, resulting in the across-shelf transport of surface material. Therefore, under steady along-shore wind forcing, surface transport within the inner-shelf region is primarily along-shore and across-shore transport in minimal. Onshore winds are therefore necessary in the advection of surface material onshore within the inner-shelf region.

The influence of spatially and temporally varying wind stress on upwelling structure, shelf circulation and vertical mixing presents several possible mechanisms as to why the broad shelf region to the north of Cape Columbine favours HAB formation. Wind shear induced by the cape may force the observed mixed layer characteristics through differential vertical mixing and Ekman pumping and an across-shore wind has been identified as necessary in the appearance of HABs at the coast during the relaxation of upwelling favourable winds. The topographical influence of the Cape Columbine peninsula on shelf circulation,

upwelling and stratification, may offer some explanation as to why this region favours HAB formation. However, in this thesis the focus shall fall only on the role of local topography and land-sea distribution in promoting local wind variations in the greater St Helena Bay region which may be conducive to HAB development.

2.5 Characteristics of the Local Summer Wind Field for the Greater St Helena Bay Region

The southern Benguela upwelling region is typical of a sub-tropical west coast region with coastal winds dominated by equatorward flow during the summer half of the year. Coastal winds which drive the upwelling circulation in the southern Benguela are forced on scales of 100 - 1000 km by the synoptic pressure field, and on smaller scales of 10 - 100 km by irregularities in topography and thermal contrasts (Jury, 1985a). Predominant upwelling favourable winds in the Marine Atmospheric Boundary Layer (MABL) are driven by the synoptic-scale across-shore pressure gradient established between the SAH and a heat low over western South Africa. A temperature inversion separates the cool, moist and turbulent well mixed air in the MABL from subsiding dry air in the upper atmosphere. Due to anti-cyclonic subsidence, this inversion thins eastwards towards the coast. The MABL flow off the west coast generally responds strongly to coastal topography in summer because the MABL is capped by a sharp inversion which inhibits vertical motion and thins to several hundred meters in depth near the coast (Edwards et al., 2001). The extent to which the prevailing summer synoptic equatorward flow in the MABL is influenced by topography depends on the depth of the MABL. Generally the inversion tilts down to a height below that of the coastal mountains. This results in the blocking of low level flow by the mountains and leads to a variety of mesoscale features in the predominantly equatorward flow field such as coastal wind jets (Chao, 1985) and coastally trapped disturbances known as coastal lows (Reason and Jury, 1990).

Coastal jets in the lower atmosphere can be generated either by the blocking and along-shore channelling of low-level across-shore flow by coastal mountains (when the inversion is well below the height of the coastal mountain), or by land and sea temperature differences (Chao, 1985). A sloping MABL implies a strong horizontal across-shore temperature gradient between the cool ocean and the warm land. A jet core of maximum along-shore magnitude is generally observed in the vertical wind profile just below the sloping in-

version. Geostrophic winds in the MABL decrease with height above the MABL due to strong across-shore temperature gradients above the inversion causing a thermal wind effect (Zemba and Friehe, 1987). The jet profile is a dual result of surface frictional drag retarding surface velocities and the decrease in along-shore geostrophic velocities above the inversion due to the thermal wind (Zemba and Friehe, 1987; Pomeroy and Parish, 2001). Jury (1985b) found evidence of an along-shore jet over the Cape Columbine headland during summer equatorward flow. This jet was found to reach maximum intensity between 100 and 300m just before sunset at 1900 South African Standard Time (SAST). Equatorward flow was found to be compressed between the inversion and the Cape Columbine headland to form a jet core.

Land-sea breeze circulation is driven directly by land-sea surface temperature contrasts. When synoptic pressure gradients are weak, sea/land breezes dominate in the coastal zone. During periods of strong synoptic across-shore pressure gradients, seabreeze effects are superimposed upon the equatorward flow, resulting in the along-shore acceleration of equatorward wind during the day time. A thermal front is established during the day as the land heats up and the across-shore horizontal thermal gradient increases. Cool SSTs established though the upwelling response to equatorward winds act to sharpen the air mass boundary between cool moist air over the ocean and warm dry air over the land. Onshore flow associated with seabreezes is rotated towards the along-shelf direction by the Coriolis effect as the day progresses. Topographic steering by coastal mountains may be as, or more, significant than the influence of the Earth's rotation in deflecting across-shore flow along-shore (Simpson, 1996). Jury (1985b) observed the development of a thermal front with a magnitude of 0.6°C km^{-1} between the Berg River valley heat low and cool marine air during equatorward flow associated with anti-cyclonic inversion conditions. The resultant diurnal variation in wind speed at Cape Columbine revealed a minimum at the onset of the seabreeze at 1100 SAST (900 GMT) with wind increasing to 10 m s^{-1} to peak at 1900 SAST (1500 GMT). The thermal front supplies momentum to the along-shore flow in the afternoon as Coriolis deflects the sea-breeze (Jury, 1985b). Weak pressure gradients and low inversions were found by Jury to favour the development of seabreezes, while westerly synoptic flow regimes were found to inhibit seabreeze development by weakening heating over the land. Cold SSTs associated with upwelling in the southern Benguela cause a downward heat flux which enhances the atmospheric subsidence inversion and results in shallower equatorward flow (Jury, 1985b). Low-level divergence associated with the seabreeze decreases the MABL depth.

According to previous observations, the wind field indicates cyclonic shear around Cape Columbine during summer equatorward flow conditions (Jury et al., 1990a,b; Kamstra, 1985). Aerial surveys were used by Jury (1985a; 1985b) to investigate topographically and thermally induced anomalies in the summer equatorward wind field between 31 and 33°S and 17 and 19°E. Below the atmospheric subsidence inversion, an equatorward coastal wind jet was found to be situated over the Cape Columbine headland, winds accelerated over the sea to the west of the cape, fanning out and decelerating with cyclonic curvature downstream over St Helena Bay. The depth of surface flow was found to affect the spatial variation of low level winds in the lee of Cape Columbine. For deep flow associated with a subsidence inversion around 2000m above ground level, onshore curvature in the lee of the headland was said to be aided by the geometry of the cape and seabreezes near the mouth of the Olifants River (Jury, 1985a). Jury suggests that the Olifants River Valley entrains the Cape Columbine jet across the coast as seabreezes induced by sharp thermal fronts north of Columbine increase the across-shore component. When the flow is shallow with an inversion around 1000m above ground level, the effects of the cape were enhanced with a wake observed in the lee of the cape (Jury, 1985a). Jury (1985b) investigated the relationship between wind forcing and the resultant upwelling response for the greater St Helena Bay region. The structure of the wind profile and its associated curl differed between shallow and deep flow, with SST images revealing different upwelling structures (Figure 2.4). Cyclonic wind curl was found over Cape Columbine for both flow depths with a distinct upwelling plume just north of the cape. During deep flow, cyclonic curvature extended further downwind of Cape Columbine. This cyclonic wind stress together with along-shore flow was found to increase the intensity of upwelling in the narrow band of coastal upwelling along the coast north of St Helena Bay. During shallow flow, this coastal upwelling was observed in SST images as being suppressed due to the wake in the lee of the Cape and anti-cyclonic wind stress curl observed further downstream.

2.6 Outline of Objectives

Variability in local wind stress forcing has been identified as a potentially important physical mechanism behind HAB development and advection in the greater St Helena Bay region. This thesis is aimed at improving our understanding of the atmospheric conditions behind HAB development and advection in the southern Benguela. To achieve this objective, the local winds are simulated over a chosen bloom event during which time hydrographic

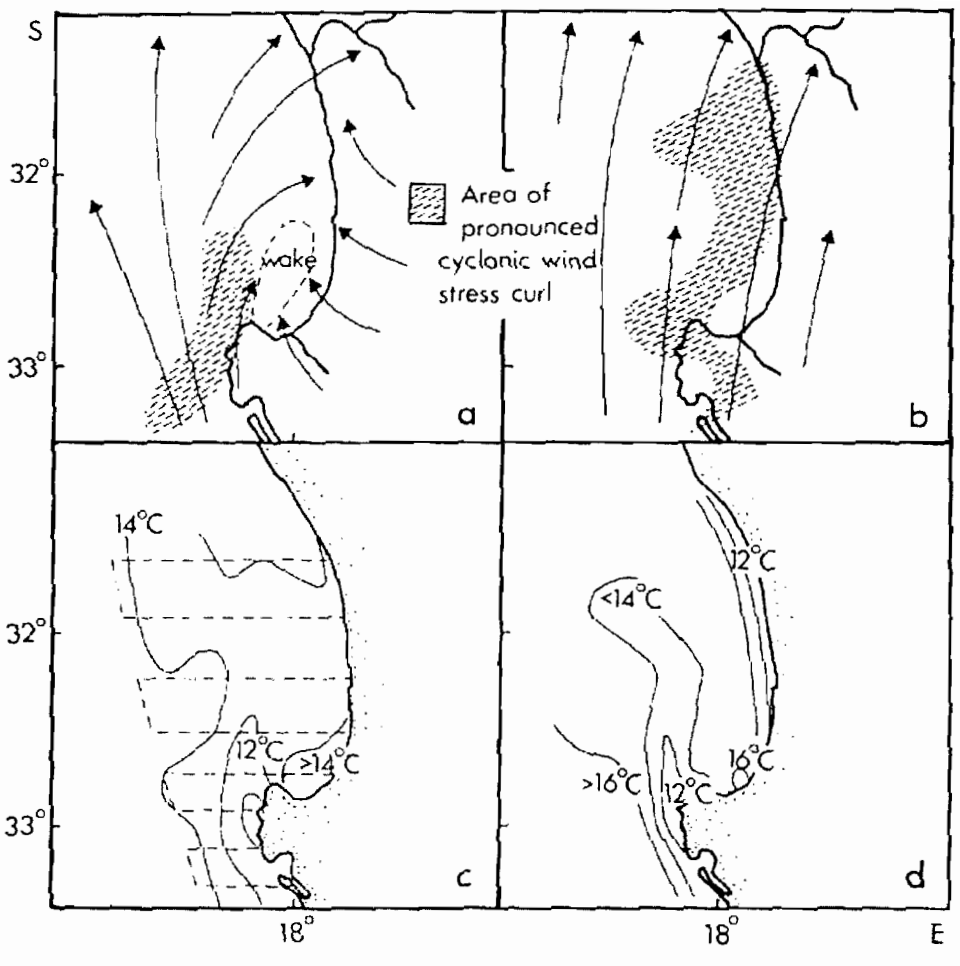

Figure 2.4: Comparison of (a) shallow and (b) deep cases of equatorward flow and (c) and (d) SSTs on corresponding days taken from Jury, 1985a.

and biological conditions offshore of Lambert's Bay were monitored by MCM. In order to assess how representative the chosen event is of the typical wind stress conditions, the nature of the case study in terms of temporal variability in along-shore wind stress forcing is considered. The simulated winds are validated with the limited observations available and the ability of the regional atmospheric model to simulate the response of synoptic flow to topography and thermal gradients is assessed. Finally, the impact of spatial variability in wind stress forcing on HAB development and advection is investigated. A range of data sets and analytical techniques are used in obtaining these research objectives, and these together with the regional atmospheric model setup are described in the following chapter.

Chapter 3

Data and Methodology

This chapter deals with the data and analytical methods used in addressing the research objectives outlined in the previous chapters. In the first section, hydrographic and biological observations conducted by MCM over the chosen March 2001 HAB event are described. The second section aims to describe the data and analytical techniques used in evaluating temporal variability in along-shore wind stress over the greater St Helena Bay region. The third section explains how the regional atmospheric model MM5 was used to simulate the atmospheric condition during the chosen case study. Data used to describe the synoptic forcing and local observations during the chosen event as well as to force and validate the model are described in this section. The final section of this chapter deals with the methods used in assessing the spatial variability in the regional wind stress.

3.1 Hydrographic and Biological Observations: 13-30 March 2001 HAB Event

The HAB division of MCM has in recent years conducted annual observations of algal bloom development. Surveys have taken place on the Namaqua shelf north of Cape Columbine towards the end of the upwelling season, when and where the incidence of HABs is known to be high. Monitoring during these surveys occurs off Lambert's Bay along an off-shore transect comprising of 14 stations, with station 1 situated in the surf-zone and station 14 approximately 24 nautical mile off-shore (Figure 3.1). Of the monitored bloom events, the March 2001 event was chosen because the clear sequence in which the initial days of active

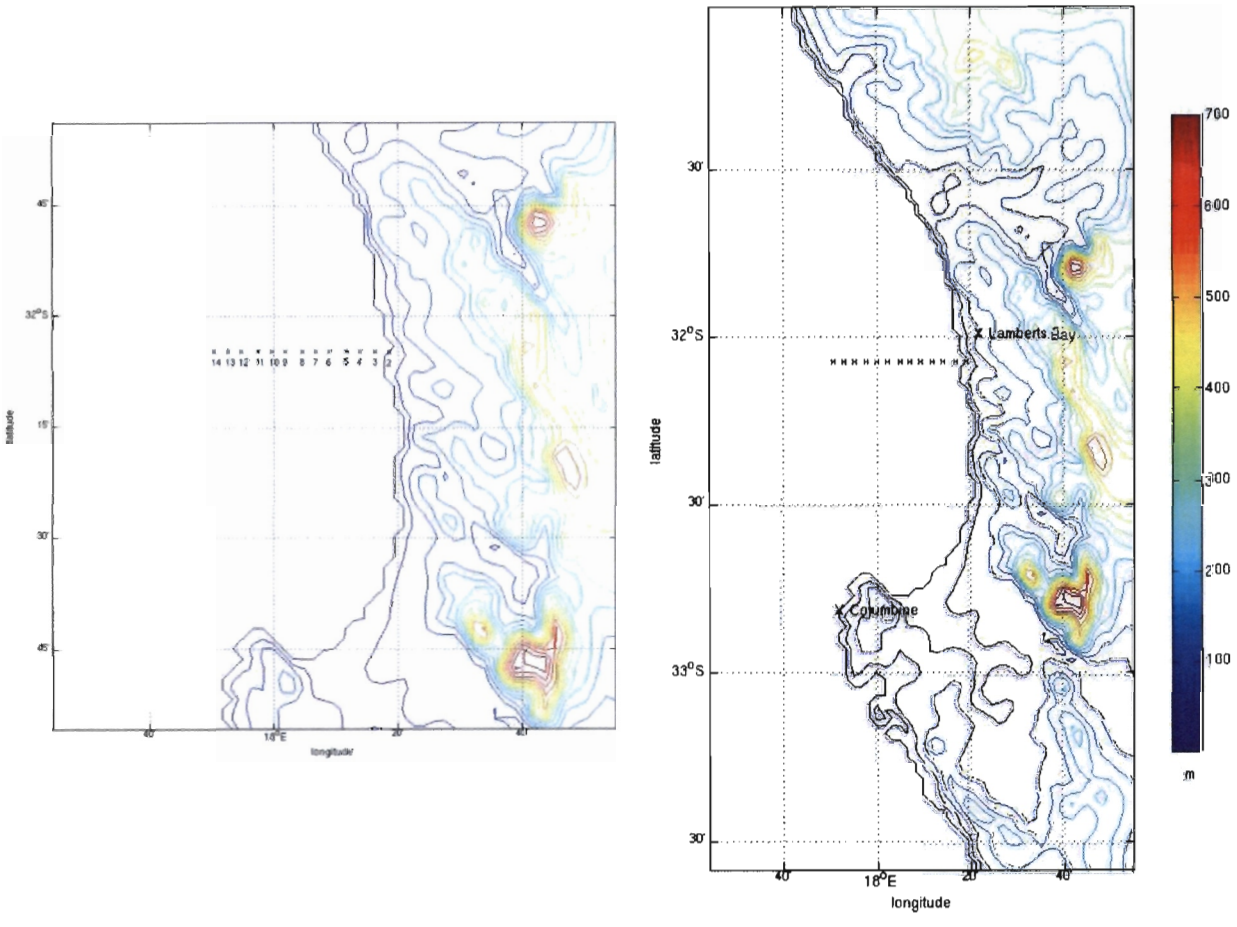

Figure 3.1: Locations of stations along MCM transect conducted offshore of Lambert's Bay and the Columbine and Lambert's Bay weather stations, plotted on topography used for the regional atmospheric model's 3km resolution nest.

at 0000, 0600, 1200 and 1800 GMT. Analysis and forecast values have been interpolated from the atmospheric model to a 2.5°x 2.5°horizontal grid. SLP ERA-40 data have been used to construct a SLPI. The SLPI has been created as a measure of the local synoptic across-shore pressure gradient which drives local along-shore wind for the greater St Helena Bay region. The SLPI has been calculated as the difference between SLP at 15°E and 17.5°E along 32.5°S. A few different ways of calculating a SLPI were tested (i.e. difference between averages taken over south-west Africa and the south-east Atlantic), however each ERA-40 value already represents a large area (2.5°x 2.5°) and so the SLPI used was found to provide the best representation of the local across-shore pressure gradient field and the best correlation with local variability in along-shore wind observed at Cape Columbine (Figure 4.12).

3.2.2 Continuous Wavelet Analysis

Continuous Wavelet Analysis (CWA) has been used to investigate dominant modes of variability in a timeseries and how those modes vary in time. CWA is a powerful tool as it allows frequency analysis of a time dependent signal locally in time (Daubechies, 1990). This is particularly appropriate for geophysical timeseries due to their non-stationary nature and the numerous scales at which geophysical processes take place (Lau and Weng, 1995). A brief explanation of the advantages of the CWA technique and the Continuous Wavelet Transform (CWT) used will be given here. More detailed explanations on wavelet analysis and the complex Morlet wavelet transform are provided by Daubechies (1992), Lau and Weng (1995) and Torrence and Compo (1998).

When dealing with frequency analysis of non-stationary timeseries over a large range of frequencies, CWT has its advantages over the Fourier transform, which is more commonly used in spectral analysis. Fourier transforms do not contain any time dependency in the signal and therefore cannot provide any local information regarding the time evolution of its spectral characteristics (Lau and Weng, 1995). A Windowed Fourier Transform (WFT) may be used to extract local-frequency information under a fixed time-frequency window (Figure 3.2), but is problematic when dealing with a wide range of frequencies. At low frequencies, there are so few oscillations within the window that the frequency localisation is impaired, while at high frequencies there are so many oscillations that the time localisation is impaired (Torrence and Compo, 1998). The advantage of using wavelet transforms is that wavelet transforms can be stretched and translated with flexible resolution in both

upwelling forced by predominant equatorward winds are followed by a prolonged quiescent phase. During the 13-30 March 2001 event, daily profiles of water column temperature and fluorescence were made at in-shore station 3 using a Sea Bird CTD and a Wetstar fluorometer. Profiles of temperature and fluorescence were performed for stations 3-14 of the transect on the 16th and 24th of March 2001. Water samples were collected on station from discrete depths for nitrate, chlorophyll a, and phytoplankton analysis as described by Pitcher and Nelson (2006). Extracted chlorophyll values were used to calibrate fluorescence profiles.

3.2 Temporal Variability in Wind Stress: Data and Analytical Methods

3.2.1 Inter-annual Timeseries

Two inter-annual timeseries have been created to assess the variability in along-shore winds within the case study region. The first was created using QuikSCAT Mean Wind Fields (MWF). QuikSCAT MWF are a CERSAT, 0.5° by 0.5° gridded data product. Using the kriging objective mapping technique, daily MWF are generated from the JPL/PO.DAAC level 2B swath product of the NASA SeaWinds scatterometer on board QuikSCAT. Blanke et al. (2005) compared MWF data with daily-averaged anemometer data at Cape Columbine from 1 September 1999 - 17 January 2002. They found very good agreement between the two timeseries with a correlation coefficient close to 0.86 for the along-shore wind component. A timeseries of local along-shore wind stress was created by extracting daily wind stress values at 32.75°S 17.25°E from 20 July 1999 - 10 January 2006 MWF.

The second inter-annual timeseries created to assess variability is a Sea Level Pressure Index (SLPI) based on daily ERA-40 re-analysis Sea Level Pressure (SLP) data from January 1979 - December 2001. The European Centre for Medium-Range Weather Forecasts (ECMWF) 40 Years Re-Analysis (ERA-40) project is a global atmospheric analysis extend

frequency and time (Lau and Weng, 1995). As a result, the timeseries signal can be decomposed in terms of wavelets which are derived from a 'mother wavelet' $\psi_0(\eta)$ by dilations and translations (Lau and Weng, 1995). The scaled wavelet is defined by Torrence and Compo (1998) as:

$$\psi\left[\frac{(n'-n)\,\delta t}{s}\right] = \left(\frac{\delta t}{s}\right)^{1/2} \psi_0\left[\frac{(n'-n)\,\delta t}{s}\right] \tag{3.1}$$

where the wavelet $\psi\left[\frac{(n'-n)\delta t}{s}\right]$ is translated along the localised time index n (translation parameter) and its scale is varied by the dilation parameter s. The 0 subscript has been dropped to indicate that $\psi\left[\frac{(n'-n)\delta t}{s}\right]$ has been normalised. A energy normalisation factor of $s^{-1/2}$ keeps the energy of the 'daughter wavelets' the same as the energy of the 'mother wavelet' ensuring that wavelet transforms at each scale are directly comparable to each other (Torrence and Compo, 1998; Lau and Weng, 1995). This also means that if the unscaled mother wavelet $\psi_0(\eta)$ is normalised to have unit energy then wavelets at each scale will have unit energy. The continuous wavelet transform of a discrete signal x_n is defined as the convolution of x_n with a set of scaled and translated wavelets (Torrence and Compo, 1998; Lau and Weng, 1995):

$$W_n(s) = \sum_{n'=0}^{N-1} x_{n'} \psi^{\star}\left[\frac{(n'-n)\,\delta t}{s}\right] \tag{3.2}$$

$\psi*$is the complex conjugate of ψ. The CWT reveals a local measure of both relative amplitude and phase at a scale of variability proportional to s and time n. Scale (s) is synonymous with the period of the wavelet and the inverse its frequency and so the CWT is a time-frequency analysis. Although it is possible to solve the wavelet transform in the time domain using equation 3.2, it is much simpler to perform the wavelet transform calculation in Fourier space using a Fast Fourier Transform (FFT) of the timeseries and the wavelet function as described by Torrence and Compo.

The Morlet wavelet was chosen for this investigation as it is the most commonly used wavelet in geophysical signal detection (Lau and Weng, 1999). The Morlet wavelet consists of a complex exponential modulated by a Gaussian function (Figure 3.3) :

$$\psi_0(\eta) = \pi^{-1/4} e^{i\omega_0\eta} e^{-\eta^2/2} \tag{3.3}$$

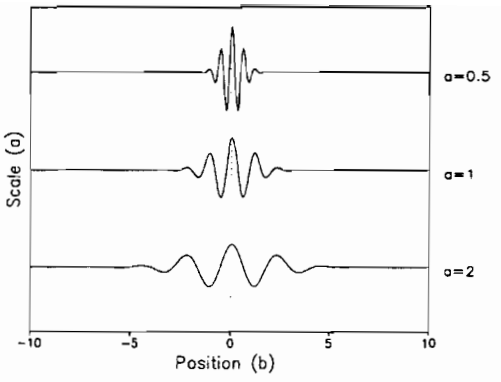

Figure 3.3: Example of the Morlet wavelet with different values of scale, taken from Lau and Weng (1995).

where $\psi_0(\eta)$ is the Morlet wavelet value at non-dimensional time η. A non-dimensional frequency $\omega_0 = 6$ (Torrence and Compo, 1998) is used, which satisfies the admissibility condition (Farge, 1992). The advantage of the Morlet wavelet transform is that its complex nature is able to detect both time-dependent amplitude and phase for different frequencies exhibited in the timeseries (Lau and Weng, 1995). The resultant wavelet transform coefficient $W_n(s)$ is complex containing both real and imaginary parts which can be used to assess the amplitude and phase of the local components of the signal. The wavelet power spectrum is defined as the absolute value of the wavelet transform squared. Depicted in two-dimensional space with time on the x-axis and period on the y-axis, the wavelet power spectrum provides a local measure of timeseries variance at each period (Torrence and Compo, 1998).

A problem with performing the wavelet transform in Fourier space is that this assumes the timeseries is cyclic resulting in a wraparound effect which is more pronounced at larger scales as the width of the wavelet in time increases. To reduce wraparound effects, one end of the timeseries is padded with zeros. This process however introduces discontinuity at the endpoints and variance near the edge is reduced with increasing scale as the influence of each wavelet extends further in time encompassing more zeros. The 'cone of influence' is therefore depicted on the wavelet power spectrum to indicate where these edge effects become important (Torrence and Compo, 1998).

Significance levels have been determined as described by Torrence and Compo (1998). An

appropriate background spectrum is chosen with the assumption that the different realizations of the geophysical process will be randomly distributed about this mean background. The actual spectrum can then be compared against this mean background spectrum and if a peak is significantly above this background spectrum, then it can be assumed to be a true feature with a certain confidence level (Torrence and Compo, 1998). For geophysical timeseries, either a white-noise or red-noise spectrum may be an appropriate background spectrum. By choosing the appropriate lag-1 autocorrelation for the timeseries, one can model a background red-noise spectrum for the timeseries. A lag-1 of 0 gives a white-noise spectrum (Torrence and Compo, 1998). The wavelet power spectrum is then distributed as chi-squared about the chosen background spectrum to define the 95% confidence contours.

The time average over all local wavelet power spectra is defined as the Global Wavelet Spectrum (GWS) (Torrence and Compo, 1998):

$$\overline{W}^2(s) = \frac{1}{N} \sum_{n=0}^{N-1} |W_n(s)|^2 \tag{3.4}$$

The GWS is equivalent to the Fourier power spectrum smoothed by the Morlet wavelet function in Fourier space (Farge, 1992). Because of the 'uncertainty principle' (Chui, 1992) the width and the height of a time-frequency window cannot be arbitrary (Figure Lau and Weng). This means that at high frequencies, high precision in time localisation can be achieved at the expense of reduced frequency resolution, while at lower frequencies time localisation it less precise and frequency resolution higher (Lau and Weng, 1995). Reduction in frequency resolution at small scales results in the peaks in the spectrum being smoothed out, while at larger scales the wavelet although wide in time is narrow in frequency and therefore the peaks are sharper and have larger amplitudes. As a result the GWS is a biased estimator and one should not use the GWS to determine the relative magnitude of peaks.

The wavelet transform is essentially a bandpass filter of uniform shape and varying location and width, extracting the different local components of the signal by providing amplitude and phase values for every frequency and time (Melice et al., 2001). The wavelet transform conserves variance so the timeseries can be recovered exactly by summing the real part of the wavelet transform over all scales using the the delta function δ (Farge, 1992; Torrence and Compo, 1998). To examine power variations over a range of scales one can scale-average wavelet power. The scale-averaged wavelet power is defined as the weighted sum

of the wavelet power spectrum over scales s_1 to s_2 (Torrence and Compo, 1998):

$$\overline{W}_n^2 = \frac{\delta j \delta t}{C_\delta} \sum_{j=j_1}^{j_2} \frac{|W_n(s_j)|^2}{s_j} \tag{3.5}$$

the delta function δ (Farge 1992) is used to reconstruct the timeseries. The factor C_δ comes from the reconstruction of a δ function from its wavelet transform using the function $\psi_0(\eta)$ (Torrence and Compo. 1998). By scale-averaging the wavelet power within a certain band of scales, one creates a timeseries of the average variance within that band.

The wavelet software used here to perform continuous wavelet analysis was provided by C. Torrence and G. Compo, and is available at URL: http://paos.colorado.edu/research/wavelets/.

3.3 Modeling Regional Winds with MM5: 11-30 March 2001

3.3.1 Synoptic Atmospheric Data

The Navy Operational Global Atmospheric Prediction System (NOGAPS), 1 August 1997 - present, global coverage, 1° gridded data product was used to assess the synoptic conditions over the event as well as to provide boundary and initial conditions for the regional atmospheric model. NOGAPS is the U. S. Department of Defence's (DOD) high-resolution global atmospheric forecast model developed and run by the Naval Research Laboratory (NRL) and the Navy's Fleet Numerical Meteorology and Oceanography Centre (FNMOC). It is spectral in the horizontal and hybrid in the vertical, following the terrain at low levels and constant pressure surfaces at upper levels. NOGAPS is run every 12 hours providing a high-resolution six-day forecast every 6 hours. NOGAPS 0000 and 1200 GMT nowcast data were used to force the regional climate model. The data assimilation system used by NOGAPS in 2001 was the US Navy's multivariate optimum interpolation (MVOI) analysis scheme (Barker, 1992). A detailed description of the operational implementation of the MVOI analysis scheme is given by Goerss and Phoebus (1992) and description of the NOGAPS forecast model is given by Hogan and Rosmond (1991). NOGAPS outputs are used to force several other DOD systems such as the Navy's Coupled Ocean-Atmosphere Mesoscale Prediction System (COAMPS), FNMOC's ocean wave model, sea ice model,

ocean thermodynamics model, tropical cyclone model, and aircraft and ship-routing programs. NOGAPS serves as the backup global atmospheric forecast system for the National Weather Service .

The National Centre for Environmental Prediction (NCEP) in collaboration with the National Centre for Atmospheric Research (NCAR) have produced re-analyses of atmospheric data from 1948-present on a 2.5° by 2.5° horizontal grid. These global analyses are based on land surface, ship, rawinsonde, pibal, aircraft, satellite, and other data, which were assimilated with the assimilation system kept unchanged over the reanalysis period. A description of this assimilation system is given by Kalnay and Coauthors (1996). NCEP re-analysis SLP data has been used for comparison with NOGAPS SLP data.

Daily South African Weather Service (SAWS) synoptic charts have also been included in Appendix A for comparison with the NOGAPS SLP data.

3.3.2 Local Weather Station Data

Data from the SAWS weather station at Lambert's Bay and a MCM weather station at Cape Columbine have been used to describe local conditions over the chosen event and for validation of the regional atmospheric model results. Figure 3.1 indicates the location of the two weather stations used. The Lambert's Bay weather station is situated approximately 5km inland at 94m above sea level. Although slightly inland, the weather station is elevated and remains exposed to the maritime wind conditions. Pressure, wind speed and wind direction data from this station have been used to compare with the model. Hourly pressure data have been corrected to sea level and are averaged values of measurements taken over the preceding hour. Hourly wind speed and direction data have been taken on the hour, based on sampling taken for a few minutes around the hour. The Cape Columbine weather station is situated near sea level and is directly exposed to maritime winds. Wind speed and direction data from this station have been used. Unlike the wind data from Lambert's Bay, weather station, the hourly wind data at Columbine are averaged values of measurements taken over the preceding hour.

3.3.3 QuikSCAT Data

Daily QuikSCAT swath data have also been used to validate model 10 meter winds over the ocean. QuikSCAT data used was produced by Remote Sensing Systems and sponsored

by the NASA Ocean Vector Winds Science Team, available at www.remss.com

3.3.4 Simulations Undertaken

The regional atmospheric model chosen to simulate the atmospheric conditions over the case study was the fifth-generation Pennsylvania State University / National Centre for Atmospheric Research (PSU / NCAR) Mesoscale Model (MM5) (Grell et al., 1995). MM5 is a limited-area, non-hydrostatic, terrain-following, sigma-coordinate atmospheric model. It has been employed in similar studies investigating the effects of topographical forcing on upwelling favourable wind stress and stress curl along the California coastline (Koracin and Dorman, 2001) as well as to simulate several cut-off low events over South Africa (Singleton and Reason, 2006). The MM5 modeling system provides a suite of programmes which are freely provided and supported by the Mesoscale Prediction Group in the Mesoscale and Microscale Meteorology Division of NCAR. Four of these programmes were used in the simulations undertaken (Appendix B).

Initially, the Terrain programme is used to set up the mother mesoscale domain together with child nests. Temporally constant elevation, land-use and land-water mask data are interpolated to the mesoscale grids defined and if a land surface model option is chosen further soil, vegetation fraction and deep soil temperature data is needed. MM5 supports both one and two-way nesting, with the nest type specified in the Terrain programme. For the purposes of obtaining high resolution within the region of interest, two way nesting was used following a 3:1 length ratio. A horizontal grid resolution of 27km was chosen for the mother/outer domain. Centred at 35°S 25°E and comprising of 123 by 123 grid points, the mother domain encompasses both easterly and westerly wave regions, ensuring adequately represented synoptic forcing. A second nest of 9km horizontal resolution focuses on the west coast of southern Africa over the region between 29°S to 35°S and 17°E to 21°E. The dimensions of this nest were carefully chosen so as to avoid any boundaries coinciding with steep topographical gradients associated with escarpment. Finally, the third nest homes in on the greater St Helena bay region at 3km resolution as depicted in Figure 3.4 . Mercator projection was chosen to represent the domain. Overlapping parabolic interpolation was used by the Terrain programme to interpolate terrestrial data onto the mesoscale grid. United States Geological Survey (USGS) topography data of 10 minute resolution was used for the 27km resolution domain, 5 minute for the 9km and 30 second for the 3km grid. 25 category 30 second resolution land-cover data from the USGS are used to provide

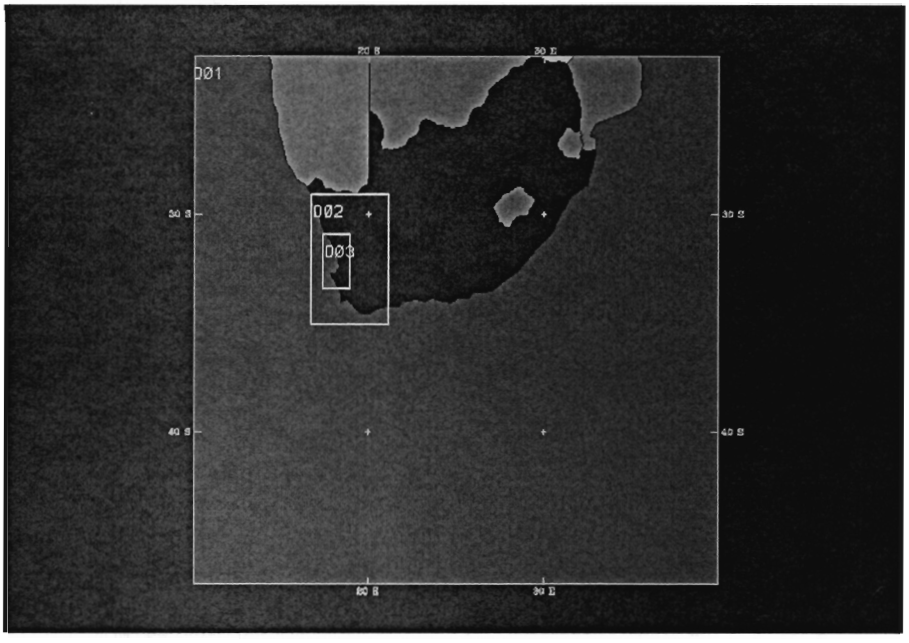

Figure 3.4: Horizontal grid used in atmospheric simulations, 27km resolution mother domain with 9km and 3km resolution nests.

vegetation and land-water mask data. Soil category, vegetation fraction and deep soil temperature data were also provided for the five-layer soil model used to compute surface heat and moisture fluxes.

The Regrid programme is then used to interpolate initial and lateral boundary conditions from their native grid to the horizontal grid defined by the terrain programme. NOGAPS twelve hourly, one degree resolution, synoptic fields were chosen to provide the initial and lateral boundary conditions. NOGAPS synoptic data used to force the model included air temperature, U and V horizontal winds, relative humidity, geopotential height and SLP.

The Interpf programme vertically interpolates model initial and lateral boundary conditions to sigma levels. The vertical grid consisted of twenty three sigma level with five falling in the lowest 1000m meters. The domain and forcing data produced by these three programmes is finally used by MM5. MM5 offers several options for the parameterisation of various sub-grid processes. Physics options chosen in the model runs include the Grell cumulus parameterisation scheme, the mixed phase explicit moisture scheme and the cloud radiation scheme which includes the effects of cloud on long-wave and shortwave radiation. The MRF parameterisation scheme (Hong and Pan, 1996) was chosen for the Planetary Boundary

Layer (PBL) due to its suitability for high resolution runs. The MRF boundary layer vertical diffusion scheme is based on the nonlocal diffusion concept of Troen and Mahrt (1986)(Hong and Pan, 1996). The MRF scheme is one of three MM5 PBL schemes which provide 10m wind results. The five-layer soil model was chosen to produce the surface physics need by the MRF scheme.

The MM5 model was run from 11-30 March 2001 with an integration step of 81 seconds for the mother domain of 27km resolution. Two model runs were undertaken. For both runs the domain setup, atmospheric forcing and physics options described above were used. Only the SST data used differed between the two runs.

For the first run, weekly 1° National Oceanic and Atmospheric Administration (NOAA) Optimum Interpolation (OI) SST version 2 (v2) data was used. These data do not capture all the details of the Benguela upwelling system and the Agulhas current. The OI.v2 analysis, described by Reynolds et al (2002), is produced weekly on a one-degree grid using in situ and satellite data. The model output was saved every four hours for the first model run.

Higher resolution SST data, resolving the mean SST structure which resulted from upwelling activity between the 11-31 March 2001, was used to force the second model run. A mean SST field of 5km resolution was created from five-day SST composite images derived from the Meteosat geostationary satellite's thermal sensor. The processing procedure for SST images from Meteosat is described by Demarcq and Citeau (1995). Applications of Meteosat SST imagery to coastal upwelling areas are given by Demarcq and Citeau (1995) and Demarcq and Faure (2000). The model output was saved every hour for the second model run. Figure 3.5 depicts, for the 9km resolution nest, the different SST data used.

3.4 Spatial Variability in Wind Stress

Neutral wind stress was derived from simulated 10 meter wind fields following Large and Pond (1981) using the bulk aerodynamic formula:

$$\tau = \rho C_d |V| V \tag{3.6}$$

τ is the stress vector, ρ is the density of air (assumed constant 1.22 kg m^{-3}), C_d is a dimensionless drag coefficient, V is the wind velocity and $|V|$is the wind speed. While C_d

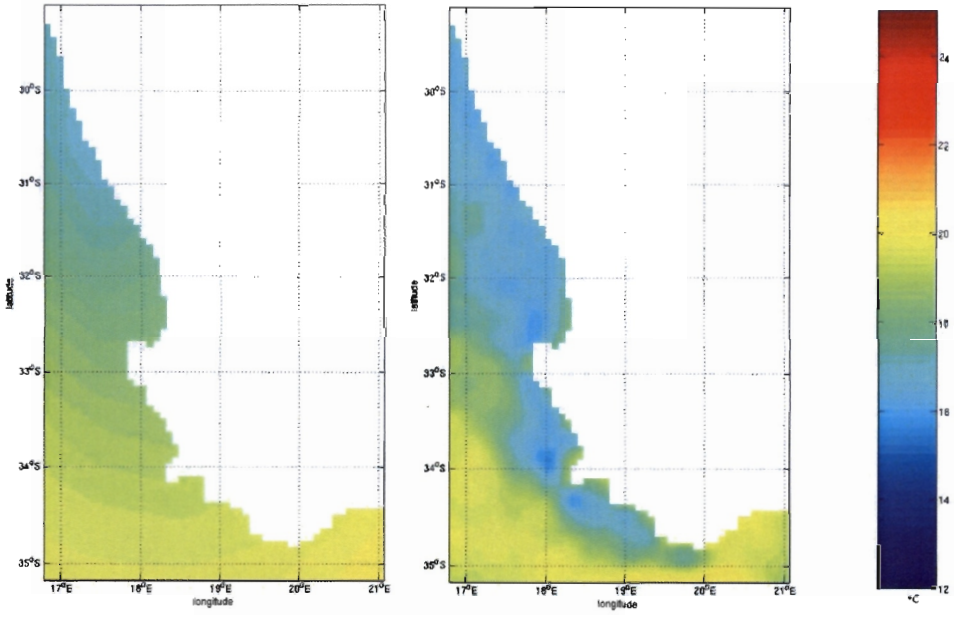

Figure 3.5: (Left) NOAA OI SST v2 used in the first model run, for the 9km resolution nest. (Right) Meteosat SST used in the second model run, for the 9km resolution nest.

is dependent on both wind stress and atmospheric stability (Large and Pond, 1981), C_d in the Large and Pond (1981) algorithm is dependent only on wind speed with atmospheric stability assumed to be neutral. Blanc (1983) showed that unstable conditions due to a upward humidity flux can increase wind stress by 10 percent and stable conditions can decrease wind stress by up to 20 percent. The southern Benguela region is considered stable due to cool upwelling induced SSTs. Hellerman and Rosenstein (1983) demonstrated that the effect of stability on large scale averages of computed stresses in the eastern boundary regions is only of the order of several hundredths of a dyn cm^{-2}. Over the unstable Agulhas current however a neglect of atmospheric stability may lead to an underestimation of wind stress of the order of 0.1 dyn cm^{-2}. The Large and Pond (1981) algorithm for estimating bulk wind stress for neutral conditions has been used in several ocean-atmosphere interaction assessments for the Californian upwelling system e.g. (Koracin and Dorman, 2001). Previous studies by Bakun and Nelson (1991) and Kamstra (1985), derived wind stress for the Benguela region from ship based wind measurements using the bulk aerodynamic formula with a constant drag coefficient of 0.0013 according to Nelson (1977). By retaining a constant ρC_d their results are equivalent to pseudo stress but scaled to carry stress units.

Spatial variability in wind stress field results in wind stress curl. Wind stress curl may play a significant role in driving upwelling/downwelling through Ekman transport divergence/convergence known as Ekman pumping. Wind stress curl C has been calculated as:

$$C = \frac{\Delta \tau_y}{\Delta x} - \frac{\Delta \tau_x}{\Delta y} \tag{3.7}$$

because of the high horizontal resolution (9km and 3km) the effects of the earths curvature in the computation of wind stress curl can be neglected (Enriquez and Friehe, 1995; Koracin and Dorman, 2001). Only curl in the wind field over the ocean is of significance and so land values have been masked out to prevent unrealistic ocean curl values due to contamination by land values.

Chapter 4

Temporal Variability in Local Winds

This chapter deals with two main subsections. Firstly temporal variability in across-shore pressure gradients and along-shore wind stress within the region of interest is assessed and the chosen event considered in terms of the observed temporal variability. The second section describes the synoptic forcing and local observations over the chosen case study.

4.1 Inter-annual Variability

The southern Benguela climate is highly variable (Reason et al., 2006). Continuous Wavelet Analysis (CWA) has been performed on two timeseries in order to asses the dominant timescales of meridional wind stress and zonal SLP gradient variability within the case study region. Details pertaining to the construction of these two timeseries together with an explanation of the CWA techniques used have been provided in the first section of Chapter 3.

The first timeseries consists of QuikSCAT meridional wind stress data for the region of interest from the 20 July 1999 - 10 January 2006. Results of the CWA performed on this timeseries are shown in Figure 4.1. The Global Wavelet Spectrum (GWS) provides an indication of the dominant timescales of variability over the entire timeseries. In Figure 4.1, periods of variability for which the GWS falls above the 95% confidence level are considered to be statistically significant. The GWS depicted in Figure 4.1, with a zoom for the higher frequencies in Figure 4.2, indicates that only synoptic variability with a period of roughly 2-8 days and the annual cycle may be considered as being significant time scales

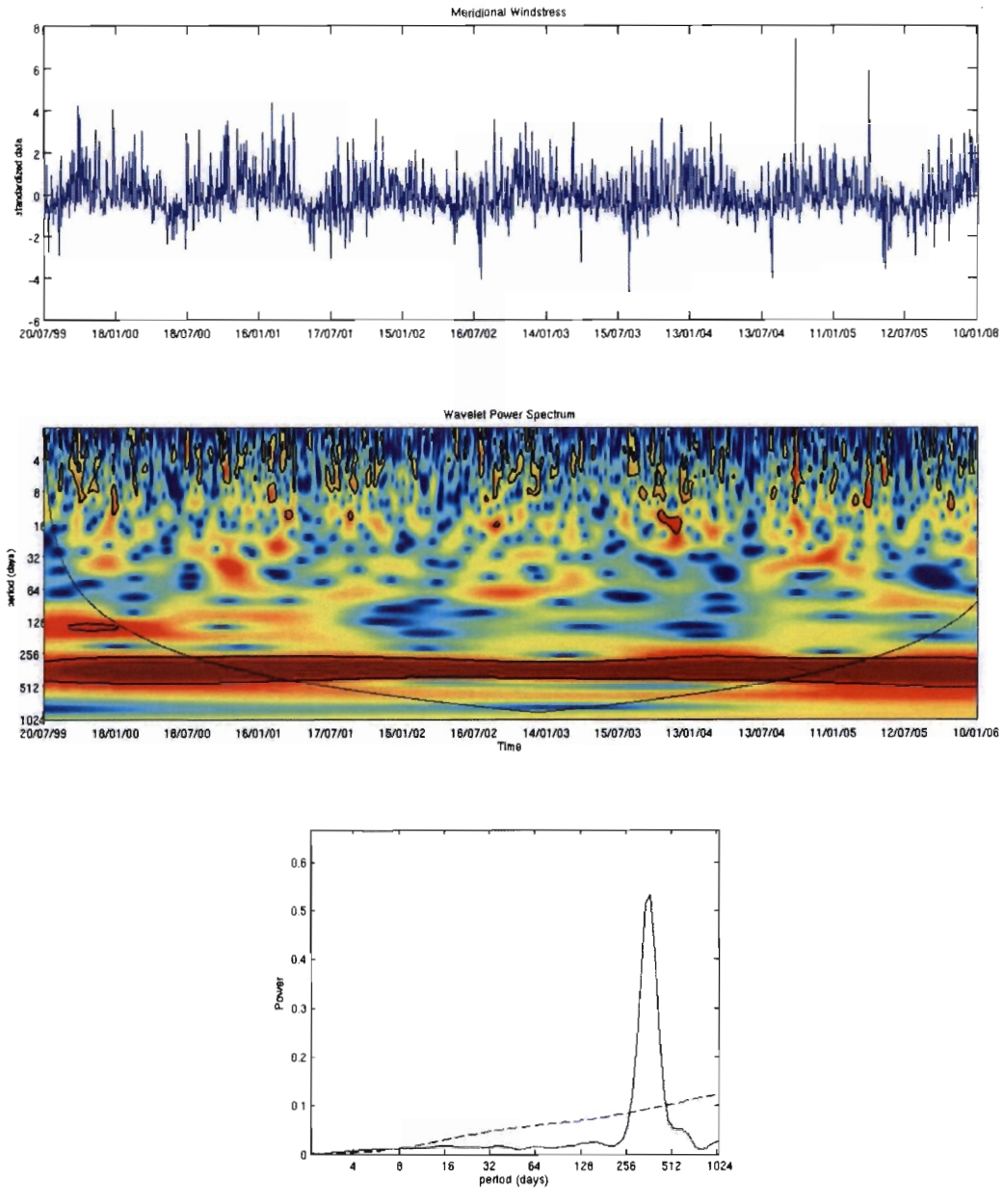

Figure 4.1: (Top) The standardised meridional wind stress timeseries from July 1999 - January 2006. (Middle) The local wavelet power spectrum with black contours indicating the cone of influence and enclosing regions of greater than 95% confidence for a red-noise process with a lag-1 coefficient of 0.6562. (Bottom) The global wavelet power spectrum (solid line) with the 95% confidence level for the global wavelet spectrum assuming a lag-1 coefficient of 0.6562 (dashed line).

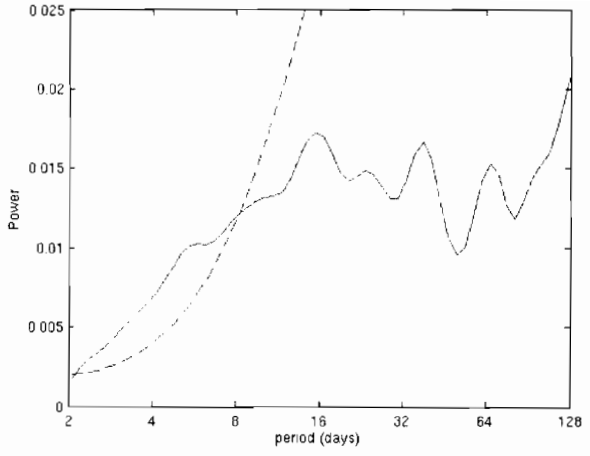

Figure 4.2: Zooming in on the 4-128 day periods, the global wavelet power spectrum for the meridional wind stress timeseries from July 1999 - January 2006 (solid line) with the 95% confidence level for the global wavelet spectrum assuming a lag-1 coefficient of 0.656 (dashed line).

of variability in meridional wind stress for the entire July 1999 to January 2006 timeseries. High frequency variability with a period of 2-8 days can be associated with the synoptic cycle. Preston-Whyte and Tyson (2000) suggest a period of 2-8 days for the synoptic cycle which occurs due to the passage of mid-latitude cyclones and migrating anticyclones south of the continent.

While the annual and synoptic cycles are the only significant signals present throughout the entire timeseries, variability at other frequencies is seen to be significant at certain stages. This is illustrated by the 95% contours on the local wavelet power spectrum in Figure 4.1. This wavelet power spectrum provides a local measure of timeseries variance at each period and from this one may ascertain what the dominant periods of variability are at each point in the timeseries. Oscillations in meridional wind stress with periods greater than the average synoptic cycle of 2-8 days do significantly contribute to timeseries variability at various stages in the timeseries. By looking at a timeseries of the average variance within the 8-64 day band (Figure 4.3), we can see that there are several stages in the timeseries where oscillations in wind stress with periods of 8-64 days (sub-synoptic to intra-seasonal) contribute significantly to the variability. In the first half of 2001, variability within 8-64 day band is seen to significantly contribute to the meridional wind stress variance on three occasions.

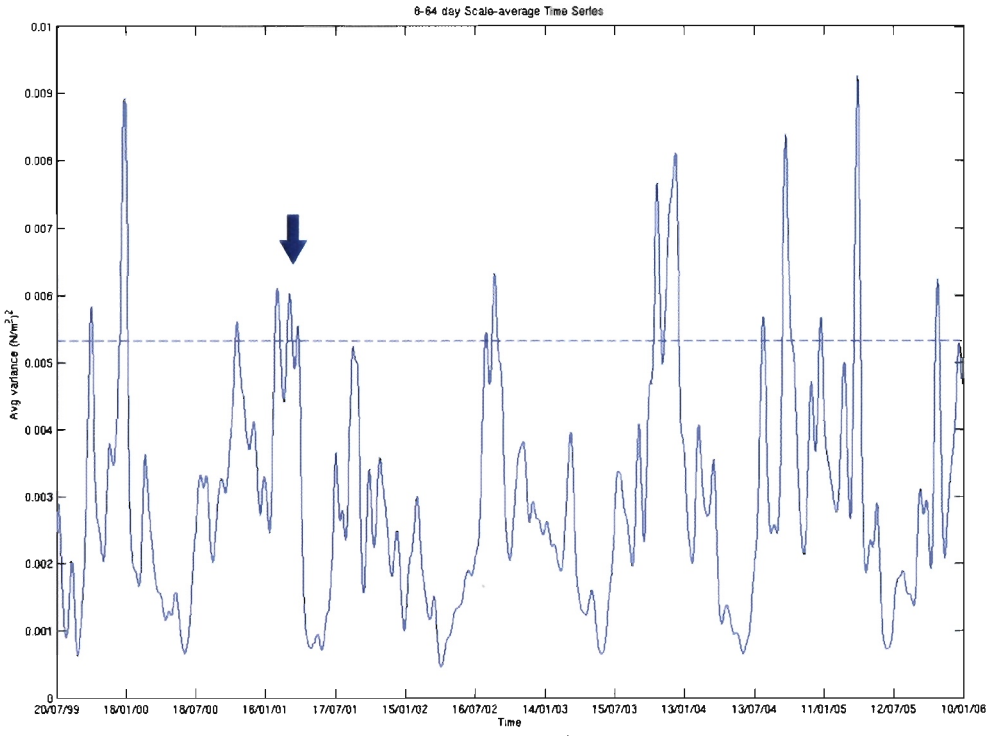

Figure 4.3: Scale-averaged wavelet power within the 8-64 day band for the meridional wind stress timeseries from July 1999 - January 2006 (solid line) with the 95% confidence level (dashed line).

Figure 4.4 zooms in on a segment of the local wavelet power spectrum from Figure 4.1 spanning from September 2000 - April 2001. The chosen case study falls within this summer season. During the 13-30 March 2001 event there is a significant peak in the local power spectrum with a period of 12-16 days (Figure 4.4). The local wavelet power spectrum from the 13-30 of March 2001 appears to be bimodal. Oscillations in wind stress with a period of 2-6 days and 12-16 days contribute significantly to wind stress variability from the 13-30 of March 2001.

The meridional wind stress is related to the zonal pressure gradient and as a result dominant timescales of variability in the zonal pressure gradients should be consistent with those of meridional wind stress. A measure of the zonal SLP gradient in the case study region is presented in the form of a SLPI derived from 23 years of ERA-40 SLP data spanning from 1979 to 2001. CWA has been performed on the SLPI timeseries in order to examine the dominant timescales of variability identified in the meridional wind stress timeseries (Figure 4.5). A first look at the GWS provides an indication of the dominant timescales of variability in the timeseries. The GWS in Figure 4.5, with a zoom for the higher frequencies in Figure 4.6, provides similar results to those of the meridional wind stress GWS (Figures 4.1 and 4.2). Once again only high frequency variability associated with the synoptic cycle of 2-8 days and annual cycle may be considered as showing statistically significant signals throughout entire timeseries.

Zooming in on the 2000-2001 summer segment of the local wavelet power spectrum (Figure 4.6), the peak in the local wavelet spectrum which falls within the 8-16 day band is considered to significantly contribute to wind stress variability from January - March 2001. This peak reaches a maximum period of 16 days towards the end of March 2001.

From the CWA of these two timeseries, we can infer that variability in the upwelling favourable meridional wind stress was occurring at a time scale longer than the period of the dominant synoptic cycle towards the end of March 2001. A significant peak in variability with a period of 12-14 days in both wavelet power spectra indicates upwelling favourable wind stress was oscillating at a lower frequency than usual which resulted in the prolonged quiescent phase in upwelling activity observed at the end of March 2001. Synoptic SLP maps discussed in the following section reveal that this prolonged period of weak across-shore pressure gradients and light variable winds can be attributed to persistent west coast trough conditions. The development of a west coast trough is associated with periods of active tropical continental convection over Namibia, together with an upper air westerly wave trough to the south-west of the continent (Preston-Whyte and Tyson,

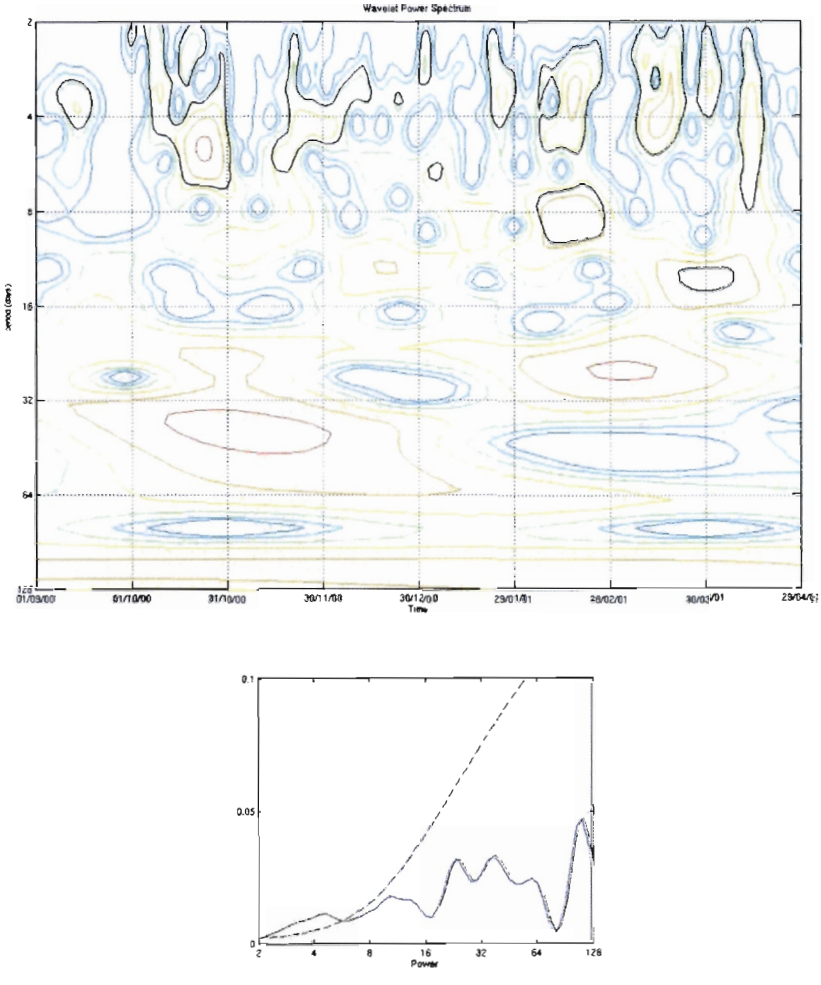

Figure 4.4: (Top) Zooming in on the summer of September 2000 - April 2001 section of the local wavelet power spectrum from Figure 4.1 with black contours enclosing regions of greater than 95% confidence for a red-noise process with a lag-1 coefficient of 0.6562. (Bottom) The time-averaged wavelet power spectrum over local wavelet power spectra from September 2000 - April 2001 (solid line) with the 95% confidence level (dashed line).

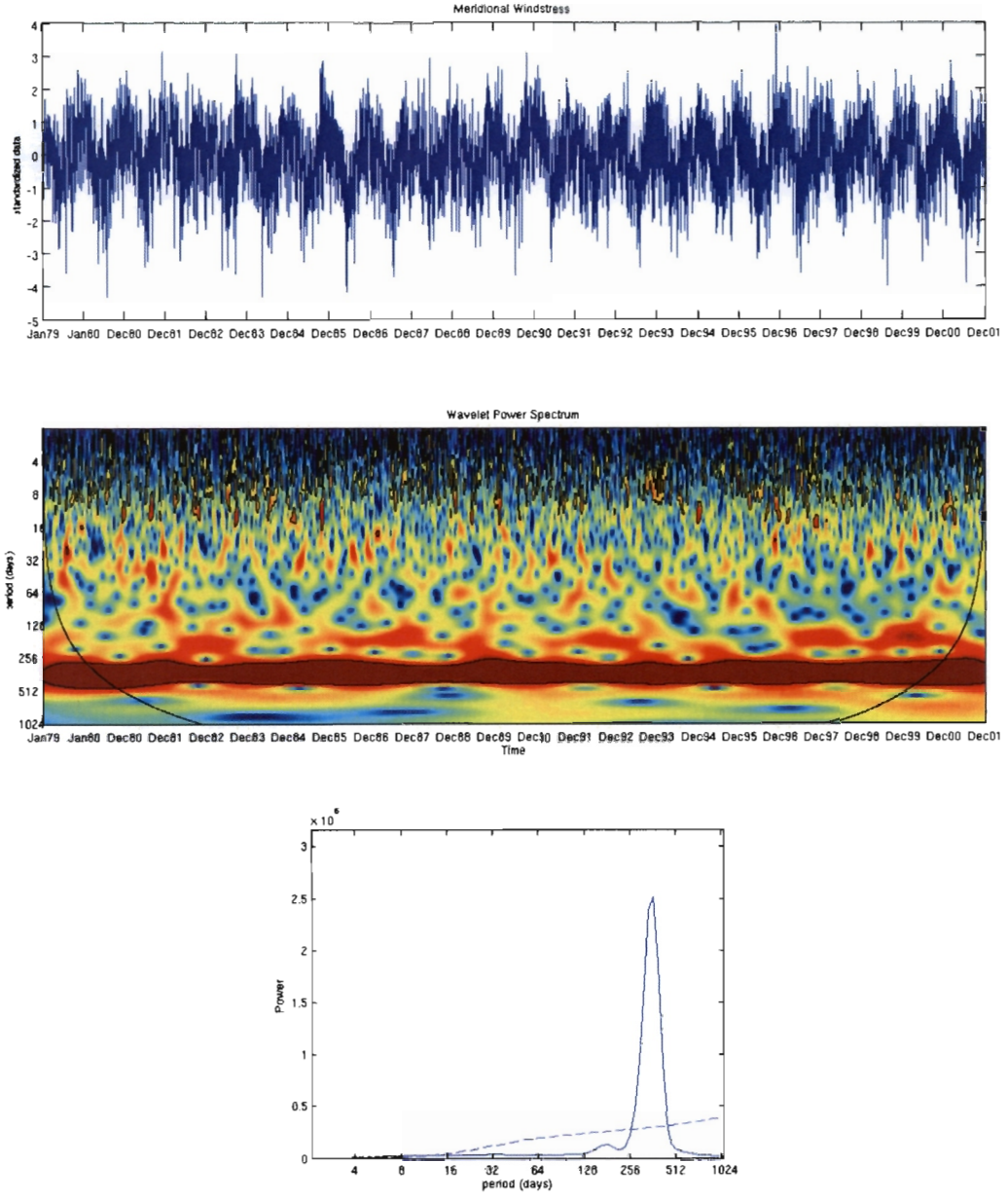

Figure 4.5: (Top) The standardised SLPI timeseries from January 1979 - December 2001. (Middle) The local wavelet power spectrum with black contours indicating the cone of influence and enclosing regions of greater than 95% confidence for a red-noise process with a lag-1 coefficient of 0.8141. (Bottom) The global wavelet power spectrum (solid line) with the 95% confidence level for the global wavelet spectrum assuming a lag-1 coefficient of 0.8141 (dashed line).

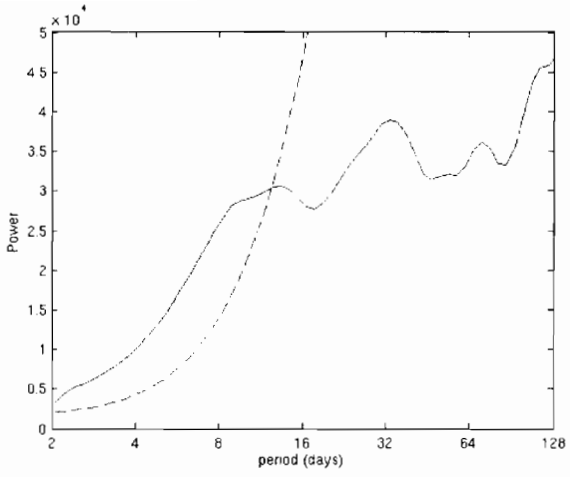

Figure 4.6: Zooming in on the 4-128 day periods, the global wavelet power spectrum for the SLPI timeseries from January 1979 - December 2001 (solid line) with the 95% confidence level for the global wavelet spectrum assuming a lag-1 coefficient of 0.8141 (dashed line).

1988). This results in a surface low pressure trough over the west coast linking tropical continental and mid-latitude marine low pressure systems and displacing the South Atlantic High pressure system westwards. NCEP re-analysis 850 and 500 hPa geopotential height anomaly plots for March 2001 indicate, cyclonic anomalies south-west of the continent (favourable for mid-latitude westerly waves) and a stronger and southward shifted Angola heat low - favourable conditions for the development a west coast trough.

4.2 Synoptic Conditions and Local Observation: 12-30 March 2001

The 13-30 March 2001 period during which hydrographic and biological observations of a bloom were undertaken by MCM, was chosen as the case study for this research project. This event was chosen because of the clear sequence in which the initial days of active upwelling forced by predominant equatorward winds are followed by a prolonged quiescent phase.

The event can roughly be divided in two with the 13-22 March dominated by strong across-shore pressure gradients and their associated along-shore wind, while from the 23rd the

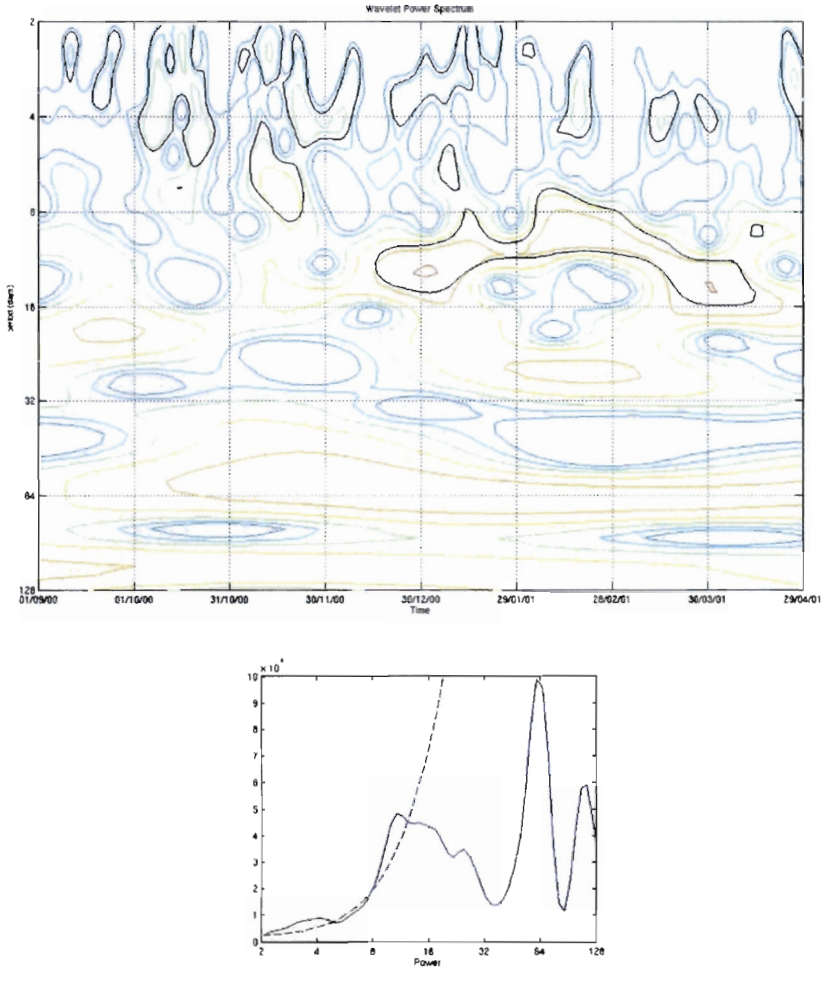

Figure 4.7: (Top) Zooming in on the summer of September 2000 - April 2001 section of the local wavelet power spectrum from Figure 4.5 with black contours enclosing regions of greater than 95% confidence for a red-noise process with a lag-1 coefficient of 0.8141. (Bottom) The time-averaged wavelet power spectrum over local wavelet power spectra from September 2000 - April 2001 (solid line) with the 95% confidence level (dashed line).

synoptic pressure gradients weakened significantly with prevailing light variable winds. A ridging high pressure to the south of South Africa was responsible for strong along-shore south easterly winds on the 13th, 16th, 17th , 18th, 20th and 21st of March (Figures 4.8 and 4.9). Weak across-shore gradients typify the days following the 23rd (Figures 4.10 and 4.11). The NOGAPS SLP data shown in Figures 4.8 and 4.10 was used in forcing the regional simulations conducted. These pressure fields compare well with corresponding NCEP re-analysis SLP fields illustrated in Figures 4.9 and 4.11 as well as the daily SAWS synoptic chart (appendix A).

Figure 4.12 shows the close relationship between across-shore pressure gradient and along-shore wind speed. The SLPI created from ERA-40 SLP data represents the difference in pressure between offshore values at 32.5°S 15°E and those inshore at 32.5°S 17.5°E. Weaker pressure gradients from the 23rd to the 27th are accompanied by light variable winds at MCM's Columbine weather station.

Timeseries of local weather station wind data over the event reveal strong diurnal oscillations. Wind speed and direction at the SAWS's Lambert's bay weather station are typified by a strong diurnal cycle in both wind speed and direction for the duration of the event (Figure 4.13). This is in agreement with Jury (1985b) who observed diurnal wind pulsing over the region due to thermally driven wind oscillations. The timeseries of wind speed and direction at MCM's Columbine weather station shows a diurnal oscillation in wind speed for the duration of the event, but only in wind direction during periods of weak synoptic forcing (Figure 4.12). Due to strong synoptic forcing, the wind direction at Cape Columbine during ridging high conditions is seen to remain fairly constant, while the wind speed is influenced by seabreeze effects which are superimposed upon the equatorward flow. The seabreeze adds momentum to the synoptically driven along-shore wind, peaking during the late afternoon when thermal contrasts reach a maximum and the seabreeze has rotated to the along-shore direction due to Coriolis effects.

Comparing wind speeds at Lambert's Bay weather station to those at Columbine weather station indicates that along-shore wind speeds tend on average to be higher at the latter station, particularly during anti-cyclonic conditions when the across-shore pressure gradient is fairly strong (Figures 4.14 and 4.15). Figure 4.14 illustrates the average diurnal oscillation in wind speed at Columbine and Lambert's Bay weather station. These oscillations reach a minimum around 0700 GMT (0900 SAST) and a maximum around 1600 GMT (1800 SAST). which is consistent with the findings of Jury (1985b). The across-shore component of the flow is on average greater at Lambert Bay's and reaches a maximum ve-

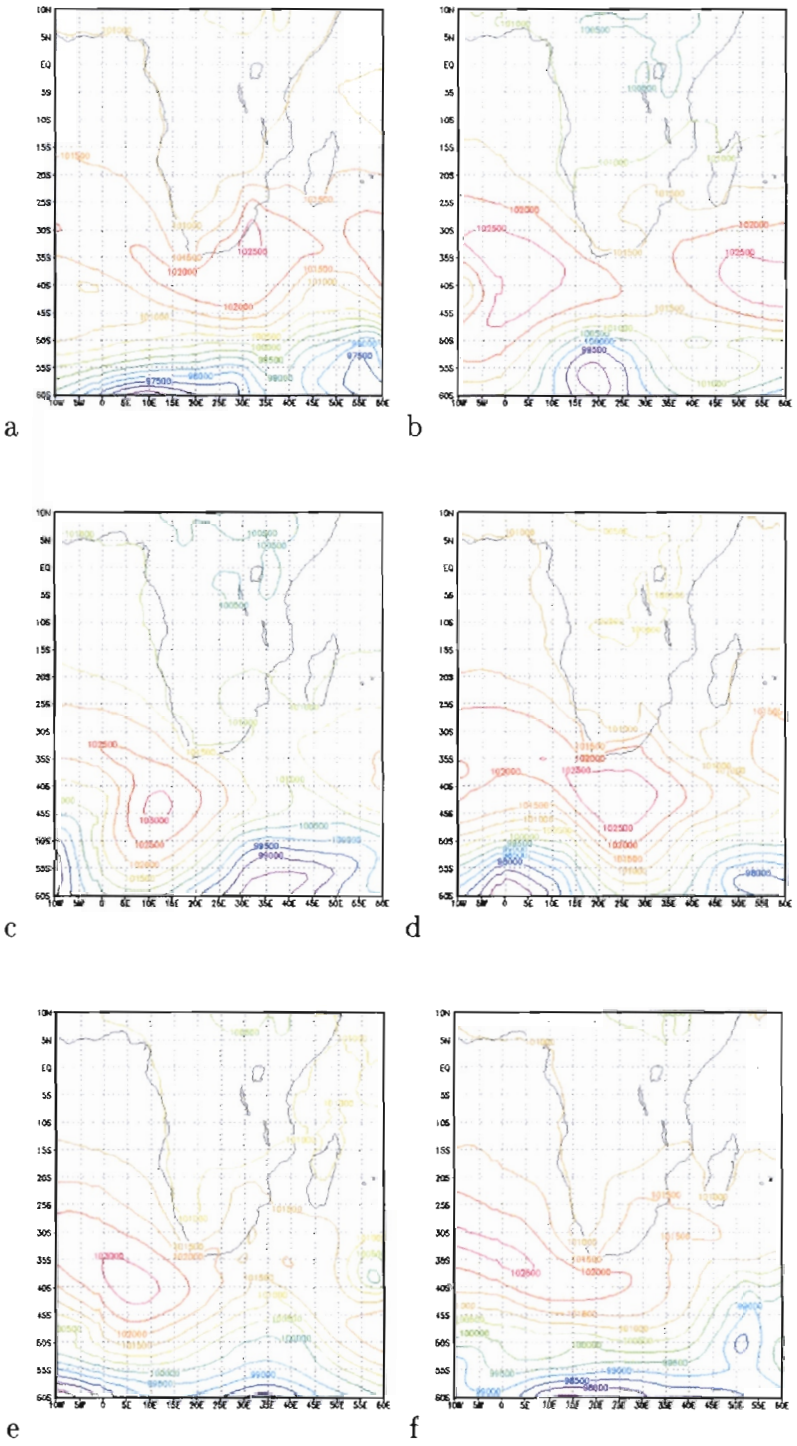

Figure 4.8: NOGAPS 1200 GMT SLP (Pa) on south easterly wind days (a) 13 March (b) 16 March (c) 17 March (d) 18 March (e) 20 March (f) 21 March.

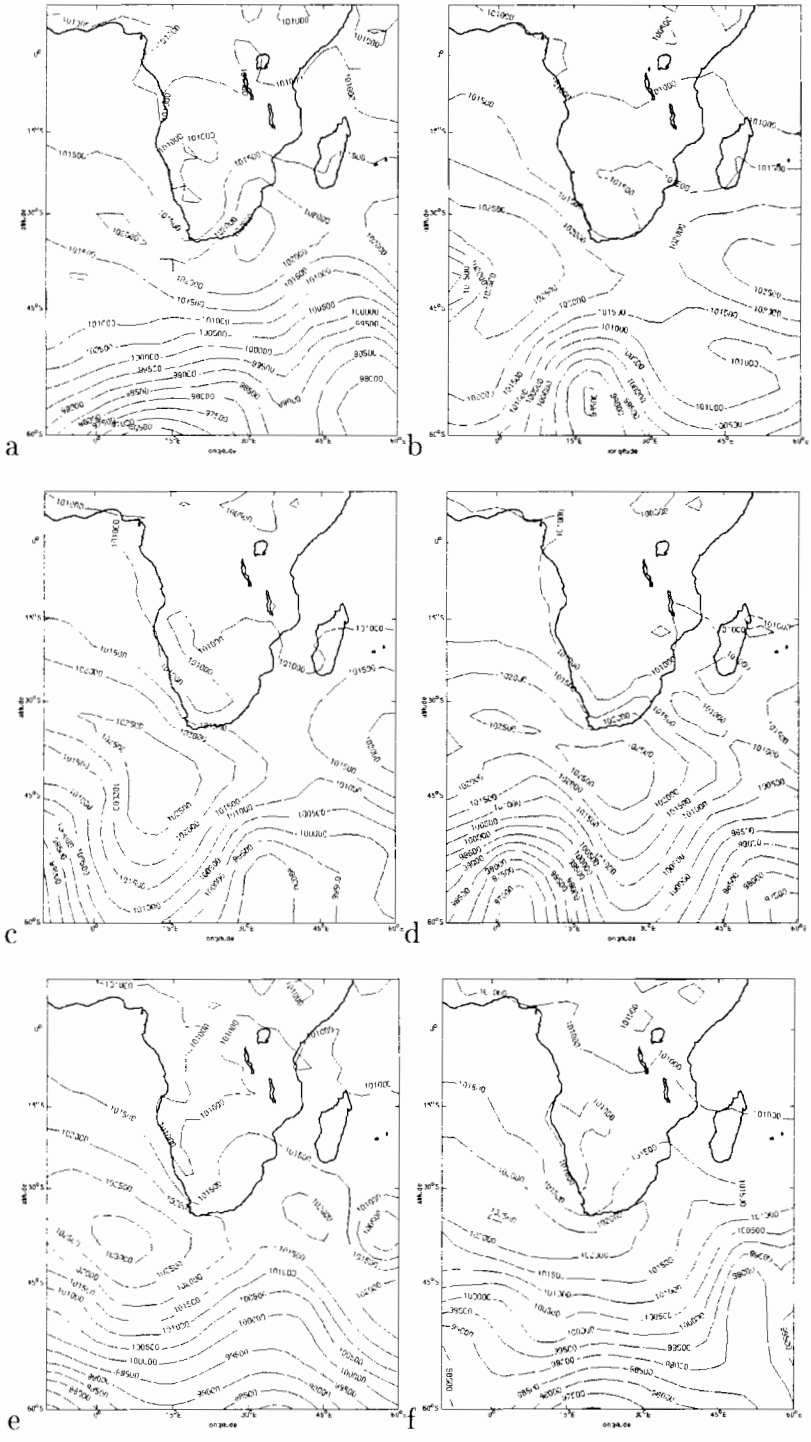

Figure 4.9: NCEP 1200 GMT SLP (Pa) on south easterly wind days (a) 13 March (b) 16 March (c) 17 March (d) 18 March (e) 20 March (f) 21 March.

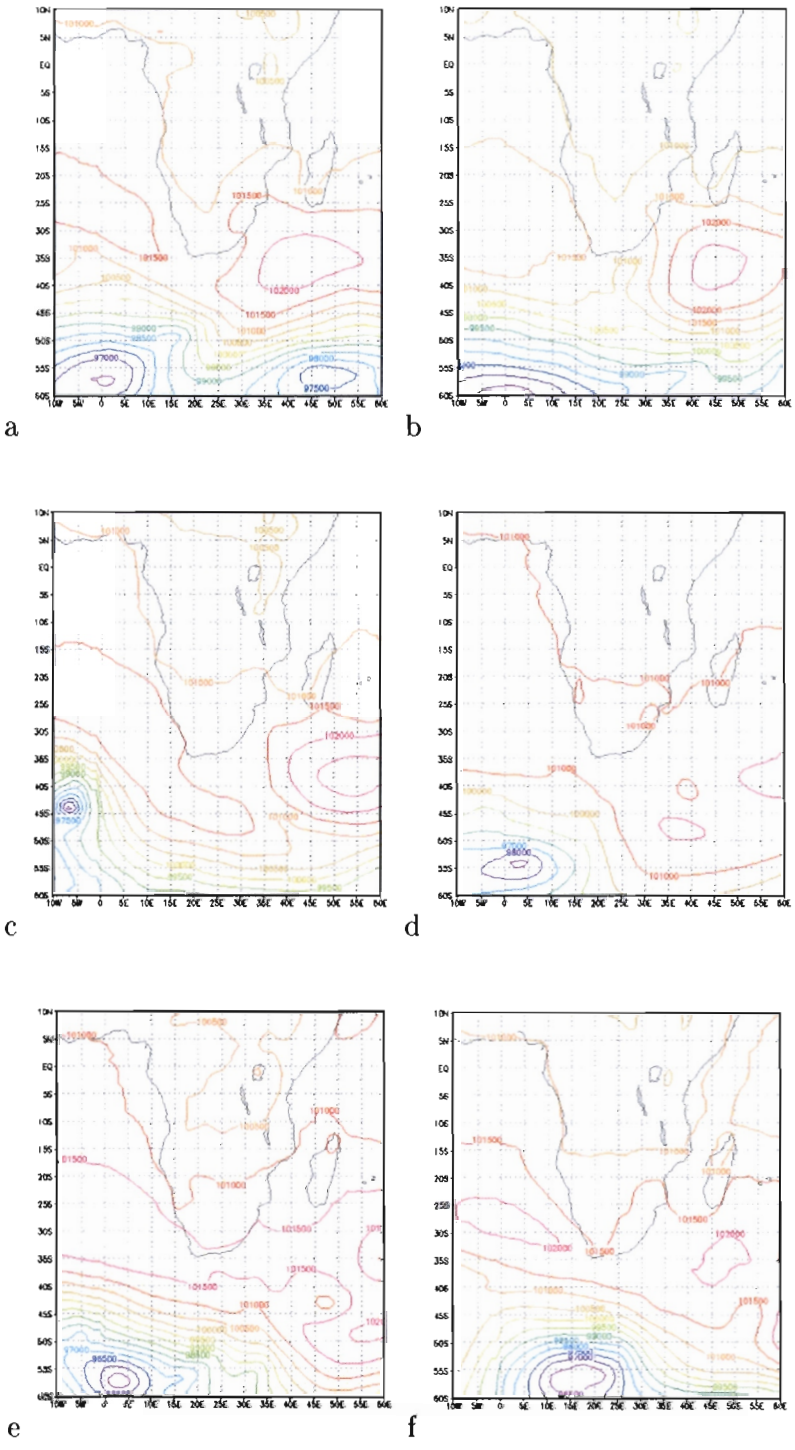

Figure 4.10: NOGAPS 1200 GMT SLP (Pa) on weak across-shore pressure gradient days (a) 23 March (b) 24 March (c) 25 March (d) 26 March (e) 27 March (f) 28 March.

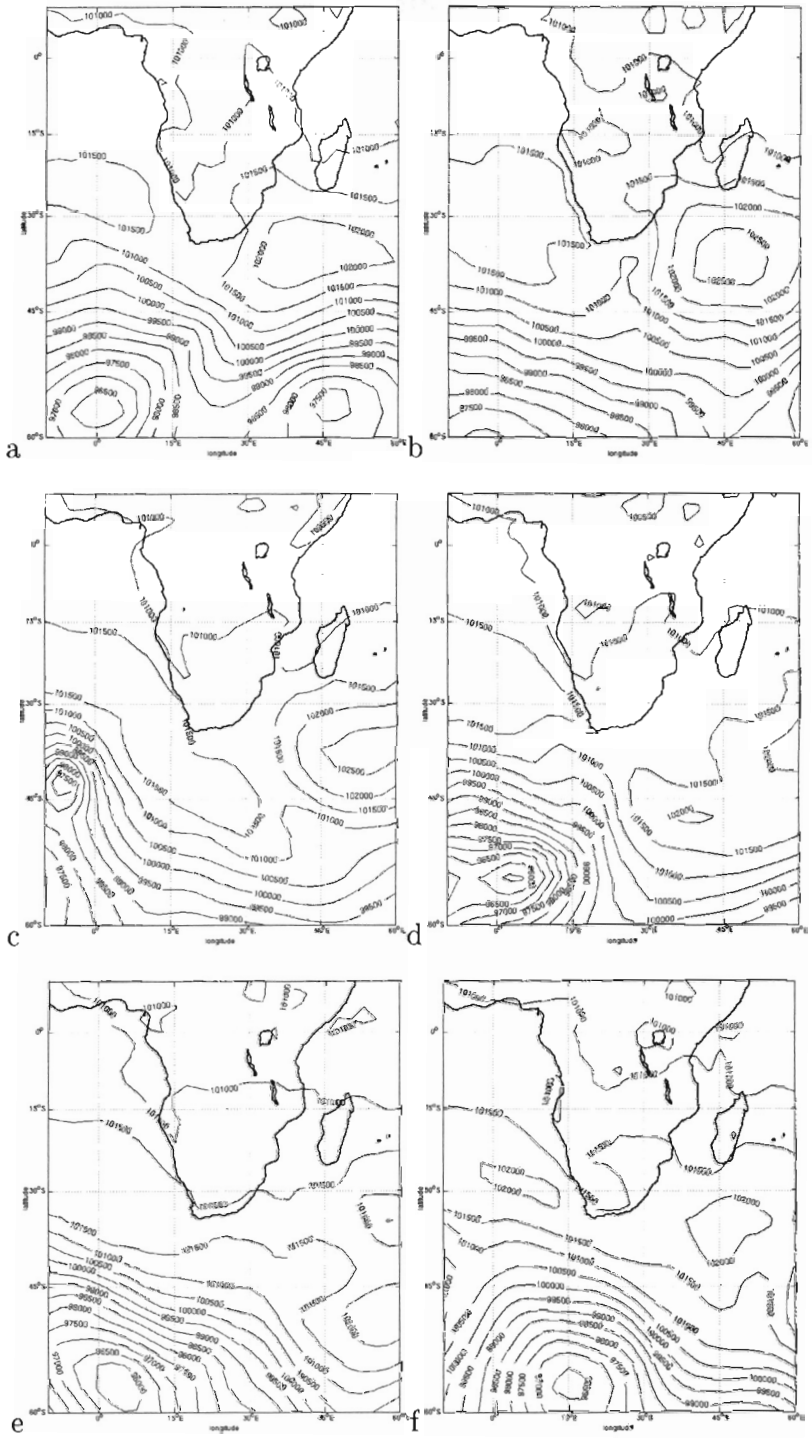

Figure 4.11: NCEP 1200 GMT SLP (Pa) on weak across-shore pressure gradient days (a) 23 March (b) 24 March (c) 25 March (d) 26 March (e) 27 March (f) 28 March.

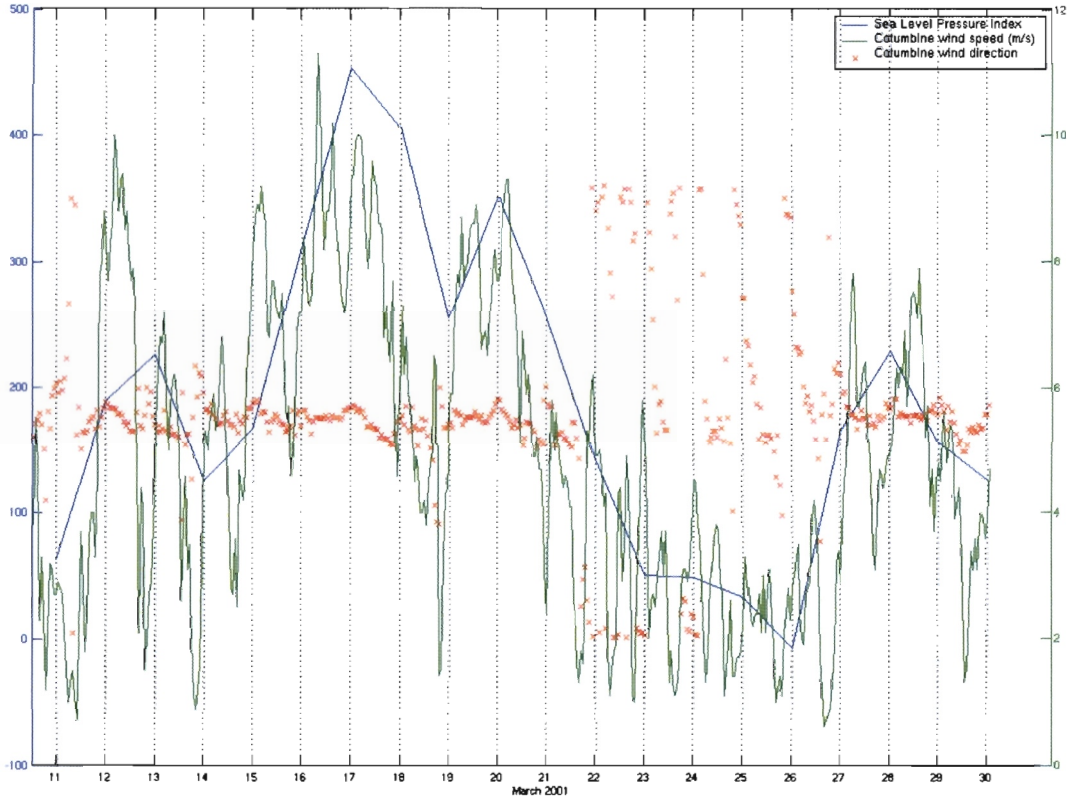

Figure 4.12: The SLPI (in Pa on the left hand y-axis) plotted together with Columbine weather station wind speed (in ms^{-1} on the right hand y-axis) and direction (in degrees from True North on the left hand y-axis) from the 11-30 March 2001.

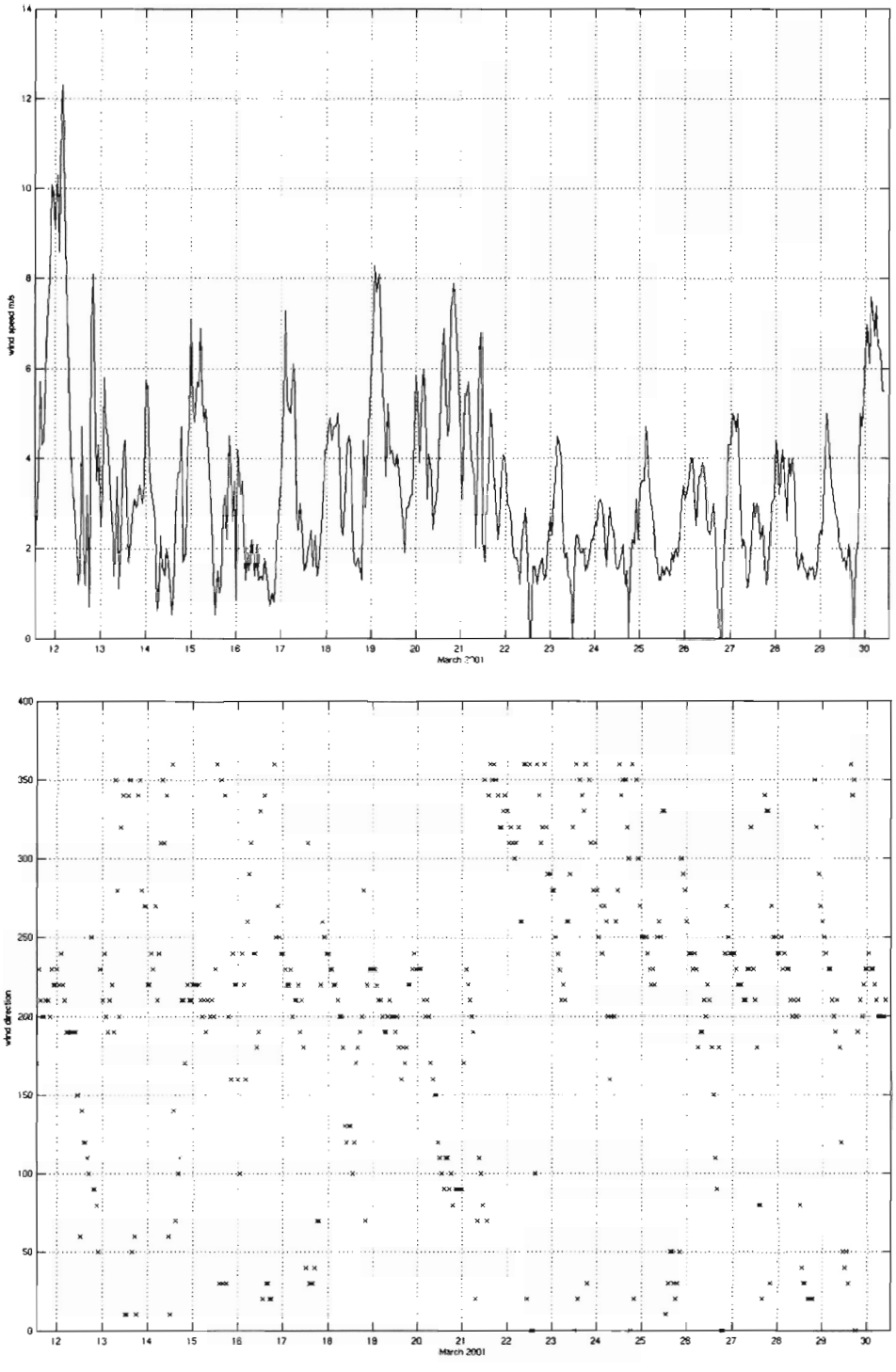

Figure 4.13: (Top) Lambert's Bay weather station wind speed in m s^{-1}. (Bottom) Lambert's Bay weather station wind direction in degrees from True North.

locity around 1400 GMT (1600 SAST) during both strong and weak across-shore pressure gradient conditions. (Figures 4.15 and 4.16).

4.3 Summary

In March 2001, variability in upwelling favourable meridional wind stress occurred at a time scale longer than the dominant period of the synoptic cycle as the result of a prolonged period of weak across-shore pressure gradients and light variable winds associated with persistent west coast trough conditions. NOGAPS SLP fields used as initial and boundary forcing in the regional atmospheric model compare well with corresponding NCEP re-analysis SLP fields and daily SAWS synoptic chart.

Timeseries of local weather station wind data over the event reveal strong diurnal oscillations in wind speed. Spatial variability in the magnitude of along-shore and across-shore wind speed is apparent from weather station data. On average wind speeds during the event were greater at Columbine weather station than Lambert's Bay weather station. Wind direction appears to be influenced more by the seabreeze at Lambert's Bay than at Cape Columbine, resulting in the average across-shore wind component being greater at Lambert's Bay weather station.

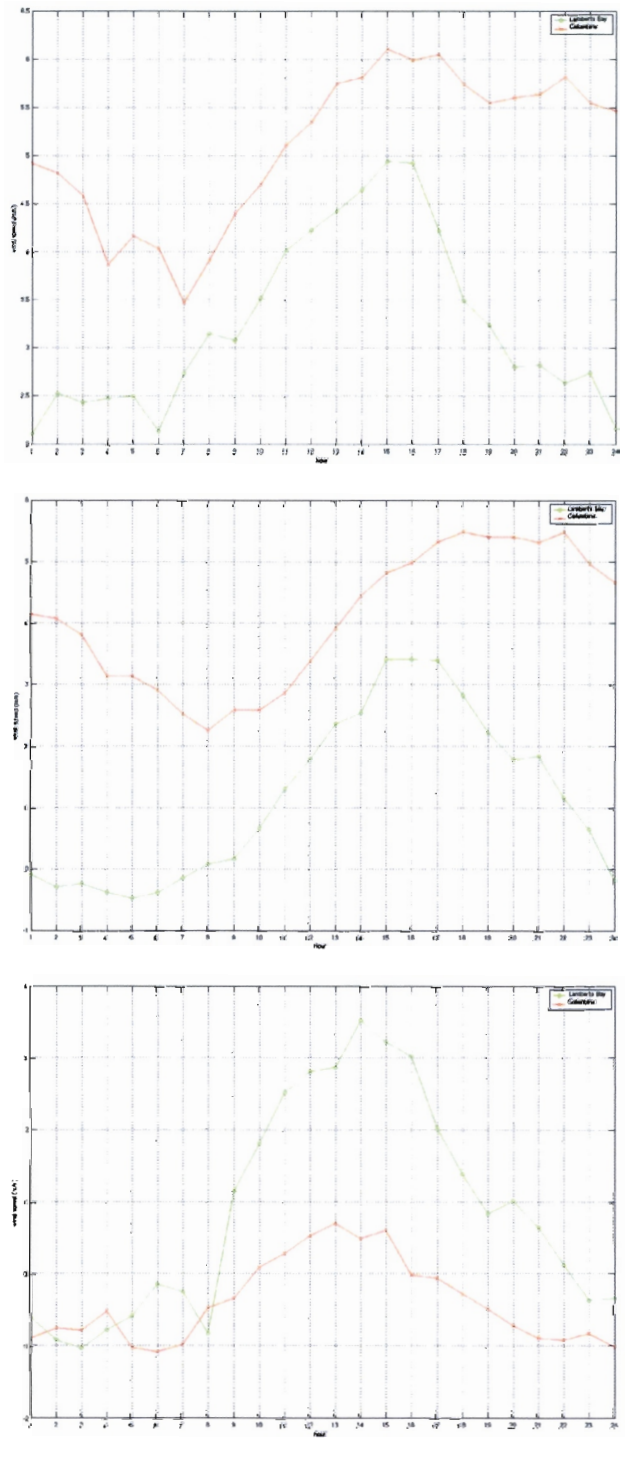

Figure 4.14: (Top) Mean 12-30 March 2001 hourly (GMT) wind speed at Lambert's Bay and Columbine weather stations. (Middle) Mean 12-30 March 2001 hourly meridional wind speed at Lambert's Bay and Columbine weather stations. (Bottom) Mean 12-30 March 2001 hourly zonal wind speed at Lambert's Bay and Columbine weather stations.

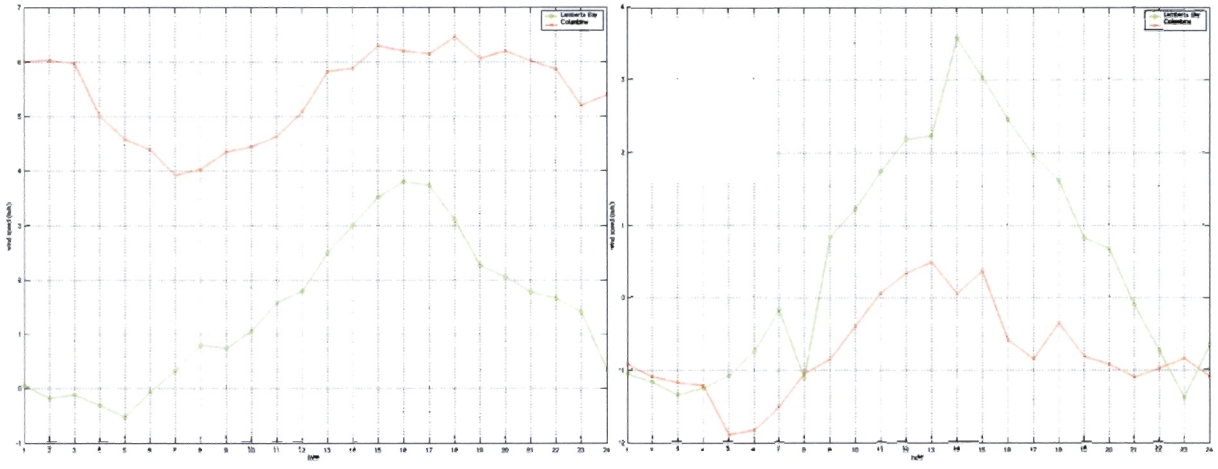

Figure 4.15: Wind observations during strong across-shore pressure gradients (Left) Mean 15-22 March 2001 hourly (GMT) meridional wind speed at Lambert's Bay and Columbine weather stations. (Right) Mean 15-22 March 2001 hourly zonal wind speed at Lambert's Bay and Columbine weather stations.

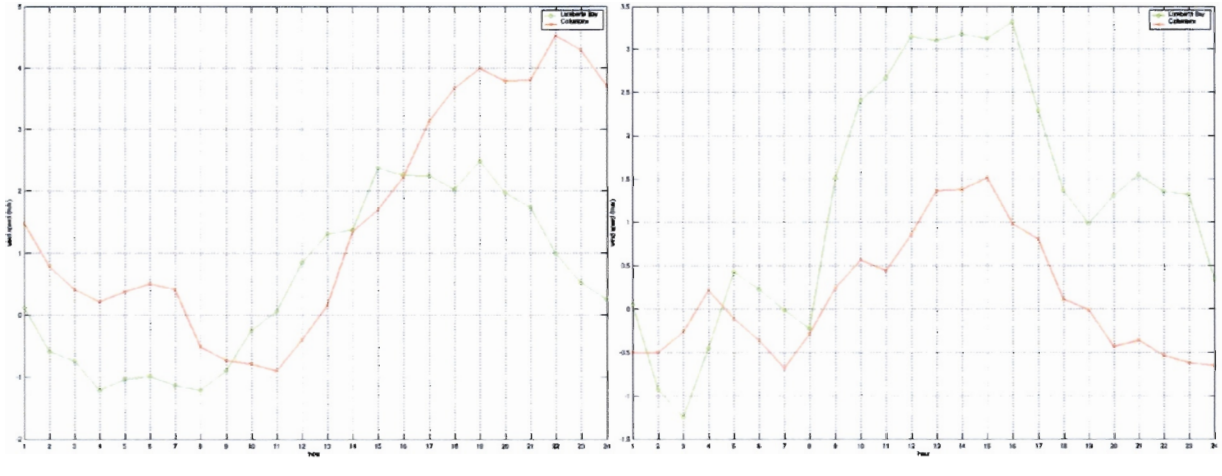

Figure 4.16: Wind observations during weak across-shore pressure gradients (Left) Mean 23-28 March 2001 hourly (GMT) meridional wind speed at Lambert's Bay and Columbine weather stations. (Right) Mean 23-28 March 2001 hourly zonal wind speed at Lambert's Bay and Columbine weather station.

Chapter 5

Model Validation

Although MM5 has been used in numerous applications and is a well accepted modeling tool, simulations for 12-30 March 2001 are validated against available observations in order to assess the ability of the model to adequately represent the atmosphere over the west coast.

A South African Weather Service (SAWS) weather station at Lambert's Bay and a MCM weather station at Cape Columbine have been used for model validation. Using linear interpolation, model data have been horizontally interpolated from the model grid to the corresponding location of each weather station. The model values will generally be smoother due to differences in sampling. Weather station measurements are taken at a specific location, while model results represent a grid averaged value.

For the first model run, four hourly model outputs have been compared with corresponding weather station measurements. Figures 5.1 and 5.2 show how the model output compares with SLP, wind speed and wind direction observations at Lambert's Bay. Model pressure and wind speeds correlate well with station measurements at Lambert's Bay, with correlation coefficients of 0.82 and 0.6 respectively. These correlations are significant at the 95% confidence level. The significance of all the correlation coefficients given below has been tested taking into account the presence of auto-correlation in the data by estimating the effective degrees of freedom (Yuan and Martinson, 2000). Model and station wind directions are less comparable, this is attributed to the location of the weather station at 94m above sea level and approximately 5km inland. While the weather station is exposed to maritime wind conditions, trees in the area and other local frictional effects on boundary layer wind direction are not resolved by the model.

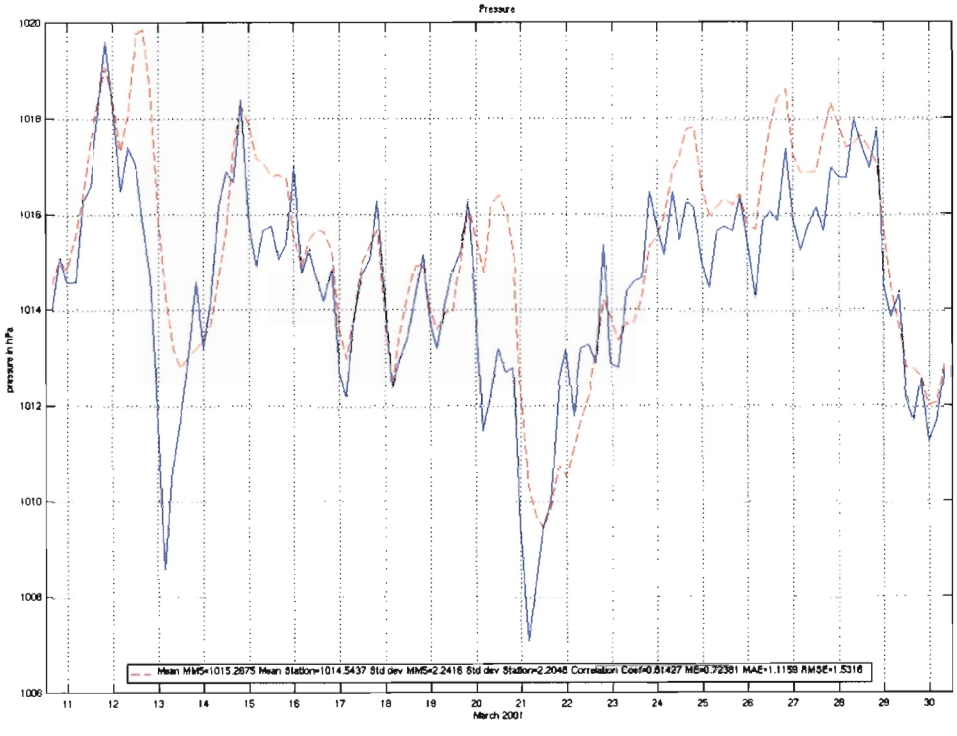

Figure 5.1: Lambert's Bay weather station (solid blue line) vs model run 1 (dashed red line) pressure (hPa).

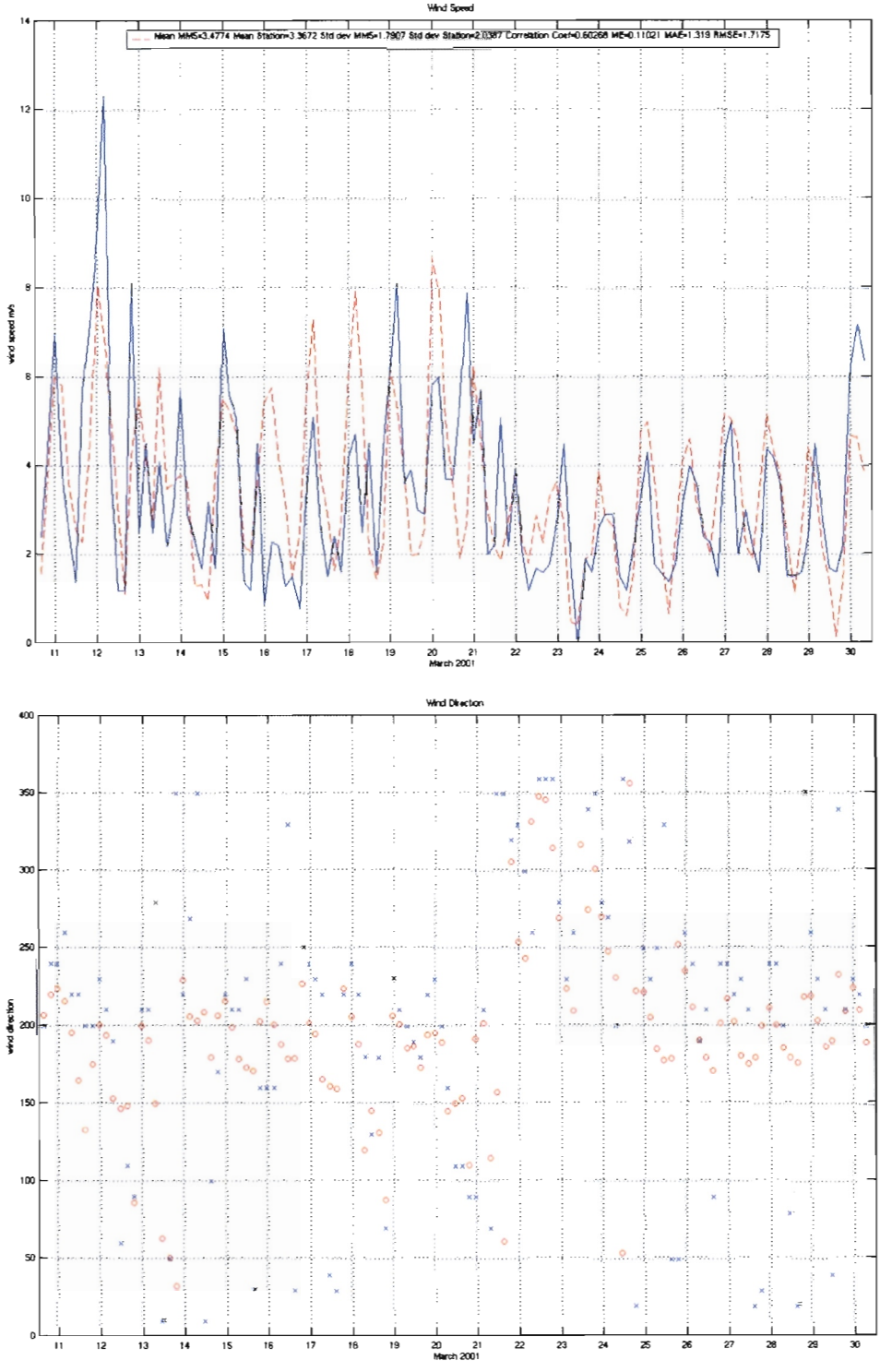

Figure 5.2: (Top) Lambert's Bay weather station (solid blue line) vs model run 1 (dashed red line) wind speed (m s^{-1}). (Bottom) Lambert's Bay weather station (blue cross) vs model run 1 (red circle) wind direction (degrees from True North).

Comparison between model and station wind speed and direction at Cape Columbine show better agreement between model and station wind direction (Figure 5.3). Situated near the coastline, the Cape Columbine anemometer is directly exposed to maritime wind conditions. Wind speeds correlate well with a correlation coefficient of 0.78 (significant at 95%), yet the model values tend to be slightly greater. This difference may be attributed to the fact that the hourly wind data provided for Columbine are averaged values of measurements taken over the preceding hour, whereas the model and Lambert's Bay wind values represent the values at a particular hour. Wind speed statistics in Figures 5.2 and 5.3 reveal that the bias between the simulated and observed wind speeds is smaller than the standard deviation of both simulated and observed wind speed timeseries.

Owing to the absence of weather buoys in the region, evaluation of model performance over the ocean could only be done using QuikSCAT surface wind estimates. Scatterometer measurements represent a 25km footprint, while the model resolution in the region of comparison is 3km. Although there are these sampling differences, simulated and satellite derived wind speeds and direction agree fairly well. Two offshore pixels at 32.125°S 17.625°E and 32.625°S 17.8750°E were used. Only days where the swath path coincided with these pixels and measurements were of an acceptable quality were used for comparison with the corresponding simulated winds. Model results were linearly interpolated in space to the location of the QuikSCAT pixel, and in time, to the time when the QuikSCAT measurements were taken. Figures 5.4 and 5.5 show how the wind speeds and directions at 32.125°S 17.625°E and 32.625°S 17.8750°E compare with correlation coefficients of 0.88 and 0.82 (significant at 95%) between the model and QuikSCAT data.

For the second model run which used higher resolution SST, the hourly outputs have been compared with corresponding weather station measurements. As with the comparisons made for the first model run, Figures 5.6 and 5.7 show how the pressure, wind speed and wind direction correlate at Lambert's Bay weather station. Figure 5.8 illustrates the agreement between simulated and measured wind speeds and directions at Cape Columbine. The correlation between observed wind speed and simulated wind speed at Columbine improved for the second model run with a correlation coefficient of 0.8 (significant at 95%) and very slightly improved at Lambert's Bay with a correlation coefficient of 0.61 (significant at 95%).

The 9km nest results for the second model run have been used for comparison with individual morning or evening QuikSCAT passes. After linear interpolation from the model grid and hourly output times to the time and location of the measurements made dur-

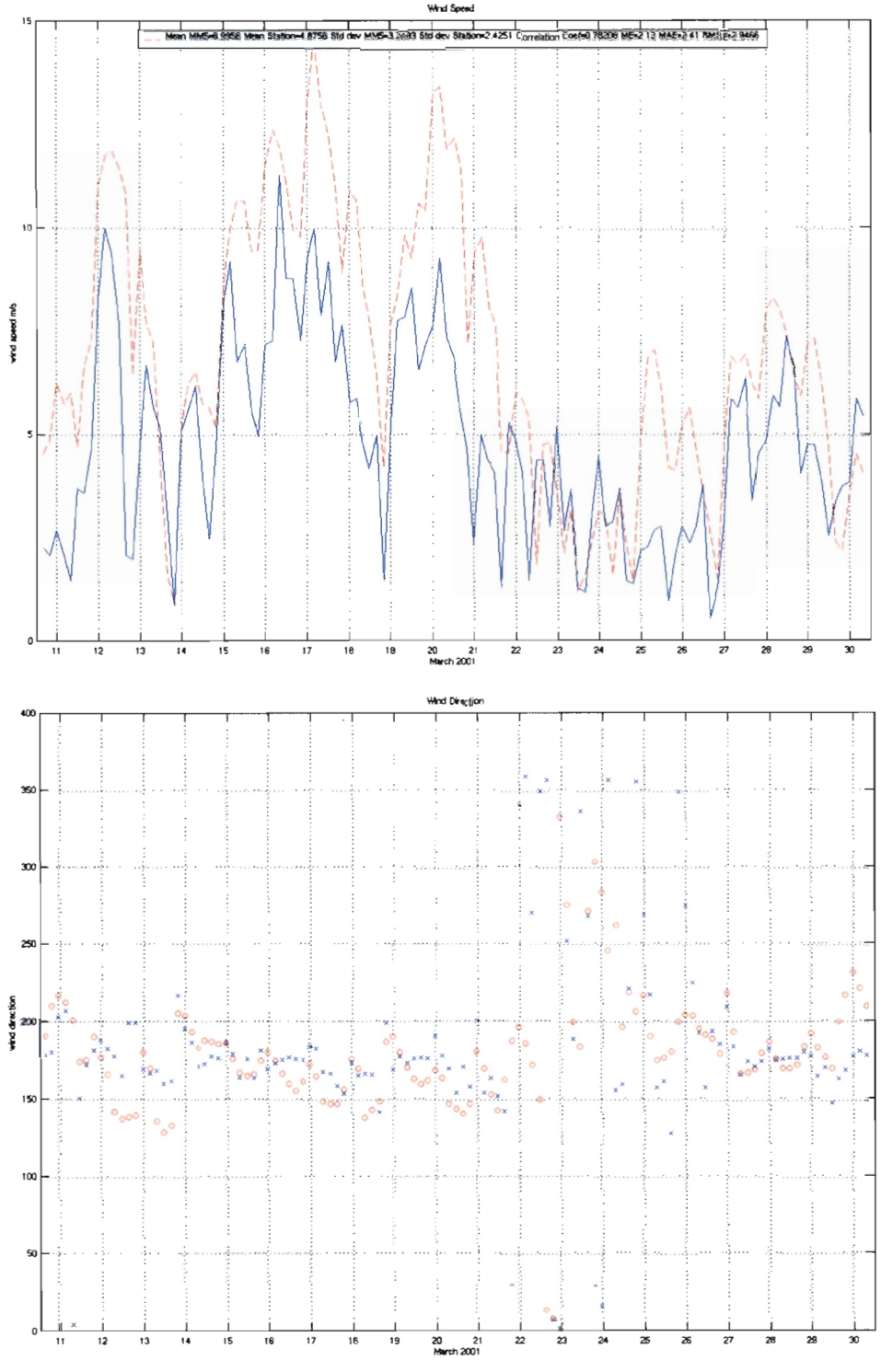

Figure 5.3: (Top) Columbine weather station (solid blue line) vs model run 1 (dashed red line) wind speed (m s^{-1}). (Bottom) Columbine weather station (blue cross) vs model run 1 (red circle) wind direction (degrees from True North).

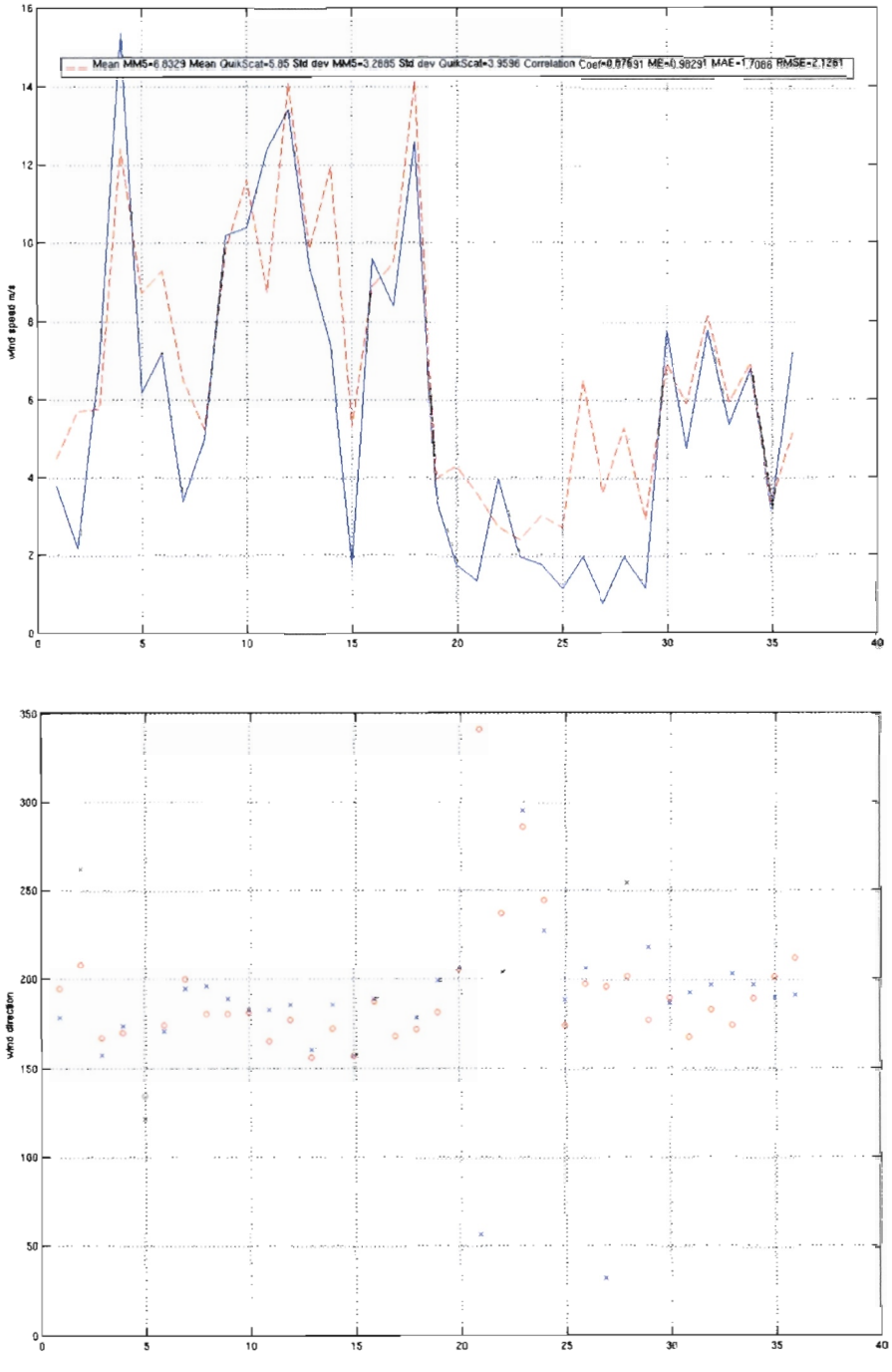

Figure 5.4: (Top) QuikSCAT pixel 32.125°S 17.625°E (solid blue line) vs model run 1 (dashed red line) wind speed (m s^{-1}). (Bottom) QuikSCAT pixel 32.125°S 17.625°E (blue cross) vs model run 1 (red circle) wind direction (degrees from True North). The number of QuikSCAT measurements available between 11-30 March 2001 for use in the comparison is shown on the x-axis.

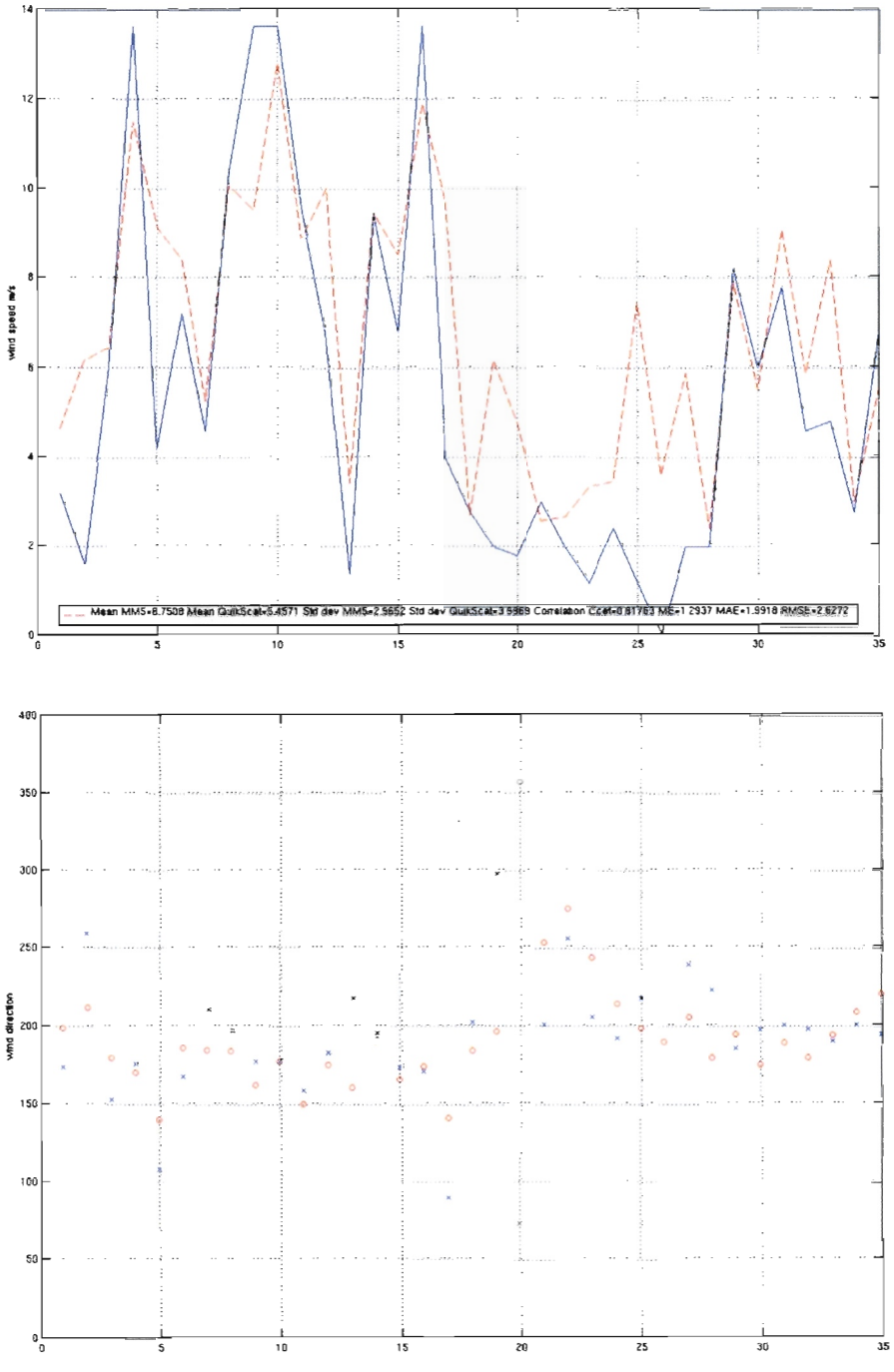

Figure 5.5: (Top) QuikSCAT pixel 32.625°S 17.8750°E (solid blue line) vs model run 1 (dashed red line) wind speed (m s^{-1}). (Bottom) QuikSCAT pixel 32.625°S 17.8750°E (blue cross) vs model run 1 (red circle) wind direction (degrees from True North). The number of QuikSCAT measurements available between 11-30 March 2001 for use in the comparison is shown on the x-axis.

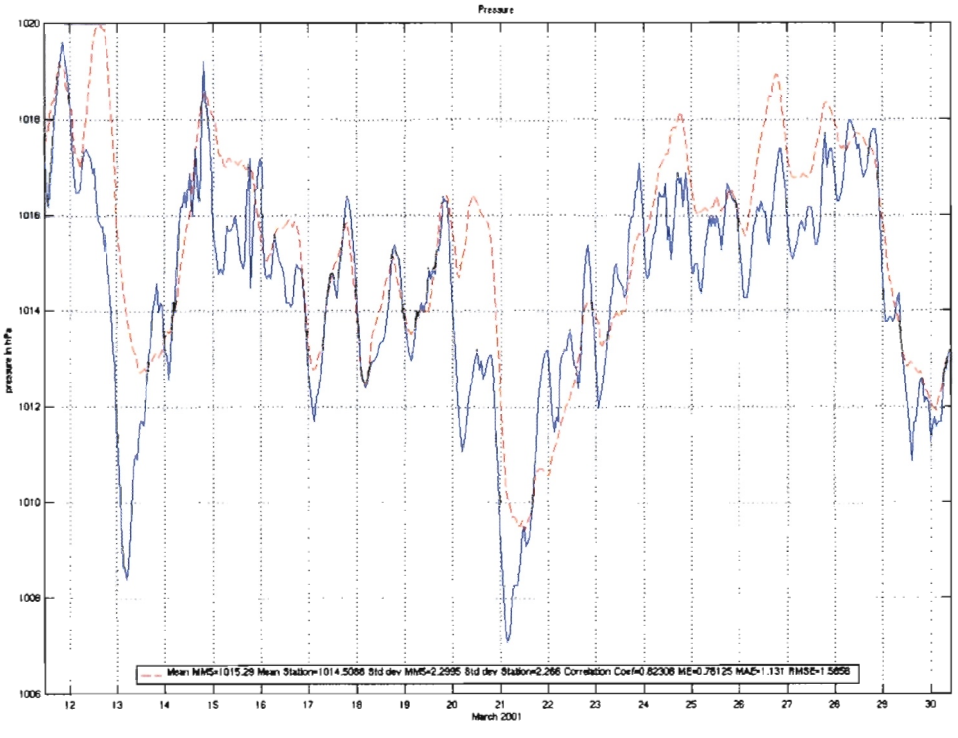

Figure 5.6: Lambert's Bay weather station (solid blue line) vs model run 2 (dashed red line) pressure (hPa).

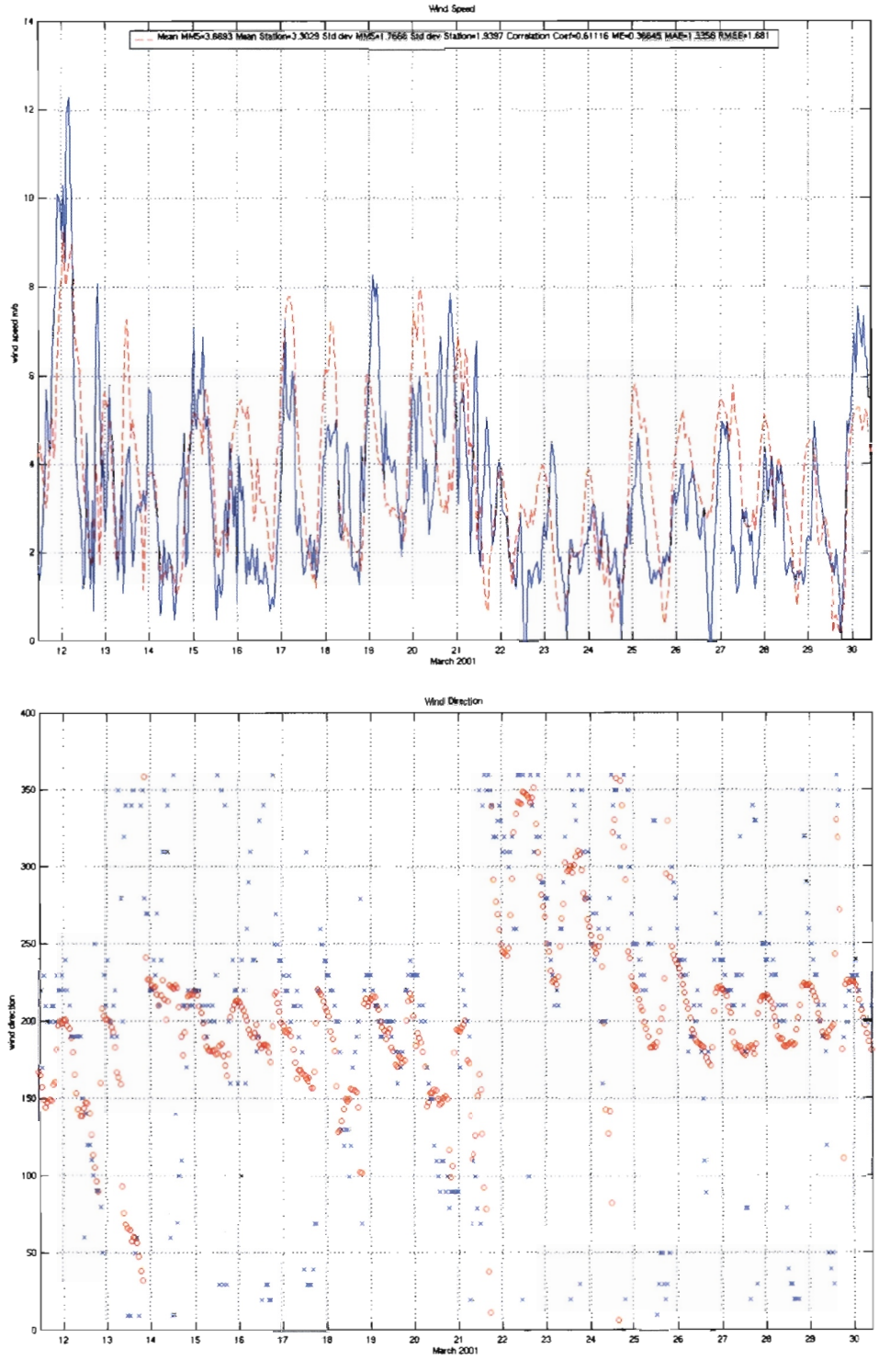

Figure 5.7: (Top) Lambert's Bay weather station (solid blue line) vs model run 2 (dashed red line) wind speed (m s^{-1}). (Bottom) Lambert's Bay weather station (blue cross) vs model run 2 (red circle) wind direction (degrees from True North).

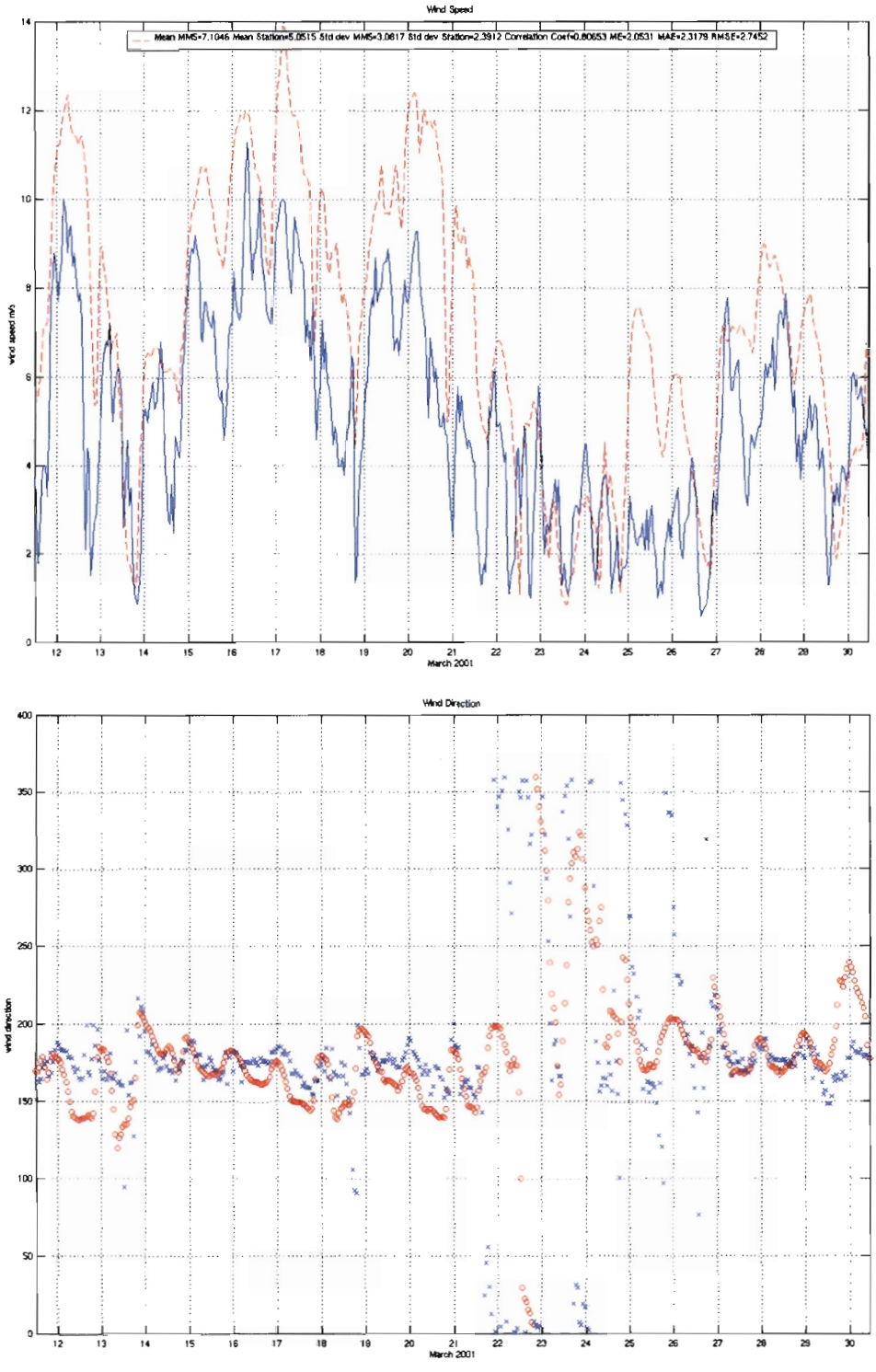

Figure 5.8: (Top) Columbine weather station (solid blue line) vs model run 2 (dashed red line) wind speed (m s^{-1}). (Bottom) Columbine weather station (blue cross) vs model run 2 (red circle) wind direction (degrees from True North).

ing each QuikSCAT pass (Figure 5.9), the model fields compare reasonably well with the QuikSCAT winds during different days of the event.

Daily radiosonde observations collected from Cape Town International Airport (33.96°S 18.6°E) have been used for comparison with simulated temperature and dew point temperature after linear interpolation from the model grid and hourly output times to the time and location of the radiosondes (Figure 5.10). While there is a good comparison between temperature values, the model struggles to accurately represent dew point temperature.

Conditions along the west coast of South Africa during summer are generally quite stable due to the presence of a strong inversion layer associated with the dominant anti-cyclonic conditions. Comparison with radiosonde data reveals that the model reproduced the variation of temperature with height and the inversion layer fairly well. The model has reproduced the main fluctuations in wind speed and pressure that occurred over the event in the region of interest. High correlation coefficients show a good quantitative agreement between observations and simulated low-level wind speed and sea level pressure. Over the ocean, comparison with QuikSCAT wind indicated that the model low-level wind fields compare reasonably well with observed QuikSCAT wind fields.

In summary, the model appears to have adequately represented the atmosphere over the west coast of South Africa between 12-30 March 2001. These results provide confidence in using the model output during the HAB period to assess the likely impacts of the low-level winds on the coastal ocean.

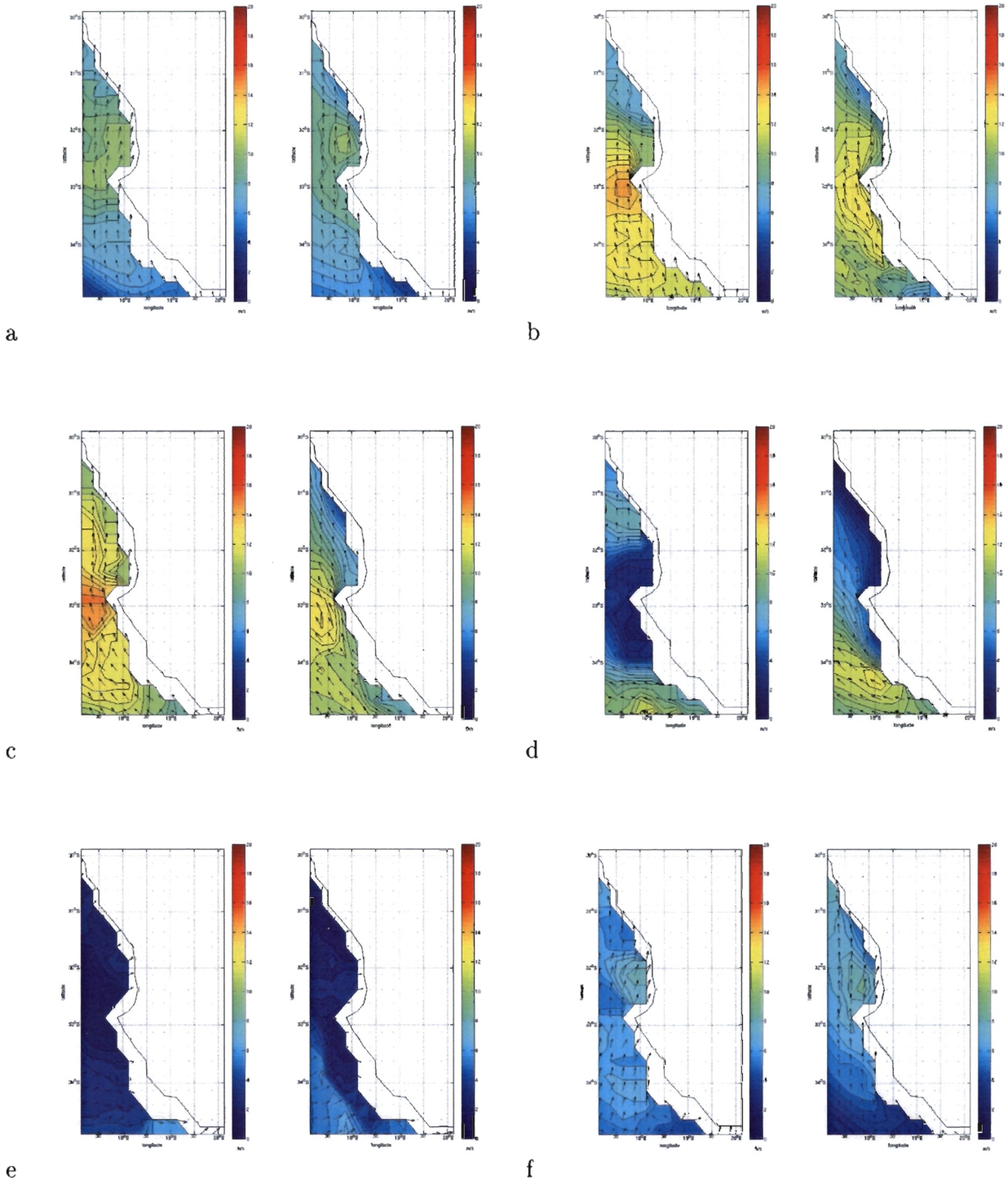

Figure 5.9: QuikSCAT pass (left) vs model run 2 (right) for March 2001. (a) 15th evening pass (b) 16th evening pass (c) 17th morning pass (d) 22nd morning pass (e) 24th evening pass (f) 28th morning pass

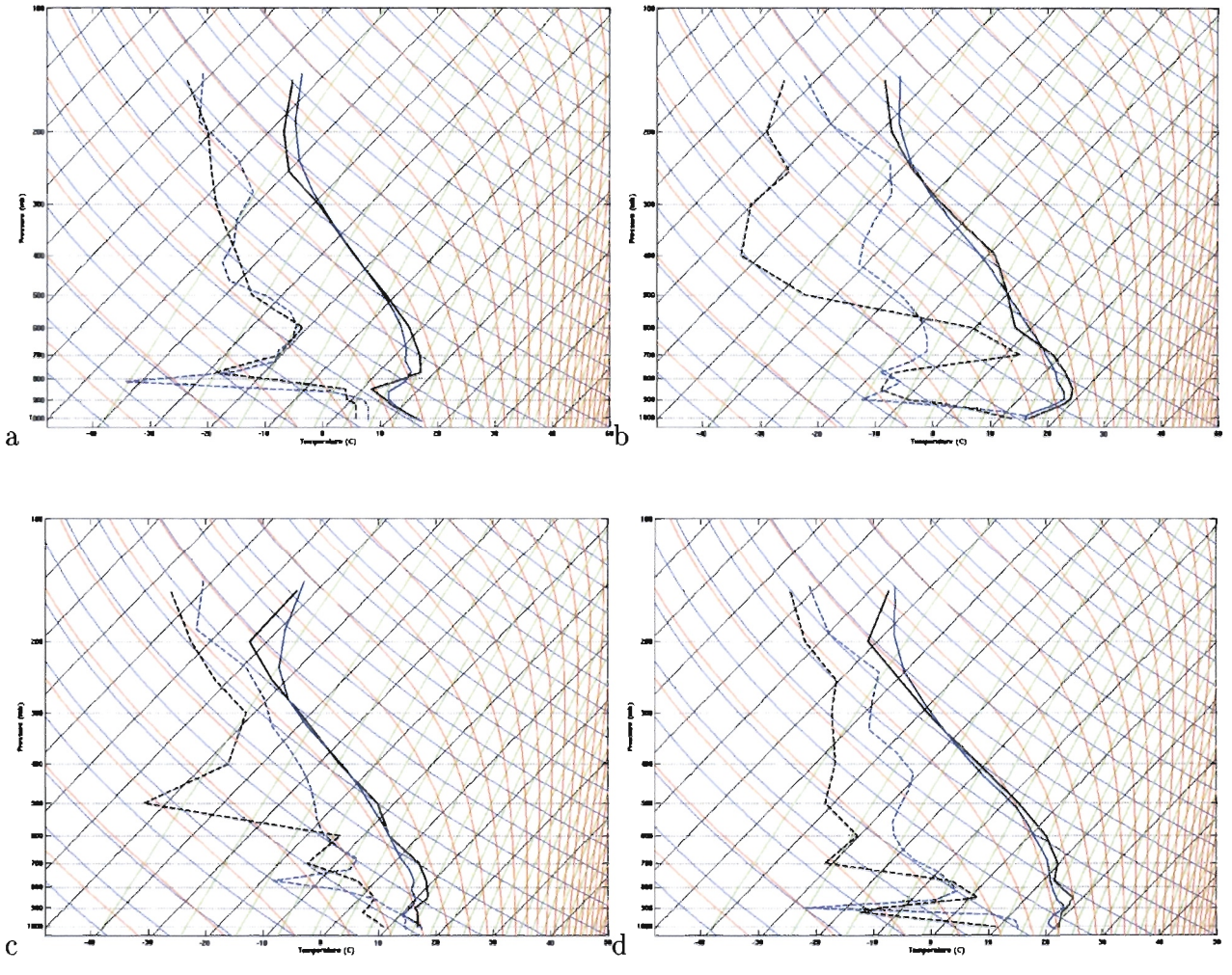

Figure 5.10: SAWS Cape Town radiosonde observations, temperature (black solid line) and dew point temperature (black dashed line) vs model run 2, temperature (blue solid line) and dew point temperature (blue dashed line). (a) 1042 (GMT) - 1242 (SAST) 12 March 2001 (b) 2313 (GMT) - 0113 (SAST) 14/15 March 2001 (c) 2312 (GMT) - 0112 (SAST) 19/20 March 2001 (d) 1123 (GMT) - 1235 (SAST) 29 March 2001.

Chapter 6

Analysis of Simulated Low-Level Coastal Winds

In this chapter, the spatial structure of the low-level wind fields simulated by the regional model over the 12-30 March 2001 case study period will be examined and compared to previous studies of the structure of the southern Benguela's low-level wind field. Initially studies dealing with a general description of the synoptic scale regional wind field are discussed to provide a background. These studies deal with climatologies and therefore cannot be directly compared with the mean regional wind field over the 12-30 March period which is the product of the synoptic flow of only a few days. As mentioned by Jury (1985a), coastal winds in the southern Benguela are forced on scales of 100km to 1000km by synoptic pressure gradients and on smaller scales of 10-100km by irregularities in topography and thermal contrasts. Smaller-scale forcing by topography and local thermal contrasts on the equatorward flow regime which dominates during the summer half of the year, results in regions of enhancement and sheltering in the low-level wind field. The ability of the model to reproduce these mesoscale effects of topography and local thermal contrasts on the low-level wind field will be assessed in this chapter.

6.1 Variations in the Low-Level Wind Field Over the Southern Benguela

Relatively coarse resolution, regional assessments of the general spatial structure of low-level winds over the southern Benguela have been conducted by Kamstra (1985), Risien (2002) and Hardman-Mountford et al. (2003). Based on 24000 ship records spanning fifty years, Kamstra (1985) described general features in the wind field over the southern Benguela. For the purpose of his analysis, Kamstra (1985) grouped ships records, which he obtained from the South African Data Centre for Oceanography (SADCO) and the SAWS, into half degree squares. Due to frictional retardation imposed by the land, the mean annual wind speed decreased from a maximum, 200-300km offshore, towards the coast. In the coastal regions, Kamstra found the strongest wind speeds were to the south of Cape Point and at the northern extent of his study area (28°S). The weakest annual average wind speeds of 3m s^{-1} were found at Elands Bay. This wind speed minimum for the St Helena Bay - Elands Bay region was attributed to a wake effect induced by the pronounced Cape Columbine headland, based on the finding of Jury (1985a) and Taunton-Clark (1985). Kamstra's (1985) data did not however resolve the presence of a near shore wind jet to the west of Cape Columbine suggested by aircraft measurements (Jury et al., 1990a,b).

Risien (2002) created a 16 month composite of QuikSCAT wind stress data for the Benguela upwelling system from August 1999 - November 2000. Risien (2002) compared this composite with a long-term wind speed climatology derived from NCEP/NCAR reanalysis data. Risien found that although the 1999-2000 period was characterised by a pronounced La Nina event the two fields were quite similar. Risien's (2002) composite showed a wind stress maximum between 25°S and 28°S situated approximately 200-250km offshore. Similar to Kamstra, Risien found an offshore annual wind stress maxima in the southern Benguela which increased in magnitude northwards towards 28°S, although the wind stress increased more rapidly with offshore extent than identified by Kamstra. Unlike Kamstra, Risien did not find a wind speed maximum south of the 34°S, nor the Elands Bay minimum. However, one would not expect the wind speed minimum in the lee of Cape Columbine to be resolved by QuikSCAT data due to the unavailability of inshore measurements. Unfortunately QuikSCAT data does not provide reliable wind measurements near the coast and therefore poorly resolves inshore conditions in wind stress and local enhancement due to the capes and other topography.

Hardman-Mountford et al. (2003) assessed the mean spatial structure of the winds using monthly maps based on 17 years of ECMWF 10 meter winds. Using latitude-time plots, they identified peaks in summer wind stress over the southern Benguela within 50km of the coast at Namaqualand/Hondeklip Bay and Cape Columbine/Cape Peninsula, which corresponded with the major upwelling cells identified from SST.

6.2 Simulated Low-Level Wind Field: 12-30 March 2001

In this section, a qualitative comparison between the model field and the aircraft wind data collected in the summers of 1978 and 1980 by Jury (1984; 1985a; 1985b; 1980) is provided, although a direct comparison is not possible due to the different summers, the prevailing southerly flow in both cases should lead to qualitatively similar features generated by the topography. Figure 6.1 shows the 12-30 March 2001 mean 10 meter winds, simulated by model runs 1 and 2, for the 9km resolution nest. Along-shore and across-shore components of the 12-30 March 2001 mean winds have been calculated according to the average 340°-160° (Jury, 1980) alignment of the coastline for the 9km nest (Figures 6.2 and 6.3). Variations in 10 meter winds due to changes in the orientation of the coastline, topographical features such as the Cape Peninsula and Cape Columbine as well as the thermal nature of the coastal interior are evident in Figures 6.1, 6.2 and 6.3.

In Figure 6.1, spatial variations in the 10 meter simulated wind field depict some of the general features identified in the regional assessments mentioned above. Similar to Kamstra (1985), wind speeds are on average weaker in the lee of Cape Columbine. Consistent with Hardman-Mountford et al. (2003), peaks in near-shore wind speeds are seen at Namaqualand/Hondeklip Bay (30°S), Cape Columbine (33°S) and Cape Peninsula (34°S). These features in the spatial structure of the coastal low-level wind field can be attributed to changes in the orientation of the coastline and topographical features such as the Cape Peninsula and Cape Columbine.

Jury (1984; 1985a; 1985b; 1980) assessed spatial variability in the low-level summer wind over the southern Benguela region by conducting several mesoscale aircraft surveys over the Cape Peninsula and Cape Columbine. Perturbations in the low-level summer wind field due to topography were identified by Jury with the local enhancement of wind speed seen near the Capes due to the compression of stream lines during equatorward flow. The increase in low-level wind speed due to the interaction of the synoptic flow with both the

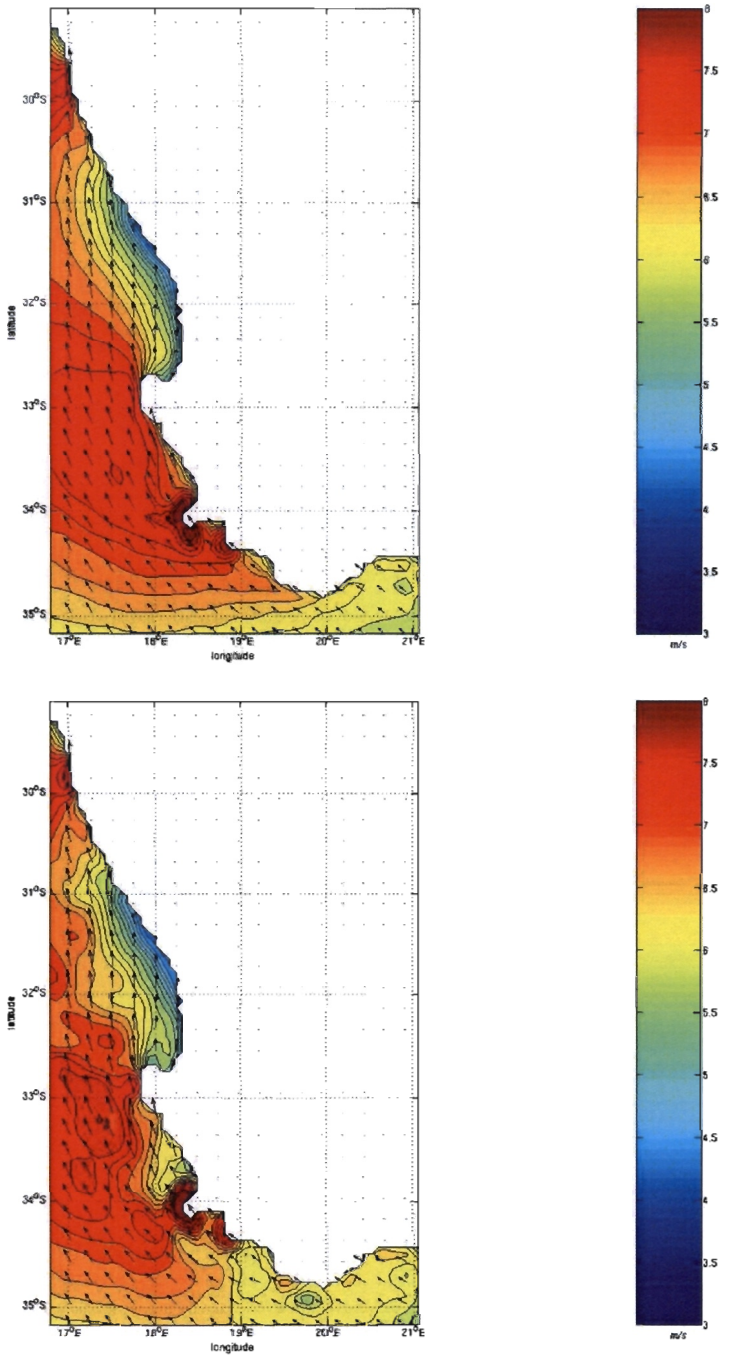

Figure 6.1: Mean 12-30 March 2001 winds for 9km resolution nest. (Top) Model run 1. (Bottom) Model run 2.

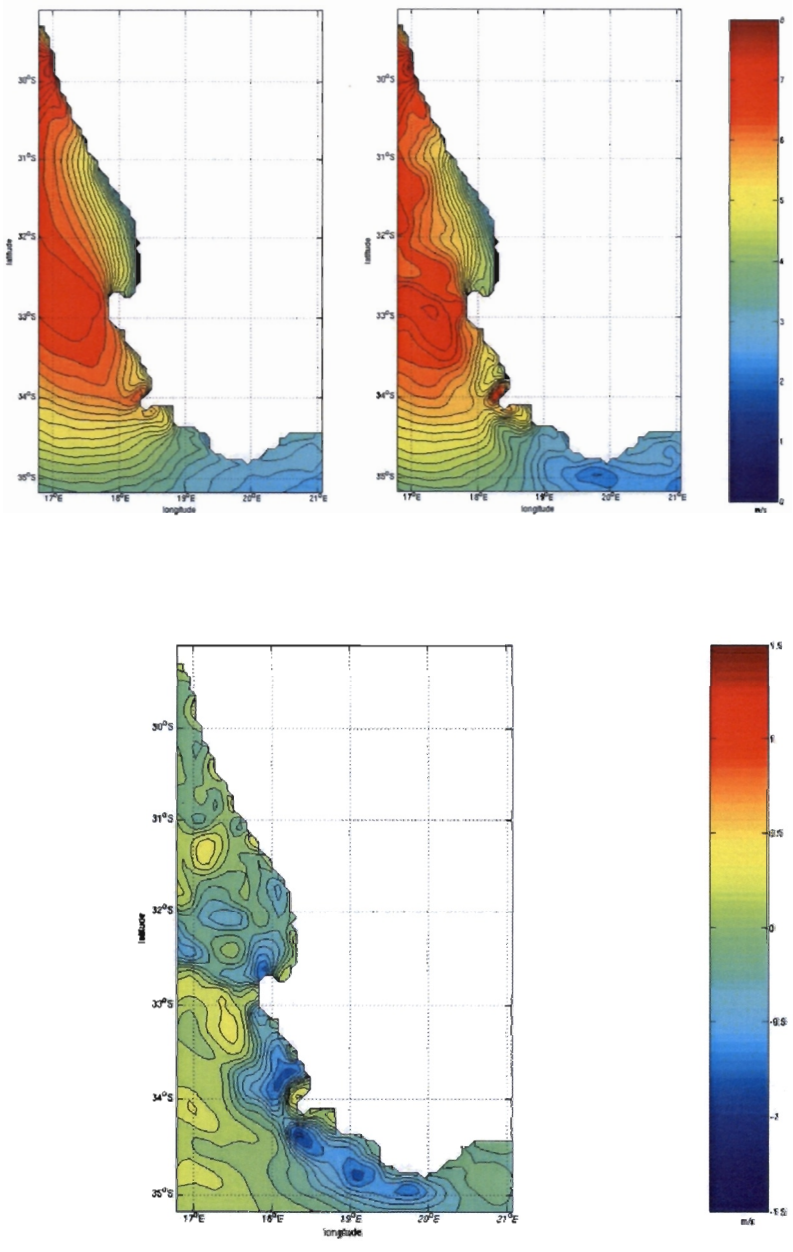

Figure 6.2: Mean 12-30 March 2001 along-shore winds (rotated to the average 340°-160°alignment of coastal topography) for 9km resolution nest. (Top left) Model run 1. (Top right) Model run 2. (Bottom) Difference in mean along-shore winds between runs one and two (model run 2 minus model run 1).

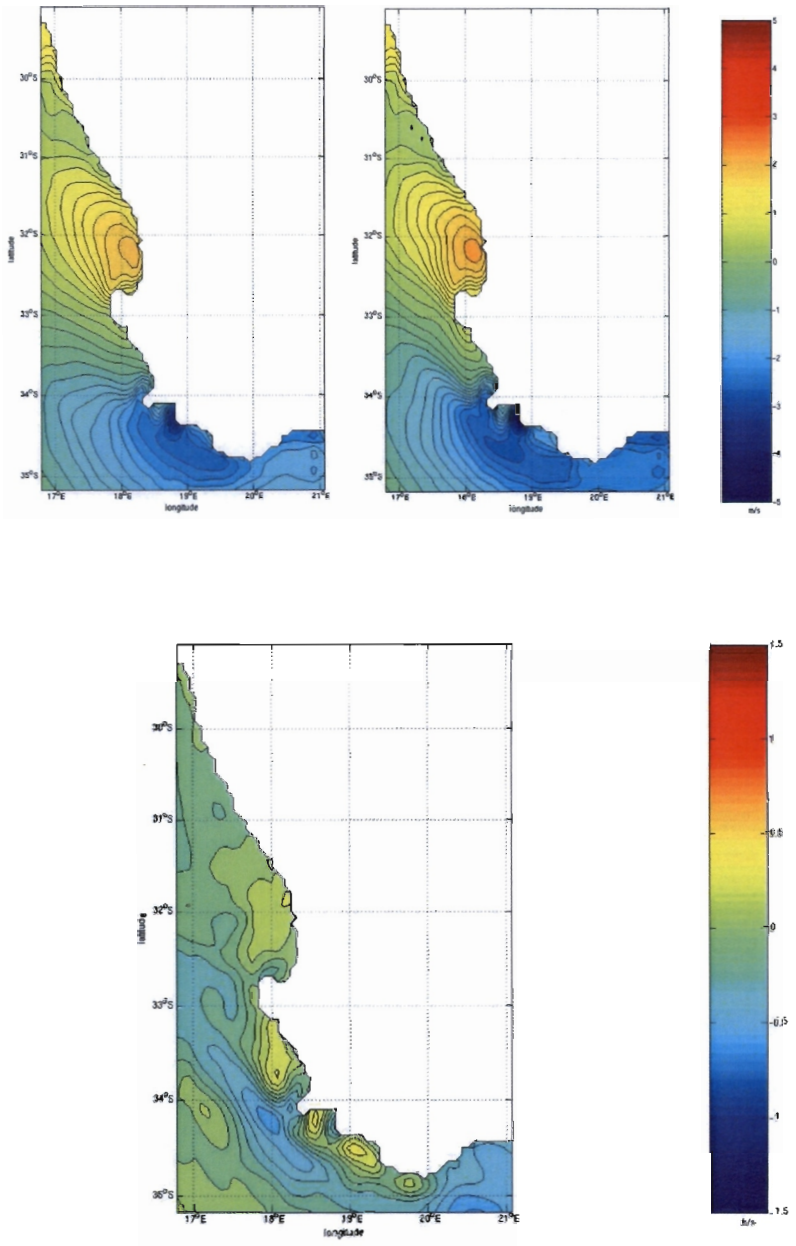

Figure 6.3: Mean 12-30 March 2001 cross-shore winds (rotated to the average 340°-160°alignment of coastal topography) for 9km resolution nest. (Top left) Model run 1. (Top right) Model run 2. (Bottom) Difference in mean across-shore winds between runs one and two (model run 2 minus model run 1).

Cape Peninsula and Cape Columbine during the 12-30 March 2001 period is evident in Figures 6.1 and 6.2 for both model runs. An average enhancement of wind speed is seen at the capes with associated bands of wind maxima, while lighter winds are seen in the lee of the capes.

During the 2-5 December 1980, four grids were flown sequentially between 30°S and 35°S (Jury, 1985a), from which a composite map of wind flow was created (Figure 6.4). A broad wind maximum in the southerly flow was observed to the north-west of Cape Columbine with a wind minimum extending 200km along the coast downstream of the cape. Weak synoptic pressure gradients and low inversions along the coast during the survey favoured the development of seabreezes in the lee of the Cape Columbine headland and resulted in an enhanced across-shore component in the flow (Jury, 1985a). Note that the two images cannot be compared directly as one is an average over a number of days whereas the other is a composite of sequential flight grids. However a general comparison between the mean simulated winds in Figure 6.1 and Figure 6.4 illustrates that the regional model was capable of reproducing a qualitatively similar effect of topographic forcing on the equatorward flow, and in particular the response of the flow to Cape Columbine. Although an intensification in simulated wind flow is seen at the Cape Peninsula, the 9km resolution of the topography does not appear to be adequate enough to resolve the finer details of the behaviour of the flow in response to the complex topography of the peninsula. Increased across-shore flow due to enhanced thermal gradients in the lee of Cape Columbine is also captured by the simulation as is illustrated in Figure 6.3.

Figure 6.2 shows that differences in mean along-shore wind stress are less then 1.5 m s^{-1} due to changes in SST forcing. The primary reason for the differences in along-shore wind stress between the two runs is the enhanced effect of coastal topography in the second model run due to a greater slope in the inversion layer towards the coast (Figure 6.5). For run 2 the mean wind speed is greater than that of run 1 in regions where topography enhances the along-shore flow and less in regions of topographic sheltering. The strong response of low-level winds to coastal topography in the southern Benguela during summer is because the Atmospheric Boundary Layer (ABL) is capped by a sharp inversion which inhibits vertical motion and thins to several hundred meters in depth near the coast. This inversion generally lies beneath the tops of the coastal topography. The extent to which the prevailing summer synoptic equatorward flow in the ABL is influenced by topography depends on the depth of the ABL. A sloping ABL implies a strong horizontal across-shore temperature gradient between the cool ocean and warm land. Cooler SSTs due to coastal

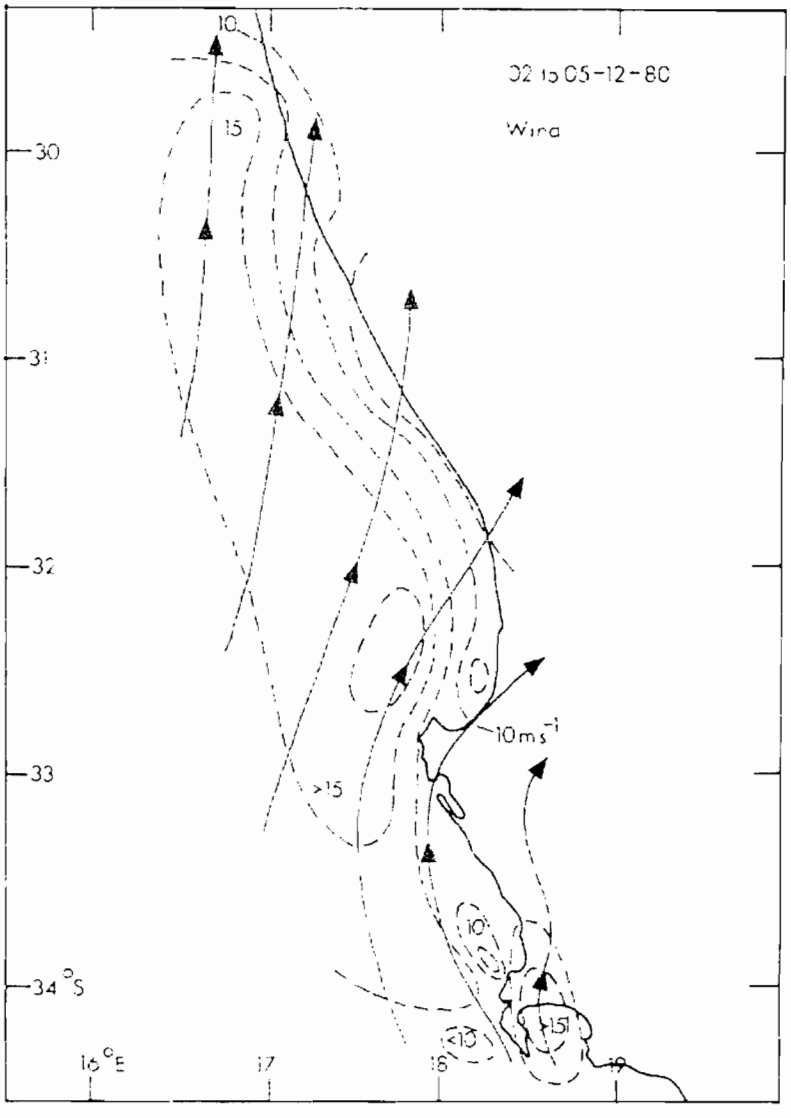

Figure 6.4: A composite map of wind flow represented by streamlines and isotachs for the 2-5 December 1980, taken from Jury, 1985a.

upwelling are better resolved by the SST forcing used in the second model run, enhancing land-sea thermal contrasts. This results in an increased slope in the inversion layer in the second run and a shallowing of the inversion towards the coast (Figure 6.5).

In the vertical wind profile near the coast, a jet core of maximum along-shore magnitude situated just below the inversion is generally observed. This jet location results from both surface frictional drag retarding surface velocities and the decrease in along-shore geostrophic velocities above the inversion due to the thermal wind (Pomeroy and Parish, 2001; Zemba and Friehe, 1987). Jury (1984) identified the presence of a low-level equatorward wind jet constrained below a sharp temperature inversion, which tilted downwards towards the coast. This jet was found to be channelled and deflected by the Cape Peninsula and Cape Columbine (Jury, 1984, 1985a). The vertical and horizontal structure of the simulated atmospheric boundary layer is investigated using the offshore cross-sections A, B and C depicted in Figure 6.6. Figure 6.7 depicts the mean 12-30 March 2001 thermal structure for cross-sections A, B and C. The depth of the constant potential temperature ABL decreases inshore in cross-sections A and B and to a lesser extent C which is situated in the lee of Cape Columbine. Above the ABL, isotherms of constant potential temperature slope down towards the coast, capping the near surface flow in the ABL. The effect of this thermal capping can be seen in Figure 6.8 which depicts the corresponding mean 12-30 March 2001 along-shore flow. The presence of a low-level along-shore coastal jet structure similar to that found in California by Zemba and Friehe (1987) and near Cape Columbine and the Cape Peninsula by Jury (1984) is evident.

Along-shore wind speeds simulated by the second model run for the 3km resolution nest (Figure 6.9) are enhanced by Cape Columbine whereas in the lee of the cape, wind speeds are on average lighter with a slight across-shore component. Below the atmospheric subsidence inversion, Jury (1985b) identified an equatorward coastal wind jet situated over the Cape Columbine headland, with maximum intensity between 100 and 300 meters and winds accelerating over the sea to the west of the cape, fanning out and decelerating with cyclonic curvature downstream over St Helena Bay. The presence of a similar jet can be seen in the model (Figures 6.8 and 6.9). Figure 6.10 shows the average land-sea surface thermal contrasts in the model. The enhanced average onshore curvature of the low-level flow in the lee of Cape Columbine is attributed to a seabreeze which develops due to the midday thermal contrasts between the marine air ($<17°C$) and the interior coastal plain ($>26°C$). Thermal gradients are further enhanced between 31.5°S and 32°S due to the presence of the Olifants River valley. The model is therefore able to simulate the coastal

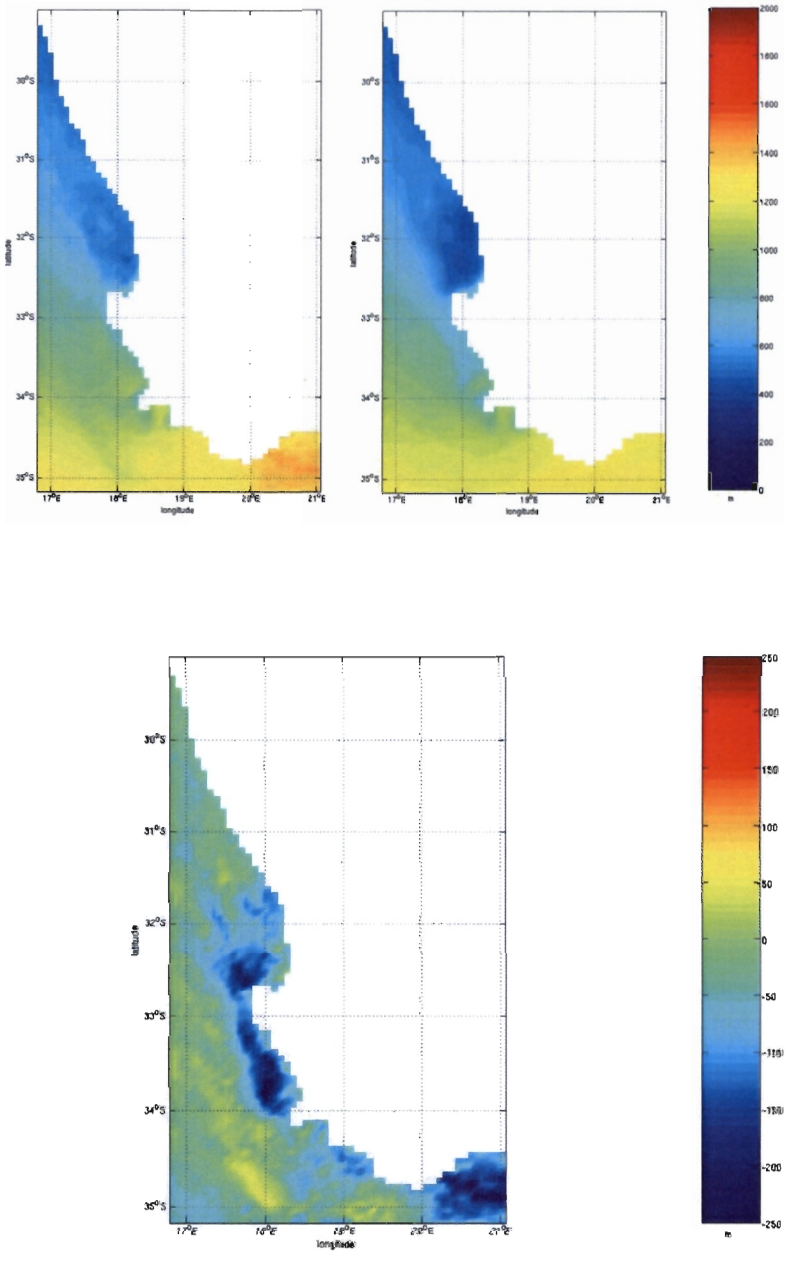

Figure 6.5: Mean 12-30 March 2001 inversion height for 9km resolution nest. (Top left) Model run 1. (Top right) Model run 2. (Bottom) Difference in mean inversion height between runs 1 and 2 (model run 2 minus model run 1).

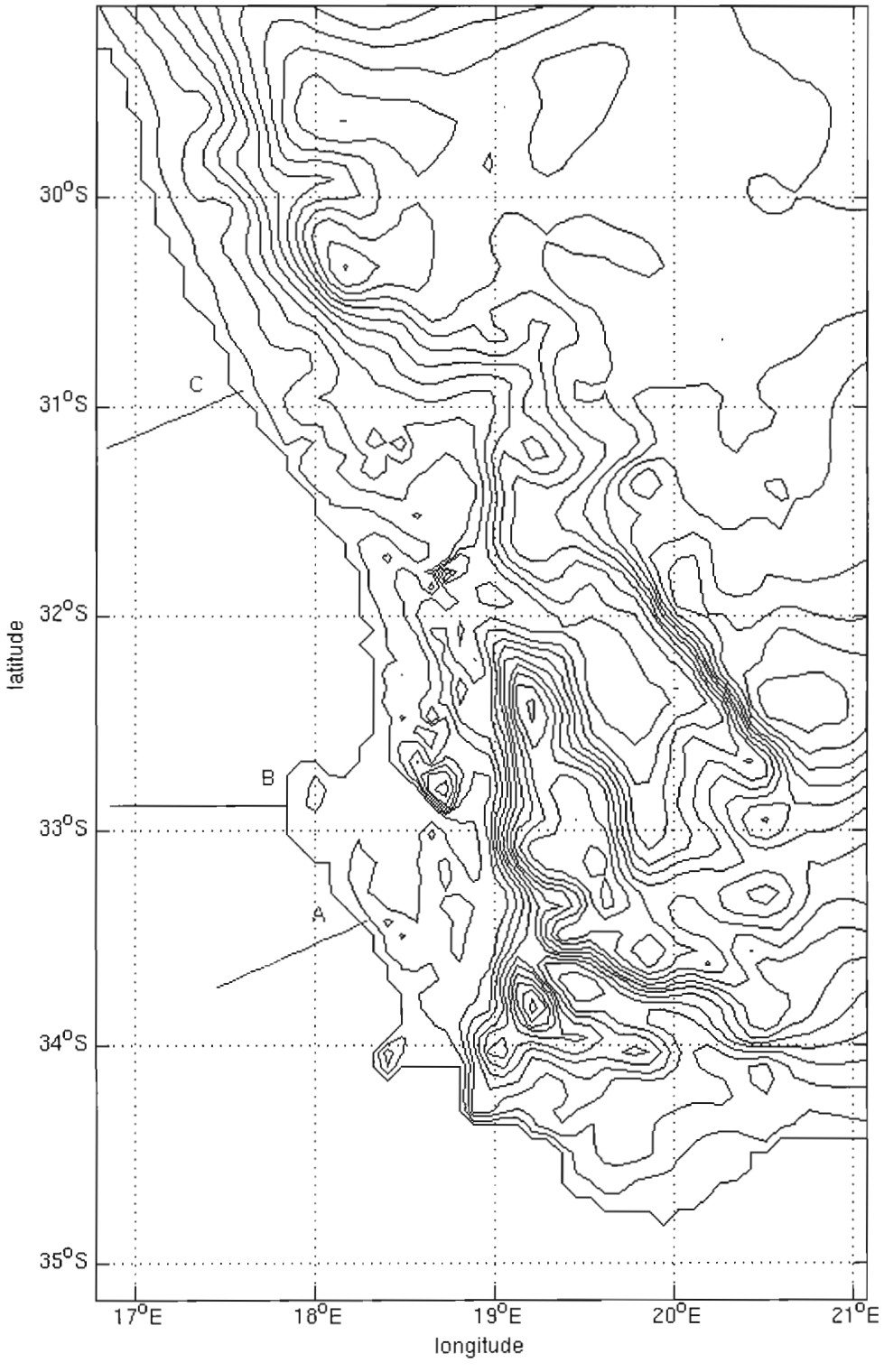

Figure 6.6: Cross-sections A, B and C with topography used for the regional atmospheric model's 9km resolution nest.

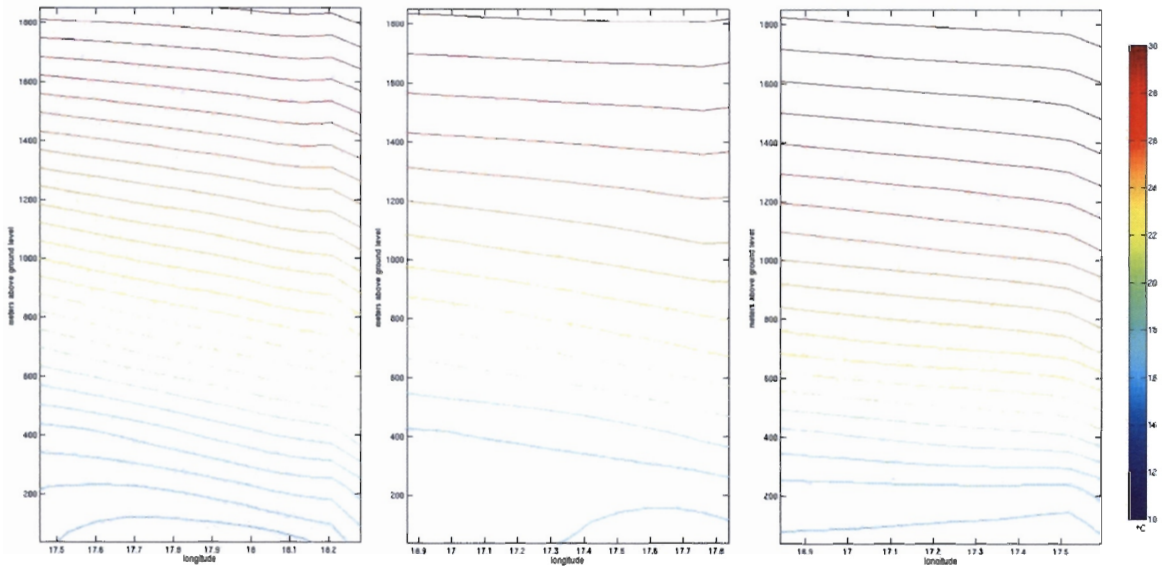

Figure 6.7: Mean 12-30 March 2001 model run 2, potential temperature for cross-sections (Left) A, (Middle) B and (Right) C.

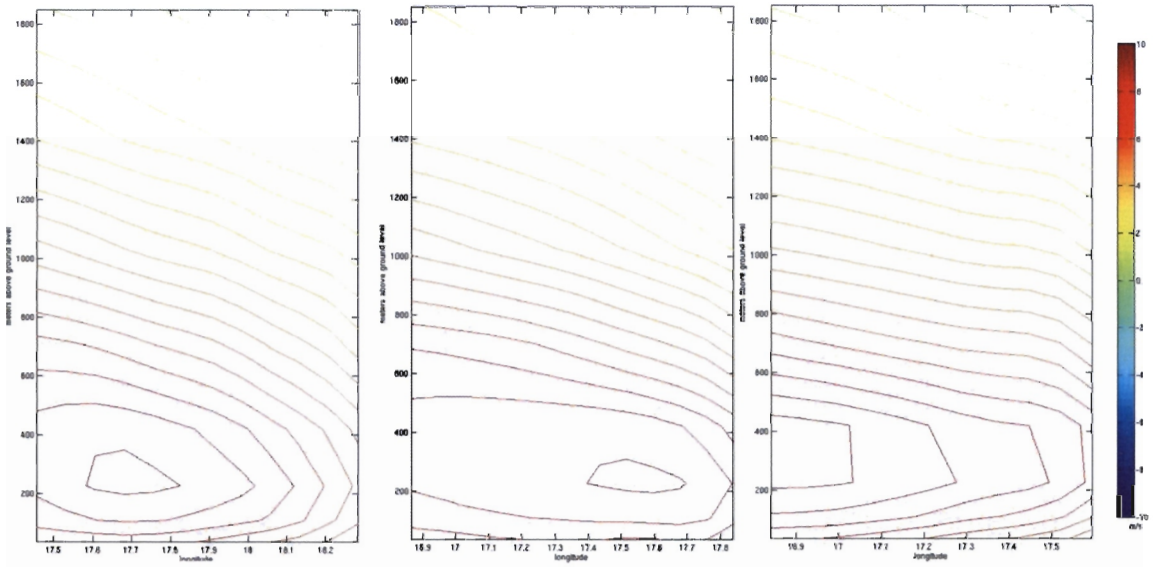

Figure 6.8: Mean 12-30 March 2001 model run 2, along-shore wind speed for cross-sections (Left) A, (Middle) B and (Right) C.

wind jet to the west of Cape Columbine, the wind wake in its lee, and the local seabreeze.

As mentioned in chapter four, the 13-30 March 2001 event can roughly be divided in two, with March 13-22 dominated by strong across-shore pressure gradients and associated equatorward flow and the 23-30 March characterised by weak across-shore pressure gradient and light variable winds. Figure 6.11 shows the temporal evolution of potential temperature and along-shore wind profiles above Cape Columbine. From Figure 6.11 and the synoptic charts (Appendix A), it is evident that anti-cyclonic along-shore flow on the 12th and 13th was interrupted on the 14th by poleward flow at Cape Columbine (Figure 6.11) and Cape Town (synoptic chart). This poleward flow was due to the passage of a mid-latitude cyclone south of the continent and the formation of a coastal low which tracked southward along the escarpment. While the coastal low is poorly resolved by the synoptic charts, the regional model is able to resolve its evolution as it tracks southward and then eastward along the escarpment (Figure 6.12). The inversion layer descended on the 13th due to the approaching coastal low (Figure 6.11) and equatorward flow resumed on the 15th. Strong equatorward flow was driven by the SAH ridging south of the continent from 16-21 March, with the exception of the 19th where it relaxed due to the passage of a mid-latitude cyclone south of the continent. From the 23rd, the across-shore pressure gradients relaxed significantly as a west coast trough developed and the winds became light and variable.

6.3 Shallow vs Deep Equatorward Flow

Using a vertical cross-section downwind of the Cape Peninsula, with a similar location to that of cross-section A in Figure 6.6, Jury (1984) evaluated the effect of upstream topographic barriers on the along-shore wind jet from the 17-19 November 1979. During this period, deep ABL flow on the 17th was replaced by shallow flow on the 19th due to a descending thermal inversion layer. This resulted in the accelerated core of along-shore wind shifting offshore and diminishing in vertical extent. Two jet cores, each greater than 15m s^{-1} in magnitude, were present in the transect on 18 November 1979, one situated at the coast and the other approximately 40km offshore. These jet cores were deflected offshore on the 19th as the ABL flow shallowed and a wind wake formed in the lee of Table Mountain (1000-1080m high) due to the descent of the thermal inversion (Jury, 1984).

Jury (1985c; 1984) also performed a comparison of the horizontal structure of the low-level

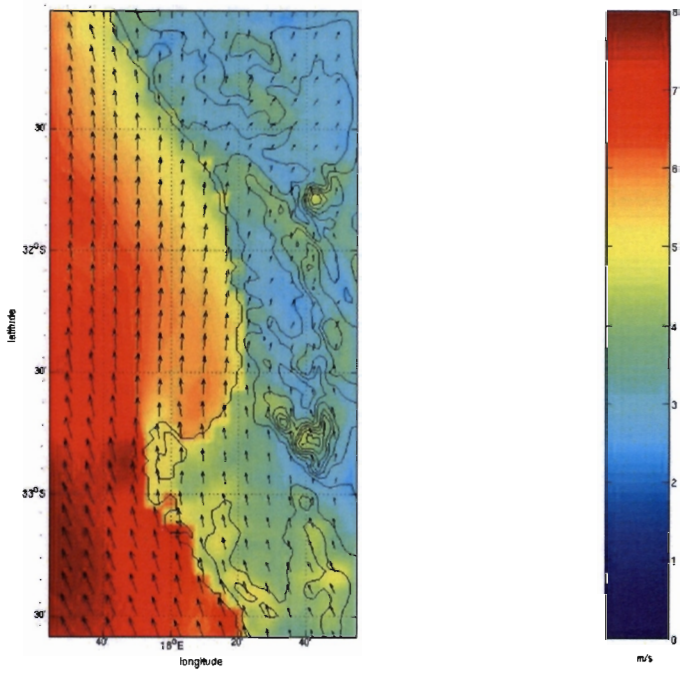

Figure 6.9: Mean 12-30 March 2001 model run 2, winds for 3km resolution nest.

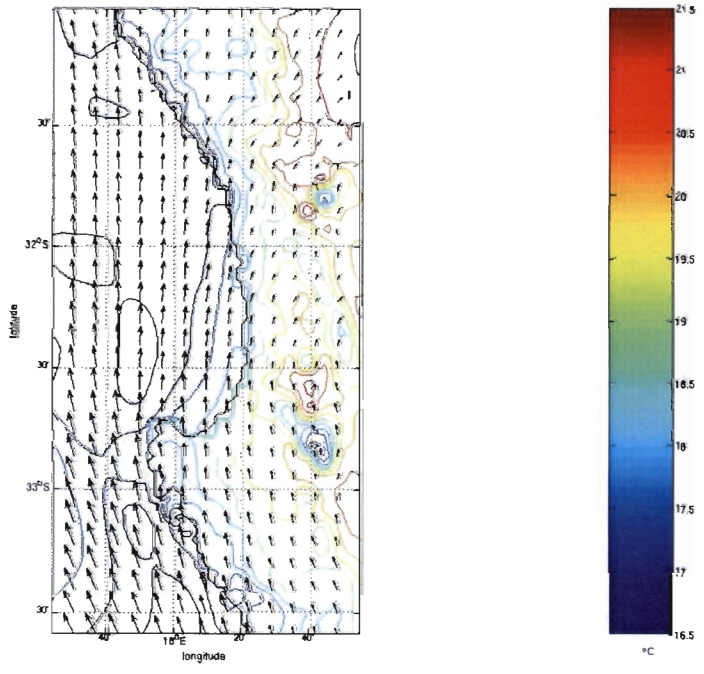

Figure 6.10: Mean 12-30 March 2001 model run 2, 2m temperature for 3km resolution nest with mean 12-30 March 2001 10 meter wind vectors overlayed.

wind field during deep and shallow equatorial flow. By conducting aerial surveys during both shallow and deep equatorward flow events, Jury (1984) established that the extent to which equatorward wind flow is perturbed by topography depended on the depth of the ABL. During a survey conducted from 21-26 January 1980, Jury (1984) investigated equatorward flow fields over the Cape Peninsula which were deep on the 22nd and shallow on the 25th. During deep flow, an axis of accelerated wind extended north-west of the Cape Peninsula while during shallow flow, the axis of accelerated wind shifted southwards and extended westwards off the Cape Peninsula. Similar results were found during a survey conducted from 11-14 December 1978. Aerial survey charts revealed the horizontal structure of deep equatorward winds on the 11th and shallow equatorward winds on the 13th due to an approaching coastal low (Jury et al., 1985c). Wind speeds peaked to the north-west of the Cape Peninsula during deep equatorward flow. The lowering of the thermal inversion caused a shift in wind speed maxima to south of the Cape Peninsula with a calm area resulting from orographic deflection of shallow flow over the northern portion of the peninsula. Jury (1984) found that during shallow flow conditions, the along-shore wind jet was deflected seawards by coastal mountains.

In order to assess whether the simulated winds respond similarly to that observed by Jury due to a shallowing of ABL flow, the mean simulated low-level winds on the 13th and 17th of March 2001 are compared. On the 13th, the inversion descended due to the approaching coastal low and resulted in shallow equatorward flow whereas, on the 17th, strong deep equatorward flow was forced by the ridging of the SAH south of the continent. Figure 6.13 illustrates the difference in cross-section A's potential temperature and along-shore wind profiles between the shallow conditions on the 13th and deep conditions on the 17th. In the former, strong southerly flow extends to roughly 600m whereas on the 17th, it extends to 1000m. The core of the flow is about 400m deeper on the 17th. The behaviour of the simulated along-shore wind is consistent with that observed in Jury's (1984) vertical cross-section downwind of the Cape Peninsula. The descent of the model inversion results in the accelerated core of along-shore wind shifting offshore and diminishing in vertical extent on the 13th relative to the 17th. The horizontal structure of the deep equatorward winds on the 17th vs shallow equatorward winds on the 13th is depicted in Figure 6.14. Similar to Jury (1985c; 1984), wind speeds peak to the north-west of the Cape Peninsula during deep equatorward flow on the 17th while the shallow thermal inversion on the 13th causes a shift in the wind speed maximum to the south of the Cape Peninsula with a calm area over the northern portion of the peninsula.

6.4 Weak Across-Shore Pressure Gradients

During 22-30 March 2001 relaxed synoptic pressure gradients persisted along the west coast of South Africa. Taking the 26 March 2001 as an example, it is apparent how local thermal contrasts control the coastal low-level wind field north of Cape Columbine during these conditions (Figure 6.15). At 0600 GMT (0800 SAST), the thermal contrast between marine air and the interior coastal plain is conducive for the seabreeze, with particular entrainment of marine air near the Olifants River mouth. By 1200 GMT (1400 SAST), insolation has passed its maximum (air temperatures have reached their day time high), resulting in large land-sea thermal gradients which drive the onshore flow associated with the seabreeze. By 1500 GMT (1700 SAST), the on-shore flow associated with seabreezes has started rotating towards the along-shore direction due to the Coriolis effect.

This diurnal evolution of the across-shore and along-shore wind components due to the seabreeze produced by the model is consistent with the local observations at the SAWS Lambert's Bay weather station and the MCM Columbine weather station discussed in chapter 4. The observed across-shore component is on average greater at Lambert Bay's than at Cape Columbine and reaches a maximum velocity around 1400 GMT (1600 SAST) during both strong and weak across-shore pressure gradient conditions (Figures 4.15 and 4.16). The observed along-shore component reaches a maximum towards the late afternoon, at roughly 1600 GMT (1800 SAST) (Figures 4.15 and 4.16).

6.5 Summary

Analysis in this chapter has shown that the model appears to do a good job of representing the mesoscale wind features which result from the interaction of synoptic flow with coastal topography and local thermal gradients. The influence of the resultant spatial variation in the low-level wind field on ocean wind stress forcing and the implications for HAB development and advection will discussed in the following chapter.

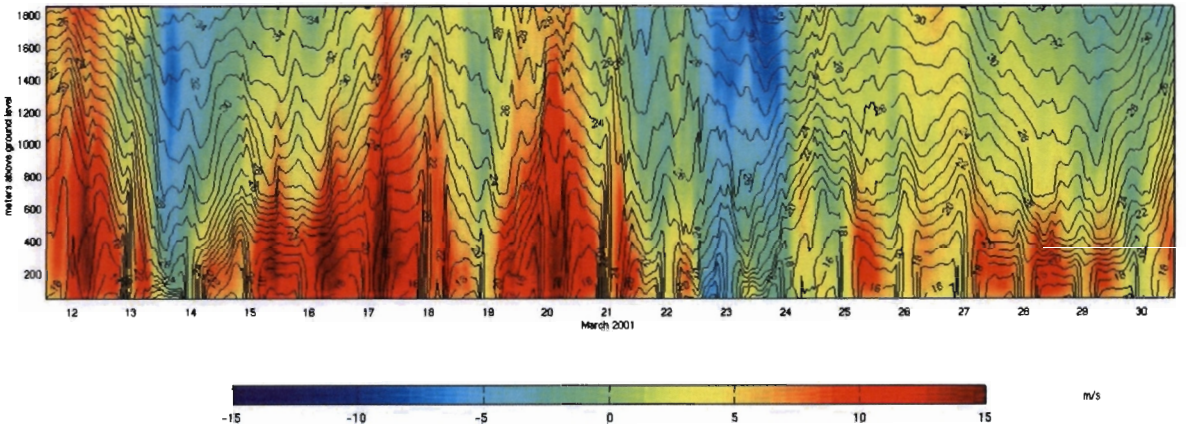

Figure 6.11: Model run 2, potential temperature and along-shore wind above Cape Columbine. Equatorward along-shore wind velocities are positive and poleward along-shore wind velocities are negative.

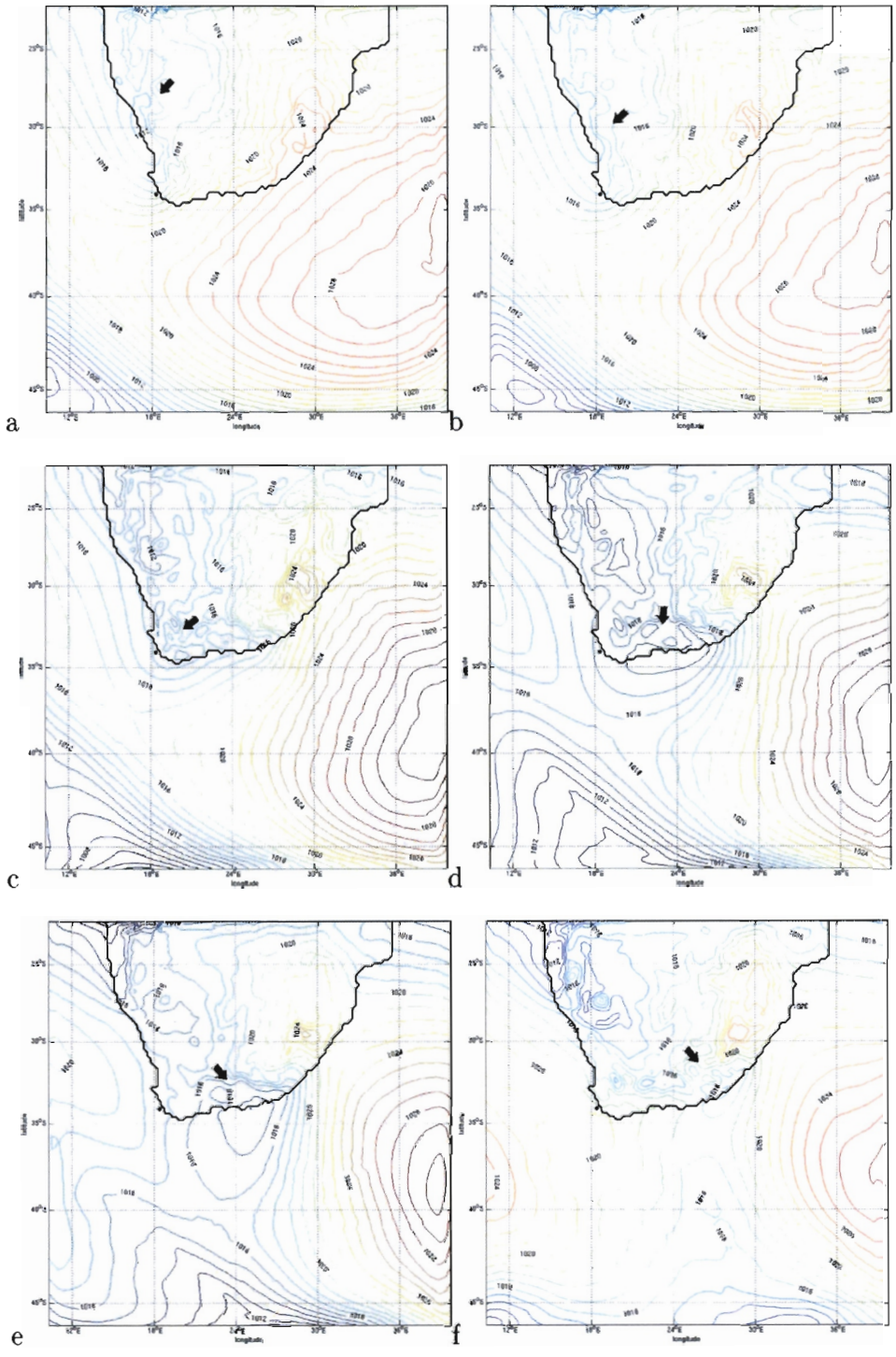

Figure 6.12: SLP (hPa) for model run 1 27km resolution nest at (a) 0000 GMT 14 March 2001 (b) 0400 GMT 14 March 2001 (c) 1200 GMT 14 March (d) 2000 GMT 14 March (e) 0400 GMT 15 March (f) 1600 GMT 15 March.

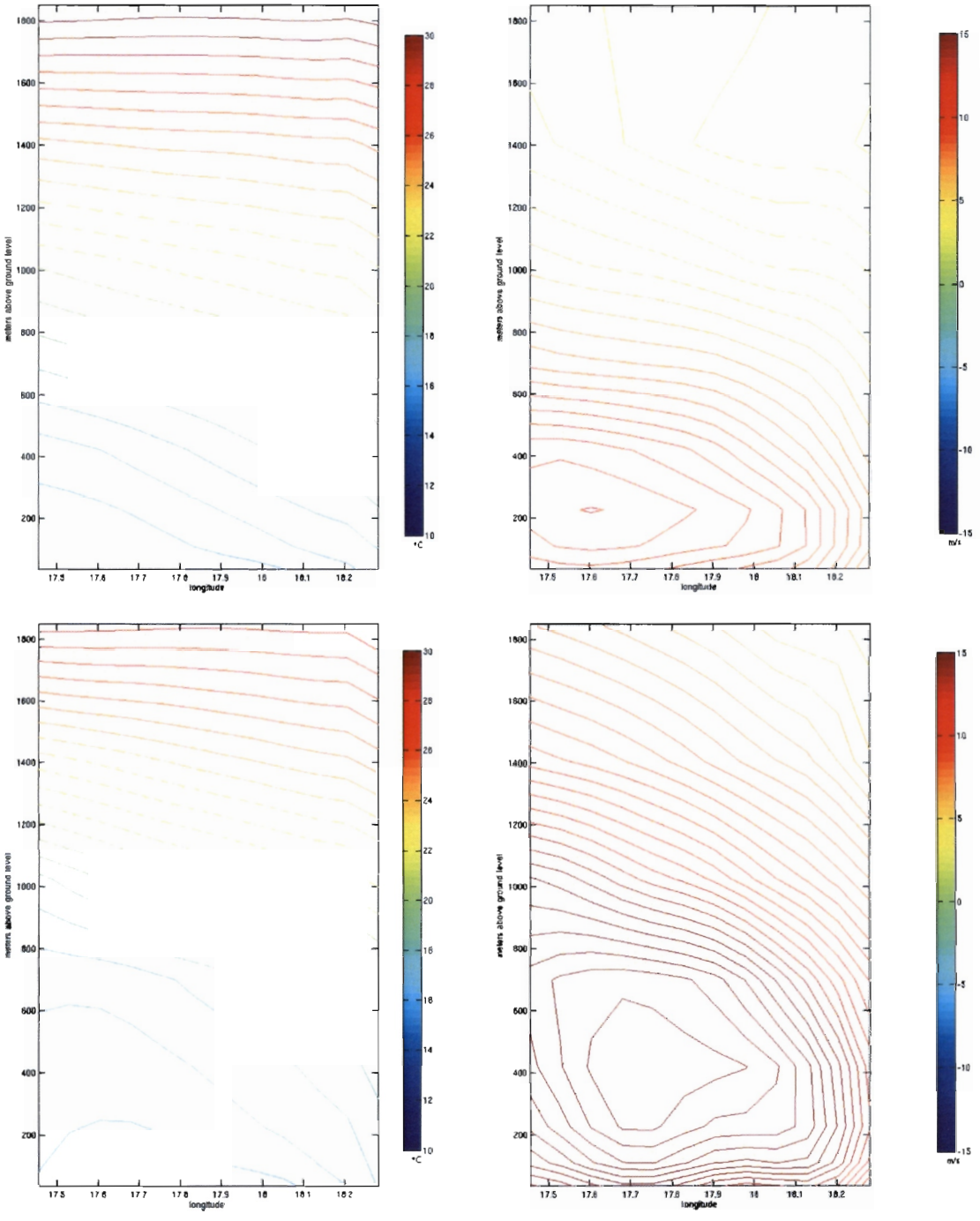

Figure 6.13: Mean cross-section A model run 2 potential temperature and along-shore wind. (Top) 13 March 2001. (Bottom) 17 March 2001.

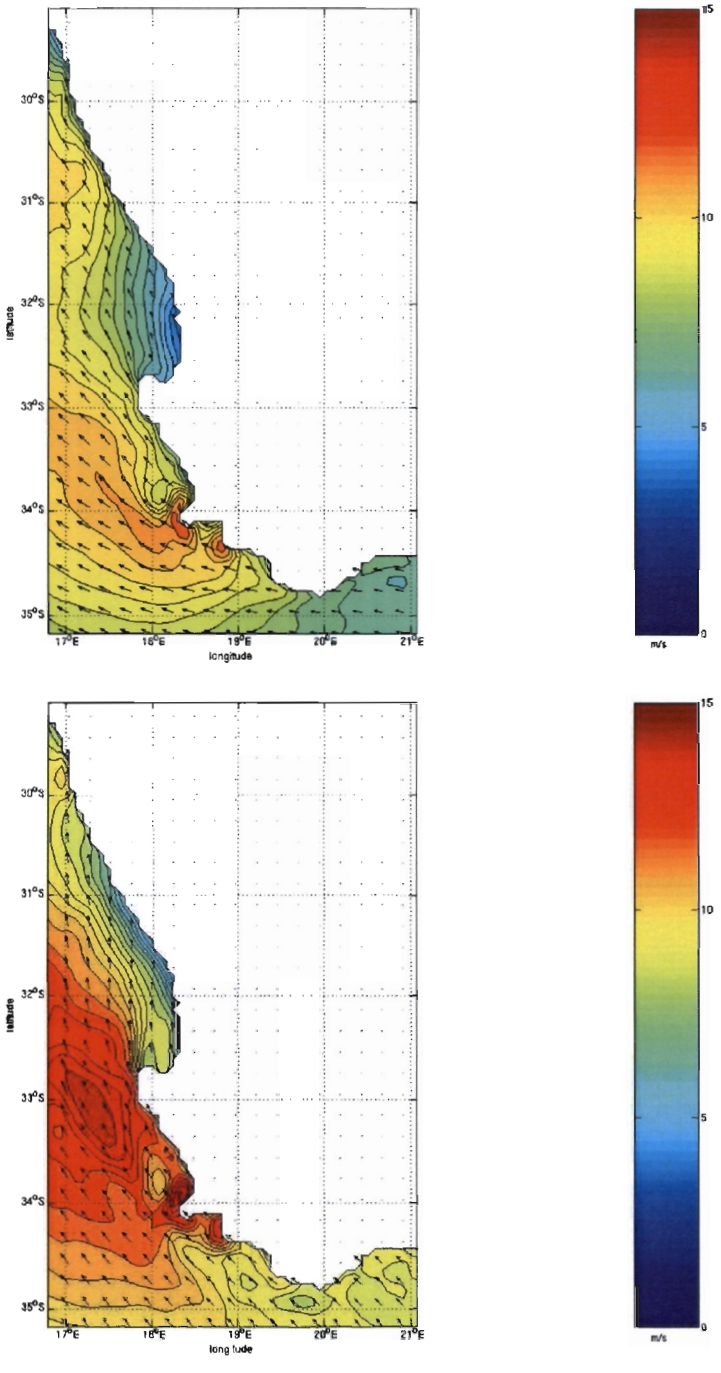

Figure 6.14: Mean model run 2 10 meter winds. (Top) 13 March 2001. (Bottom) 17 March 2001.

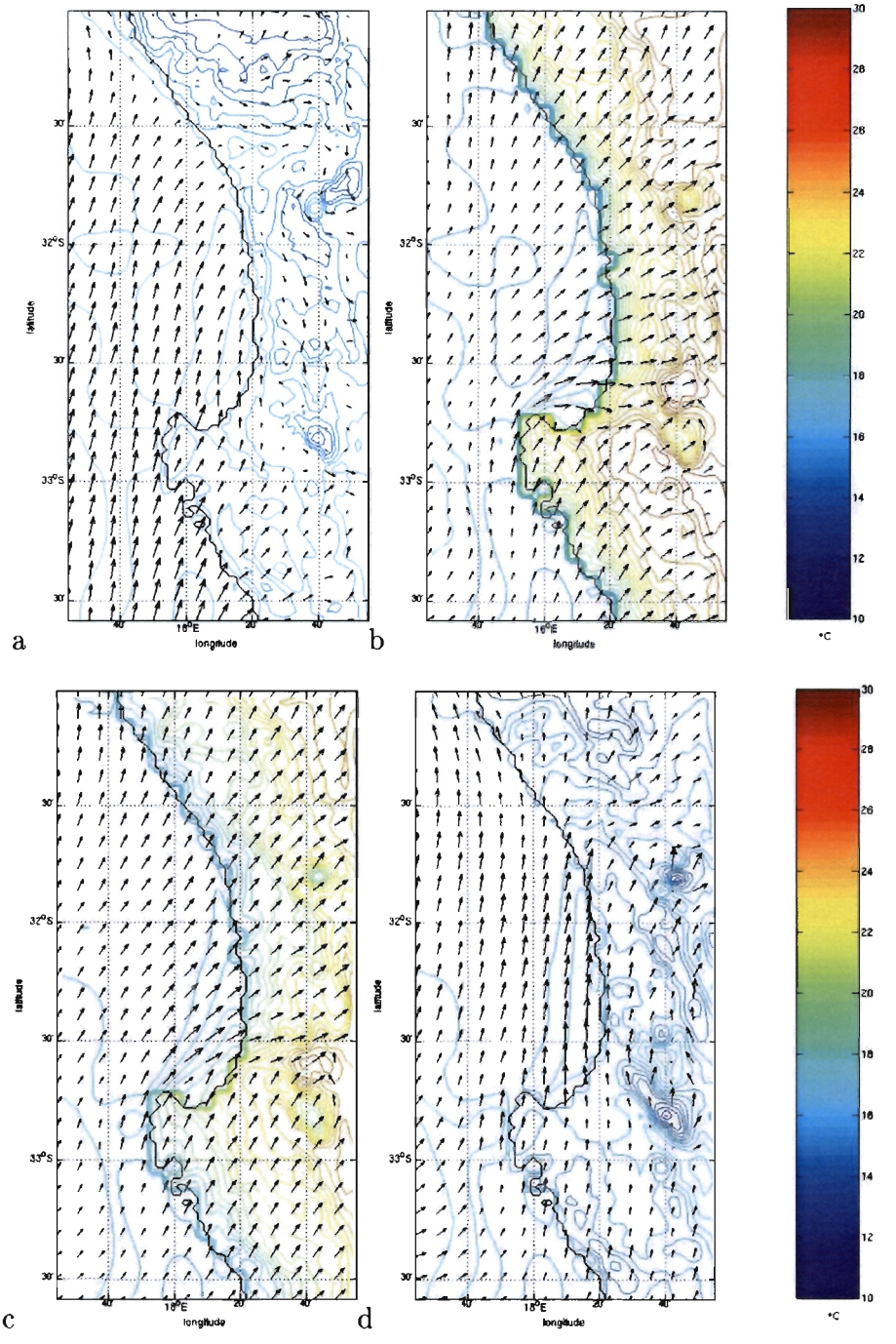

Figure 6.15: Model run 2, 2m temperature for 3km resolution nest with wind vectors overlayed at (a) 6000 GMT (b) 1200 GMT (c) 1500 GMT (d) 2100 GMT on 26 March 2001.

Chapter 7

Spatial Variability in Wind Stress with Potential Implications for HAB Development and Advection

As discussed in Chapter 2, both wind stress and wind stress curl could play an important role in determining ocean mixed layer characteristics and hence phytoplankton species dominance over the broad shelf region north of Cape Columbine. The magnitude of wind stress controls the mixed layer depth through vertical mixing whereas Ekman divergence induced by the coastal cyclonic wind stress curl may act to lift the base of the thermocline, increasing stratification and decreasing the depth of the mixed layer in regions of strong cyclonic curl. These two mechanisms may be responsible for the observed mixed layer characteristics and resultant phytoplankton species distribution off-shore of Lambert's Bay during upwelling favourable winds.

The upwelling favourable equatorward winds which prevail in the southern Benguela during summer are interrupted every so often by transient weather events. HAB events may develop during these quiescent periods in upwelling, as dinoflagellate-dominated surface water becomes strongly stratified encouraging dinoflagellate growth and resulting in a high biomass bloom. A significant onshore wind stress component during quiescent phases in upwelling is needed to advect these high biomass blooms into the near-shore environment where they have the greatest impact upon coastal communities. In this chapter, wind stress and wind stress curl are derived from the simulated 10 meter winds in an attempt to establish the role of spatial variability in the low-level wind stress field in the development of

HAB events prone to the greater St Helena Bay region. In addition, surface fluxes, Ekman depth, the Monin-Obukhov length scale and other diagnostic parameters are analysed.

7.1 Wind Stress and Wind Stress Curl: 12-30 March 2001

Wind stress has been calculated according to the bulk parameterisation method of Large and Pond (1981), assuming near-neutral stability conditions, as described in Chapter 3. Figure 7.1 depicts the mean 12-30 March 2001 wind stress derived from model run 2 for the 3km resolution nested grid and indicates the intensification of wind stress seaward of the Cape Columbine and sheltering in the lee of Cape Columbine. The inshore wind stress values are significantly less in the lee of Cape Columbine than those to the south of the cape and further off-shore during this period.

In-shore of the maximum equatorward wind stress values, is an area of wind stress decrease leading to cyclonic wind stress curl over the region (Figure 7.2). Note that the land has been masked out when calculating the curl in wind stress to prevent contamination by land values. In agreement with the observations of Jury (1985b; 1985a), an enhanced region of cyclonic wind curl extends north of the cape due to the strong across-shore shear in the mean along-shore flow which exists between the equatorward low-level wind jet to the west of the cape and sheltering in its lee.

7.2 Bloom Dynamics: 13-30 March 2001

Temperature and chlorophyll data for the upper ocean collected from station 3 (Figure 3.1) during the course of the case study (13-30 March 2001) are depicted in Figure 7.3. Station 3 is situated approximately 2 nautical miles off-shore of Lambert's Bay. During periods of active upwelling, station 3 lies inshore of the coastal upwelling front associated with the narrow band of coastal Ekman upwelling. Upwelling favourable winds on the 13, 16-18 and 20-22 March 2001 resulted in low sea surface temperatures at this station. Slight warming associated with the passage of a coastal low occurred on the 14th and also on the 19th as the equatorward wind stress relaxed. Relaxation of equatorward upwelling favourable winds from the 23rd onwards led to warming of the surface waters.

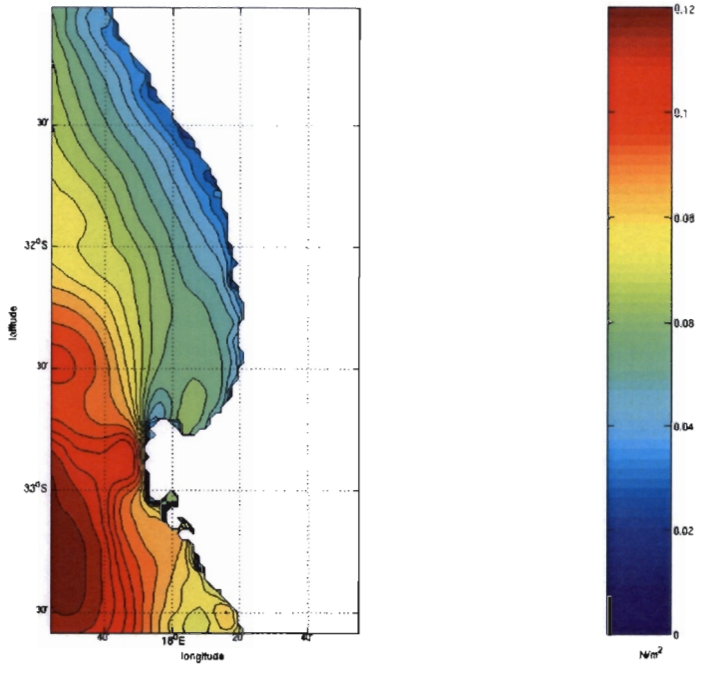

Figure 7.1: Mean 12-30 March 2001 model run 2, wind stress for 3km resolution nest.

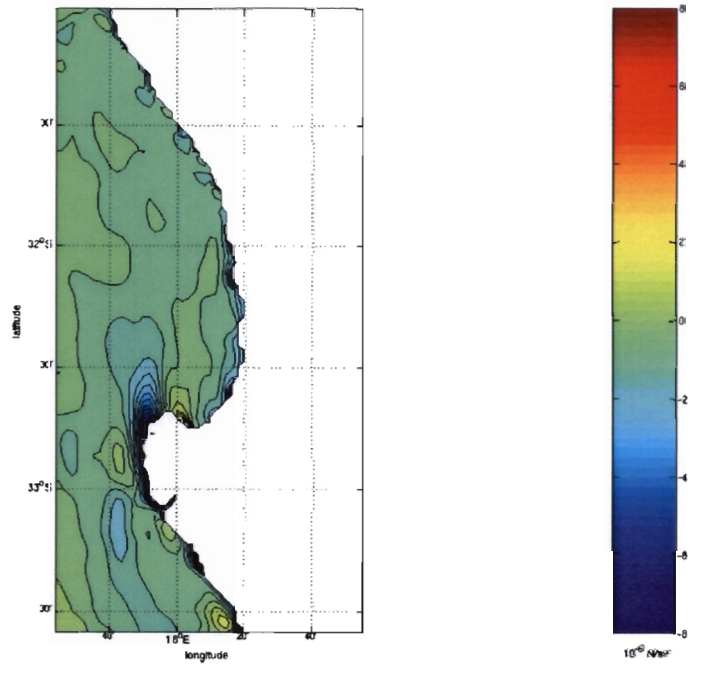

Figure 7.2: Mean 12-30 March 2001 model run 2, wind stress curl for 3km resolution nest.

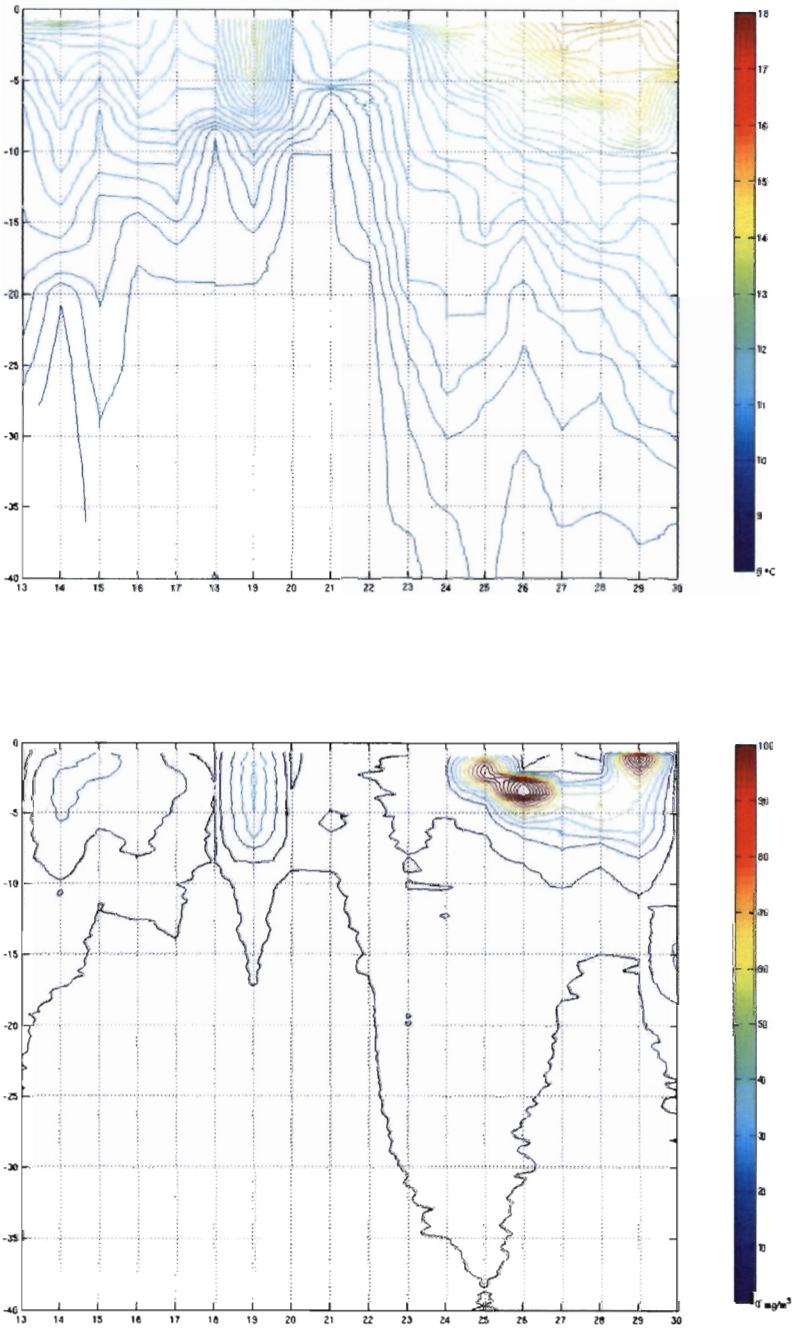

Figure 7.3: Station 3 timeseries 13-30 March 2001 with depth represented in meters on the y-axis. (Top) Temperature. (Bottom) Chlorophyll concentrations.

The correspondence of the station surface species composition with ocean surface boundary layer characteristics was assessed by Pitcher and Nelson (2006). The surface boundary layer was characterised in terms of surface mixing using a stratification index and nutrient availability using nitrate concentrations. Diatoms dominated station 3 samples during upwelling conditions, when nutrient concentrations were high and the index of stratification was low as a result of turbulent mixing within the surface layer. The samples of intermediate composition were characterised by intermediate stratification index and nutrient concentration values. A dinoflagellate bloom was associated with a high index of stratification and lower nutrient concentrations which persisted from the 23rd.

From the timeseries of temperature and chlorophyll at station 3, it is evident that the period can roughly be divided into two, with March 13-22 characterised by upwelling, cool surface temperature, low chlorophyll values and diatom dominated samples at station 3 whereas from the 23rd, the prolonged relaxation of upwelling favourable winds led to significant warming, increased stratification and the appearance of a high biomass dinoflagellate bloom. This dense bloom then impacted upon the coast at Lambert's Bay as a result of onshore flow (Pitcher and Nelson, 2006).

The appearance of this bloom at the coast can be directly attributed to the coastal wind forcing and its temporal variability. Strong equatorward winds which brought nutrients to the surface through upwelling and vertical mixing were followed by a prolonged quiescent phase, which allowed near-shore surface waters to warm and stratify through radiative heating and horizontal advection (Pitcher and Nelson, 2006). Pitcher and Nelson (2006) and Fawcett (2006) have shown that the southward advection of warmer waters from the north, by a poleward barotropic current which occurs under relaxed equatorward wind conditions, may be responsible for rapid warming events at this station.

Wind stress forcing clearly plays an important role in determining mixed layer characteristics and hence phytoplankton species dominance. Spatial variability in wind stress forcing could therefore pose as an important mechanism in determining phytoplankton species distribution over the broad shelf region north of Cape Columbine. More stratified conditions tend to favour the growth of dinoflagellates and hence the formation of HABs. The role of spatial variability in wind stress forcing in influencing the upper ocean off-shore of Lambert's Bay during 13-30 March will now be investigated. While wind stress induces turbulent vertical velocities which mix surface waters and deepen the surface mixed layer, a positive buoyancy flux acts to stratify and stabilise surface waters, reducing turbulent mixing within the surface boundary layer. In order to assess the tendency of wind and

buoyancy fluxes to influence the upper ocean, Ekman depth and Monin-Obukhov length scale are calculated from the model winds and surface fluxes. Although the validity of the model 10 meter winds from which wind stress values are derived has been assessed in previous chapters, the ability of the model to simulate realistic surface fluxes has not been discussed. These surface fluxes are used to assess the buoyancy forcing. An assessment of the representativeness of these fluxes is provided in Appendix C.

7.3 Active Upwelling: 13-22 March 2001

Quantifying the role of spatial wind stress variability in determining ocean mixed layer characteristics north of Cape Columbine should ideally be performed by means of a numerical model of the upper ocean. Such a task is bigger than the scope of this thesis. However, certain diagnostic variables illustrating the mixed layer depth scales related to the wind stress and buoyancy forcing can be derived. From these depth scales, some conclusions may be drawn as to the role spatial variability in the horizontal wind structure north of Cape Columbine may play in influencing the mixed layer characteristics and in promoting HAB development in this region.

A transect extending off-shore of Lambert's Bay (Figure 3.1) was conducted on the 16th of March during the period of active upwelling. The across-shore temperature and chlorophyll structure from this transect is depicted in Figure 7.4 to show the off-shore changes in mixed layer characteristics and thermocline depth as described by Pitcher and Nelson (2006).

From this across-shore transect together with previous transects conducted in 2000, Pitcher and Nelson (2006) identified that dinoflagellates typically dominate surface waters in the inshore half of the transect. High phytoplankton biomass, dinoflagellate dominated, surface water is typically associated with the frontal region immediately off-shore of the narrow band of coastal Ekman upwelling, while further off-shore the dinoflagellate contribution decreases relative to diatoms due to a deepening of the mixed layer (Pitcher and Nelson, 2006). The changes in the mixed layer depth appear to be greatest mid-transect.

Pitcher and Nelson (2006) suggest two physical mechanisms which may be responsible for the deepening of the mixed layer depth and subsequently the change in phytoplankton species composition off-shore. The off-shore deepening of the mixed layer could be driven by wind stress shear resulting in increased wind mixing off-shore, or by greater shear instabilities at the base of the mixed layer due to stronger surface currents off-shore which

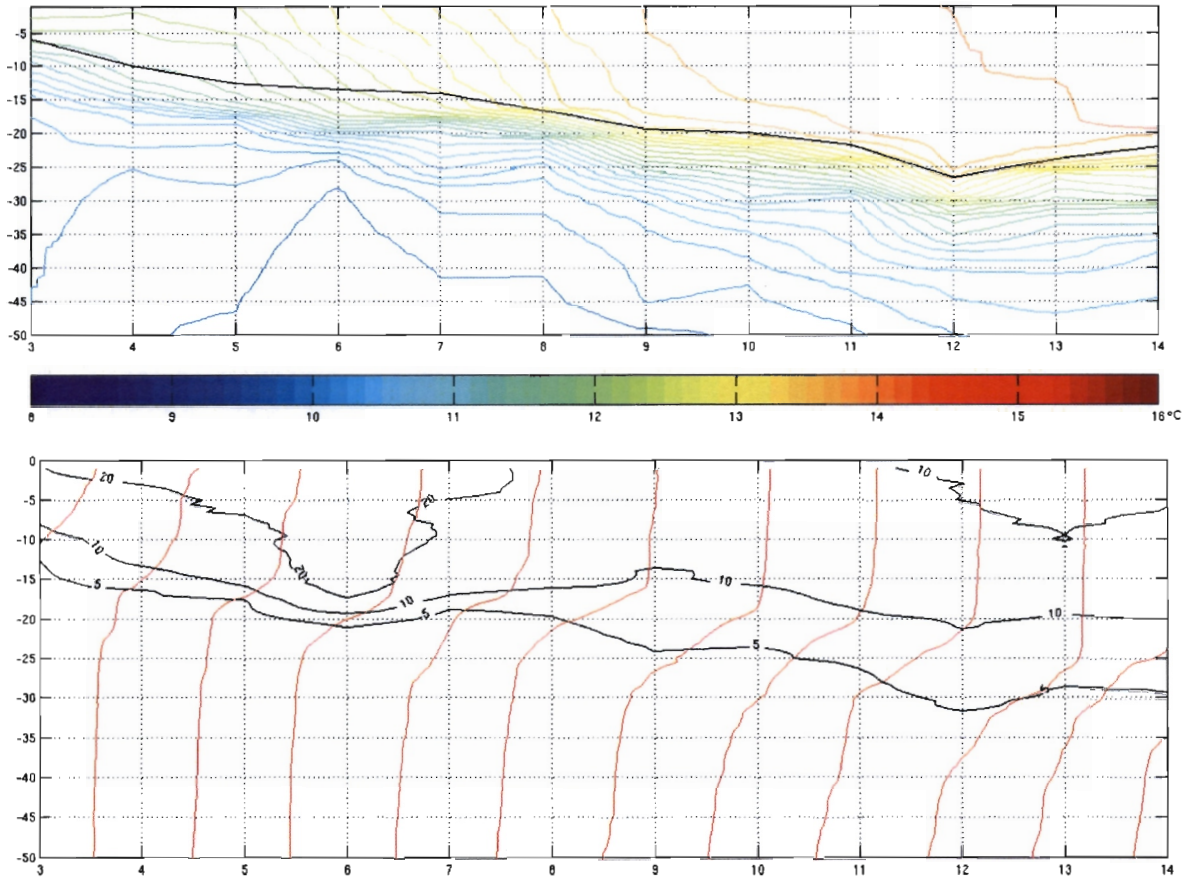

Figure 7.4: Transect 16 March 2001 with depth represented in meters on the y-axis and transect stations from in-shore station 3 to off-shore station 14 represented on the x-axis. (Top) Temperature with the isotherm layer depth (defined as the depth at which the temperature value is 0.5 °C less that the SST) over-layered in black. (Bottom) Chlorophyll concentrations with individual station temperature profiles in red.

enhance entrainment and deepen the mixed layer. However, a lack of wind and current data has made it difficult to determine the physical processes responsible for this off-shore change. Since the model appears to do a reasonable job of capturing the effect of Cape Columbine on the low-level wind flow, the model winds are used to calculated the wind shear and assess the impact of wind mixing off-shore.

7.3.1 Wind Mixing

Figure 7.5(a) shows the average across-shore decrease in wind stress along the transect, after the wind stress values have been horizontally interpolated from those derived from the 3km and 9km resolution simulated 10 meter winds. The across-shore decline in wind speed within the narrow coastal band due to land-sea changes in surface drag and atmospheric boundary layer depth, remains a difficult atmospheric modeling issue. Capet et al. (2004) found the structure of the across-shore wind profile produced by the U.S Navy model COAMPS differed significantly with differing resolution, with the region over which the decline in wind stress occurs decreasing with increasing resolution. This results in higher wind stress curl within the narrow coastal region with increasing resolution. Similarly, Figure 7.5(a) shows that the on-shore decline in wind stress between in-shore stations 3-6 differs between the 3km and 9km grids. With increasing resolution, the across-shore region over which the decline occurs decreases, and hence the associated curl increases in magnitude. Off-shore of station 6, the across-shore decline in wind stress due to sheltering induced by Cape Columbine is the same for both resolutions. With no in-situ data available to determine the actual decline in wind stress within the narrow coastal region, it is difficult to ascertain which resolution provides a more accurate representation of the decrease in wind stress between stations 3-6. For the purpose of this investigation, wind stress and wind stress curl values derived from the 3km resolution simulated 10 meter winds will be used. Caution must however be exercised when looking at stations inshore of station 6, particularly when dealing with wind stress curl values for near-shore stations 3 and 4.

A diagnostic length scale which may be used to assess the relative effects of wind mixing within the region north of Cape Columbine, is the Ekman depth as described by Large et al. (1994):

$$h_E = 0.7u^\star/f \tag{7.1}$$

where the frictional velocity $u^\star = \sqrt{|\tau_0|/\rho_0}$ and f is the local Coriolis parameter. The Ekman depth calculated here represents the depth of a neutrally stratified boundary layer

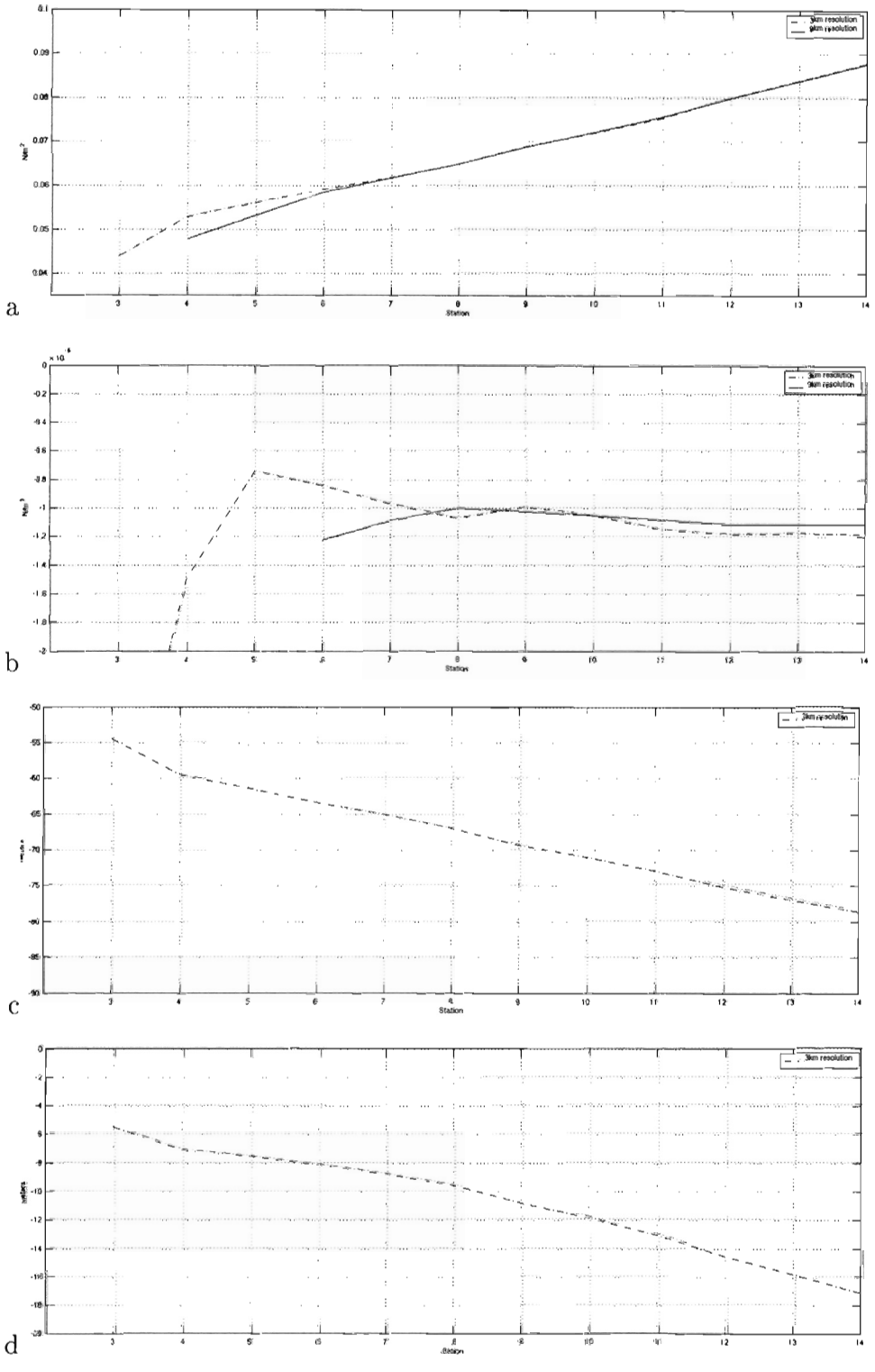

Figure 7.5: Mean 13-22 March 2001 (a) wind stress (b) wind stress curl (c) Ekman depth (d) Monin-Obukhov depth, for transect conducted off-shore of Lambert's Bay from in-shore station 3 to off-shore station 14.

due to wind stress forcing. The frictional velocity used for the Ekman depth has been calculated using the hourly wind stress values derived from the simulated winds while the surface sea water density was derived using the model SSTs and a typical surface salinity value of 34.8 PSU taken from the transect CTD data. Figure 7.6 depicts the mean 13-22 March 2001 Ekman depth derived from the 9km grid of model run 2. An extended region of shallow Ekman depth can be seen along the shelf region north of Cape Columbine, during upwelling favourable winds. The spatial extent of this region correlates well with the region of high average chlorophyll concentrations north of Cape Columbine depicted in Figure 2.3. The wind shadow which occurs in the lee of Columbine during the equatorward flow appears to favour a shallower mixed layer depth over the broad shelf region north of Cape Columbine, which may explain why this region is prone to high phytoplankton biomass.

The mean Ekman depth scale calculated over 13-22 March 2001 for the transect from the transect wind stress values is depicted in Figure 7.5(c). The Ekman depth increases with off-shore extent as a result of increasing average wind stress off-shore. From this we can infer that wind induced turbulent mixing may be responsible for the off-shore increase in mixed layer depth typically seen in transects conducted off-shore of Lambert's Bay (Figure 7.4).

However, the Ekman depth scale represents the depth of a neutrally stratified boundary layer due to wind stress forcing and does not consider the effects of stratification which may result from a positive buoyancy flux. A positive buoyancy flux tending to give stable stratification will result in the mixed layer depth being less then the Ekman depth scale. A diagnostic length scale that accounts for buoyancy forcing is the Monin-Obukhov depth scale defined as (Large et al., 1994):

$$L = u^{\star 3}/(\kappa B_f) \tag{7.2}$$

where $\kappa = 0.4$ is von Kármán's constant, $u^\star$ is the frictional velocity and B_f is surface buoyancy forcing. The frictional velocity was calculated as for the Ekman depth. The buoyancy forcing for each transect station was calculated according to Large et al. (1994) using hourly solar, longwave, latent and sensible heat fluxes obtained from the second model run. The buoyancy forcing is similar to the buoyancy flux in equation C.1 except that the contribution of solar radiation is not included in the net heat flux Q as its contribution is considered as a separate term due to the fact that some of the insolation passes through the mixed layer into the deeper ocean. In order to assess the amount of insolation contributing

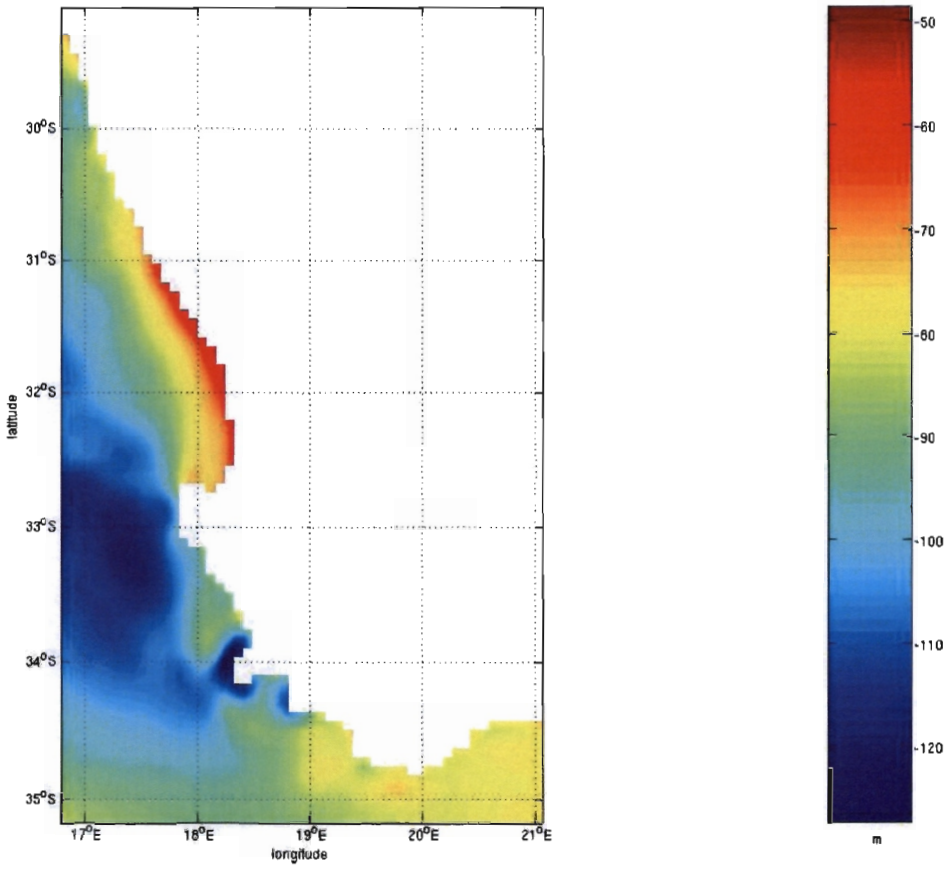

Figure 7.6: Mean 13-22 March 2001 model run 2, Ekman depth for the 9km resolution nest.

to the surface buoyancy, the distribution of solar irradiance in the water column is modelled according to a double exponential depth dependence (Kraus, 1972) using Paulson and Simpson (1977) parameters for Jerlov (1968) water type three applicable to the coastal waters of the Benguela. Only insolation absorbed in the top 10 meters was assumed to contribute to the buoyancy as this depth appears to be the mean mixed layer depth observed in the transects. The specific heat capacity, density and the thermodynamic expansion coefficients were derived using the model SSTs and a typical surface salinity value of 34.8 PSU.

The Monin-Obukhov length scale is only positive for a positive buoyancy forcing. While insolation during the day ensures a positive buoyancy flux, the buoyancy forcing is negative at night and the stratification established during the day is slowly eroded. However, for the purposes of this scale analysis, an averaged positive buoyancy forcing value has been used in calculating the mean Monin-Obukhov length scale over a desired period. The average Monin-Obukhov depth scale shown in Figure 7.5(d) was derived using the mean positive buoyancy flux and frictional velocity values for the 13-22 March 2001 period (note it is depicted as negative to illustrate increasing depth). Unlike Ekman depth, the Monin-Obukhov depth scales are very similar to the mixed layer depths observed in the transects conducted off-shore of Lambert's Bay (Pitcher and Nelson, in press). Figure 7.5(d) therefore suggests that the wind stress and buoyancy flux forcing during upwelling favourable winds can help explain the typically observed depths of the mixed layer and why it changes in depth off-shore of Lambert's Bay.

Figure 7.7 compares the March 16 transect mixed layer depth, determined as the isotherm layer depth at which the temperature decreases by 0.5°C less then SST, with the Monin-Obukhov depth scale derived from the mean buoyancy forcing and frictional velocity values averaged over the 24 hour period before the transect was completed. It appears that the Monin-Obukhov depth scale gives a good representation of the mixed layer depth and its off-shore variation in the Lambert's Bay region on 16 March 2001. Slightly stratified conditions within the first few meters of the surface at stations inshore of station 8 during upwelling favourable winds may be attributed to the effect of strong solar heating and weaker wind conditions in the sheltered wind wake which resides in the lee of Cape Columbine.

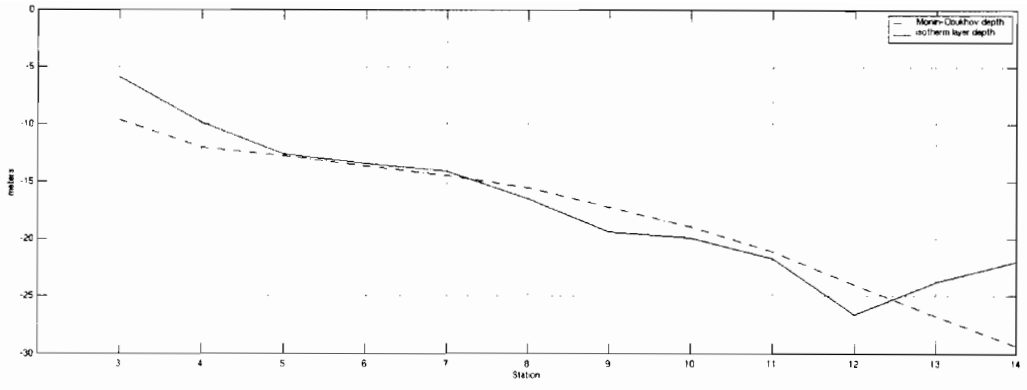

Figure 7.7: Isotherm layer depth (defined as the depth at which the temperature value is 0.5°C less that the SST) derived form the transect conducted on the 16th of March 2001 and the Monin-Obukhov depth scale derive from the mean buoyancy forcing and frictional velocity values averaged over the 24 hour period before the transect was completed.

7.3.2 Ekman Pumping

The previous subsection has shown that the depth of the mixed layer appears to be largely determined by the balance between vertical mixing due to wind stress and stratification due to a mean positive buoyancy flux. Curl patterns induced by Cape Columbine may result in Ekman pumping which acts to lift the base of the thermocline bringing nutrient rich sub-thermocline water closer to the surface and increasing stratification below the wind mixed layer, over the broad shelf region north of the Cape. Ekman pumping may play an important role in supporting dinoflagellate growth during upwelling favourable wind. Growth in dinoflagellate populations which occur in a subsurface stratum associated with the thermocline may be enhanced due to increased light levels as the base of the thermocline is uplifted through Ekman pumping, promoting HAB development.

The effects of wind stress curl in driving upwelling through Ekman pumping and circulation through Sverdrup balance is known to be diminished by the presence of coastal boundaries due to frictional effects. Studies in California have shown that the wind stress curl associated with capes induces upwelling velocities through Ekman pumping comparable to those induced by coastal Ekman transport divergence (Enriquez and Friehe, 1995; Koracin and Dorman, 2001; Pickett and Paduan, 2003). Capet et al. (2004) also showed that wind stress curl due to the decrease in wind speed within the narrow coastal band results in a gradual rise and doming of the thermocline within a band 10-30km off-shore of the coast. The Californian continental shelf is however generally much narrower than

the broad shelf region north of Cape Columbine. In an investigation of the relationship between wind forcing and the resultant upwelling response for the greater St Helena Bay region, Jury (1984; 1985a; 1985b) found a strong correlation between the differing negative curl patterns north of Cape Columbine during shallow and deep equatorward flow and the respective SST patterns. Based on Jury's findings, it shall be assumed here that although the Ekman pumping may be somewhat reduced over the broad shelf region north of Cape Columbine compared to its possible values over the open ocean, it still drives upwelling which acts to uplift the thermocline.

Figure 7.2 indicates that the highest cyclonic curl values are found immediately north of Cape Columbine and along the narrow coastal strip north of this cape. The region of enhanced cyclonic curl immediately north of the cape corresponds with the position of the upwelling plume which develops north of the cape during upwelling favourable wind (Taunton-Clark, 1985). Although Penven (2000a; 2000b) illustrated that development of the upwelling plume observed north of Cape Columbine could be attributed to the horizontal advection of water upwelled south of Cape Columbine around the attached cyclonic eddy, wind stress curl presents another mechanism which may be causing this plume to develop. High curl values in this region could result in an uplifted doming thermocline due to strong vertical velocities driven by Ekman pumping, with vertical wind mixing bringing cool thermocline water to the surface. However, an ocean modeling study quantifying the relative contribution of these two mechanism in creating the upwelling structure associated with the plume would be needed in order to determine the importance of the small-scale features in the wind.

Further north, in the region of the Lambert's Bay transect, average curl values during upwelling favourable winds are negative and cyclonic as wind stress decreases shoreward due to wind sheltering in the lee of the cape. During upwelling favourable winds, the cyclonic wind stress curl which occurs over the entire transect may drive upwelling velocities which act to uplift the base of the thermocline and enhance stratification below the wind mixed layer (Figure 7.5(b)). Ekman pumping velocities at the base of the mixed layer caused by wind stress curl (C) are given by $C(\rho f)^{-1}$for the open ocean. Figure 7.8 indicates that on average during upwelling favourable winds, upwelling velocities in the region of 1 meter per day could be driven by Ekman pumping for stations 5-14.

Closer inshore, the curl values become increasingly cyclonic as they are enhanced by a stronger decline in the wind stress due to land-sea changes in surface drag and atmospheric boundary layer depth. This increased inshore decline and associated curl is illustrated in

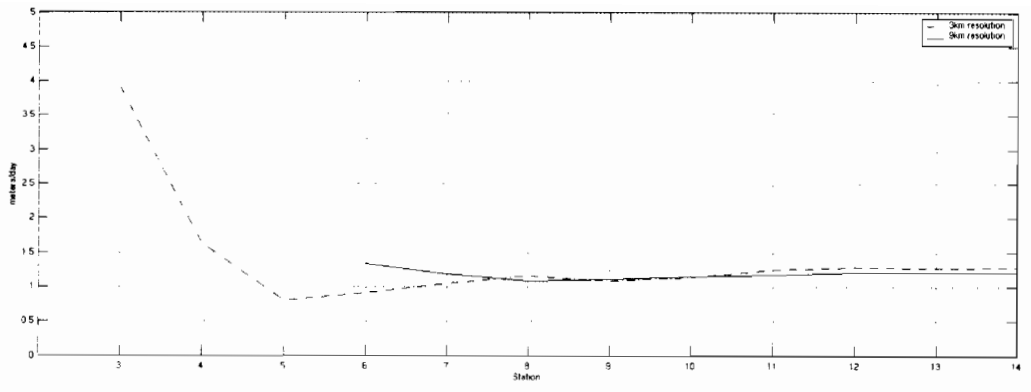

Figure 7.8: Mean 13-22 March 2001 Ekman pumping velocities calculated for transect conducted off-shore of Lambert's Bay from in-shore station 3 to off-shore station 14.

Figure 7.5(a). As already mentioned, wind stress curl values inshore of station 6 must be treated with caution because the decrease of wind stress in this narrow coastal band is dependent on model resolution. The atmospheric model can only qualitatively represent this region of enhanced curl for inshore stations. Enhanced cyclonic curl at these inshore stations due to land-sea contrasts in surface friction may however be responsible for the gradual rise of the base of the thermocline as Ekman pumping velocities increase inshore (Figure 7.4).

Increased uplift of the base of the thermocline due to enhanced Ekman pumping at inshore stations, together with shallower average mixed layer depths at these stations, appears to be consistent with the resulting region of enhanced surface water stratification typically observed at these inshore stations during upwelling favourable winds. These stratified surface waters together with the availability of nutrient rich sub-thermocline water near the surface may in turn promote dinoflagellate growth during upwelling favourable winds, hence pre-conditioning the region prior to HAB events.

7.4 Quiescent Phase: 22-30 March 2001

A transect extending off-shore of Lambert's Bay was also conducted on 24 March 2001 which falls within the period characterised by a prolonged quiescent phase in upwelling favourable winds. The across-shore temperature and chlorophyll structure from this transect (Figure 7.9) shows that the light winds have resulted in strongly stratified conditions in

the upper few meters of the ocean at all the stations along the transect. Lower mean wind stress values (Figure 7.10(a)) result in less turbulent mixing, and reduced mean Ekman depth values for this period (Figure 7.10(c)). Although turbulent mixing has decreased, the insolation remains high resulting in a very shallow average Monin-Obukhov depth scale (Figure 7.10(d)) and in the warming and stratification of surface waters as seen in Figure 7.9. The bloom distribution remains similar to that which was set up during the preceding upwelling favourable condition, with the core off the bloom (>30 mg chl a m^{-3}) situated between station 5-7 where the thermocline has been uplifted. In this region, nutrients below the thermocline are available fairly close to the surface and the water column is very stratified and stable resulting in enhanced growth of dinoflagellates and the development of a high concentration bloom.

During this period of relaxed equatorward winds, the bloom was advected on-shore impacting upon the coast. As discussed in chapter two, an on-shore wind component is necessary for the on-shore advection of surface material within the inner-shelf region. Figure 7.11 illustrates that the average zonal component of the wind stress was onshore in the greater St Helena Bay region during the 23-30 March 2001 quiescent period. Spatial variability in the mean low-level wind field during periods of weak synoptic across-shore pressure gradient results in an enhanced on-shore component in wind stress north of Cape Columbine as the weak synoptic activity allows seabreezes to develop over the region.

7.5 Summary

Spatial variability in the low-level wind field north of Cape Columbine forced by topography and thermal land-sea gradients is suggested as being favourable for HAB development and on-shore advection in the greater St Helena Bay region. Wind stress and wind stress curl derived from the simulated 10 meter winds and simulated surface fluxes have been used to derive, certain diagnostic variables. Ekman depth and the Monin-Obukhov length scale have been calculated in order to assess mixed layer depth scales related to the wind stress and buoyancy forcing. From these depth scales, some conclusions have be drawn as to the role spatial variability in the horizontal wind structure north of Cape Columbine may play in influencing the mixed layer characteristics and in promoting the HAB development in this region. The finding of this and previous chapters will now be summarised in the final chapter.

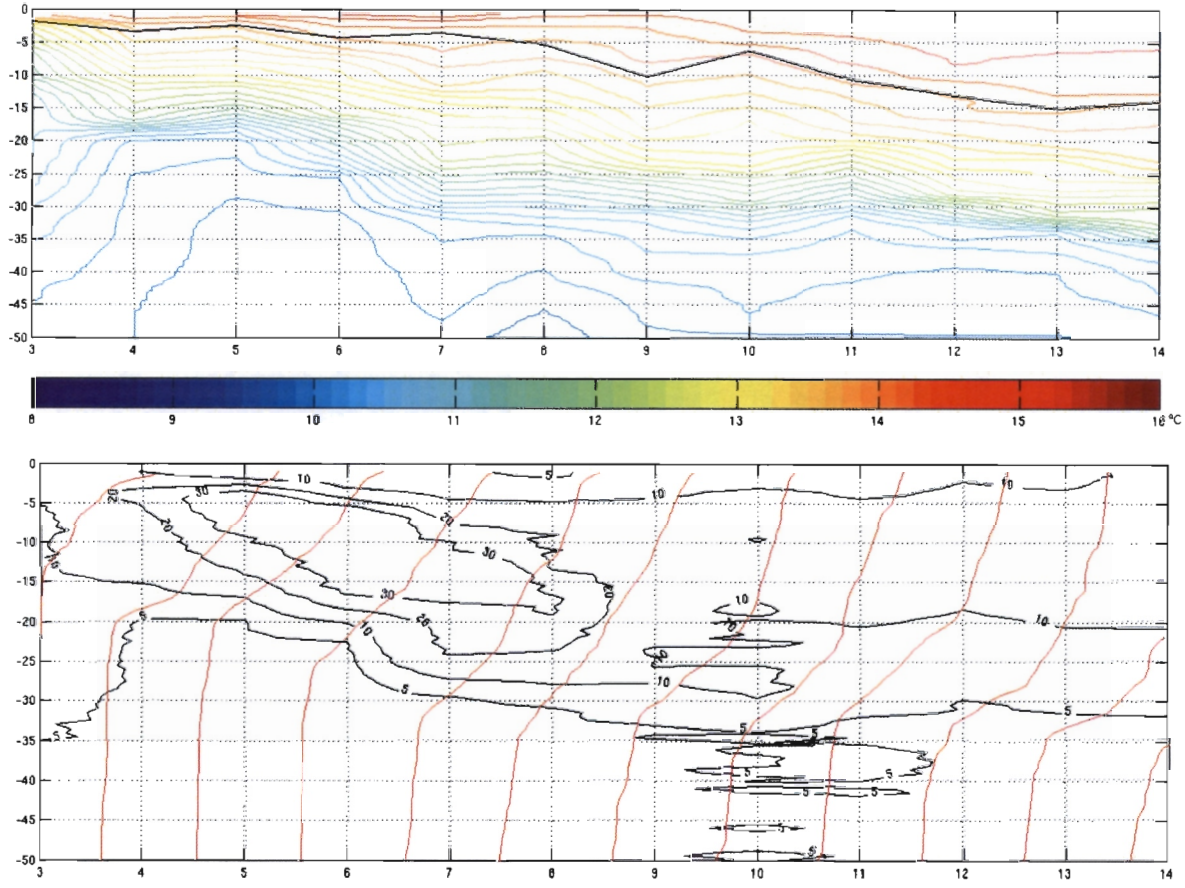

Figure 7.9: Transect 24 March 2001 with depth represented in meters on the y-axis and transect stations from in-shore station 3 to off-shore station 14 represented on the x-axis. (Top) Temperature with the isotherm layer depth (defined as the depth at which the temperature value is 0.5 °C less that the SST) over-layered in black. (Bottom) Chlorophyll concentrations with individual station temperature profiles in red.

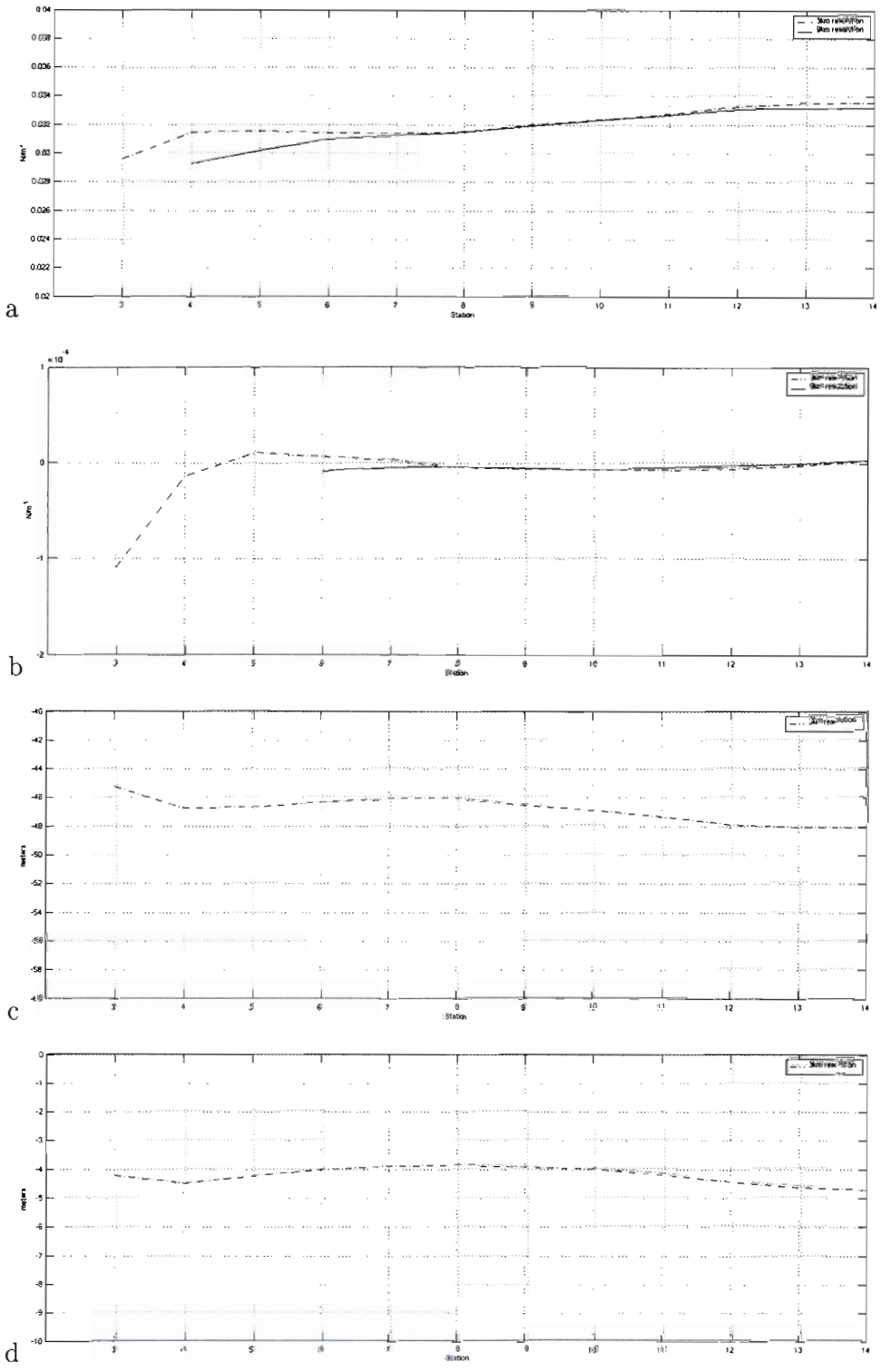

Figure 7.10: Mean 23-32 March 2001 (a) wind stress (b) wind stress curl (c) Ekman depth (d) Monin Obukhov depth, for transect conducted off-shore of Lambert's Bay from in-shore station 3 to off-shore station 14.

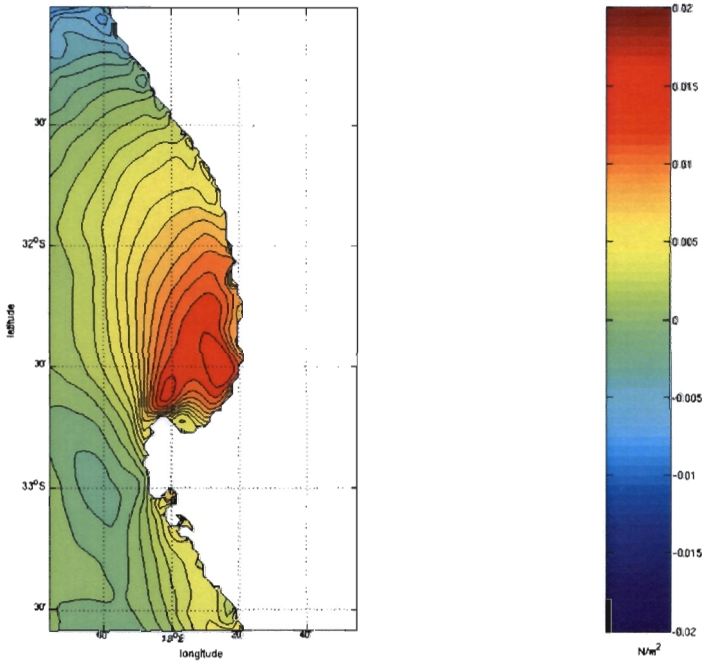

Figure 7.11: Mean 23-30 March 2001 model run 2, across-shore wind stress for 3km resolution nest.

Chapter 8

Summary and Conclusions

A key question this thesis hoped to address was how local winds adjust to the topography of the greater St Helena Bay region to produce conditions that are conducive to the HAB development and advection which is unique to this region. Temporally, it is fairly well established that the prolonged relaxation of dominant equatorward flow during late summer results in quiescent phases in upwelling which favour bloom development. Synoptic weather patterns responsible for this temporal variability in upwelling favourable winds are also well understood. However the spatial variability in the local winds which results from the adjustment of the large scale flow to regional topography and thermal gradients is less well understood and it is this aspect that has been examined in this thesis.

Previous studies have indicated that the summer synoptic wind field over the southern Benguela is in fact influenced by coastal topography and land-sea thermal gradients resulting in mesoscale (10-100km) features in the low-level wind field (Jury, 1985a,b; Kamstra, 1985). Observations of mesoscale spatial variability in coastal winds over the southern Benguela are however limited. Mesoscale climate modelling provides an alternative and so an attempt was made to utilise a regional atmospheric model to resolve mesoscale spatial variations in coastal wind stress forcing.

Based on MCM hydrographic and biological data, the March 2001 HAB event was selected as a case study and the MM5 regional atmospheric model used to simulate low-level coastal winds at high resolution (3km) over the case study period. In order to assess how representative the chosen event period is of the typical wind stress conditions, the nature of the case study period in terms of temporal variability in along-shore wind stress forcing was investigated.

From continuous wavelet analysis conducted on inter-annual timeseries of local along-shore wind stress and across-shore pressure gradients, we can infer that variability in upwelling favourable meridional wind stress towards the end of March 2001 occurred at a time scale longer than the dominant period of the synoptic cycle (2-8 days). A significant peak in variability with a period of 12-14 days in both wavelet power spectra indicated that upwelling favourable wind stress was oscillating at a lower frequency than usual. This resulted in a prolonged quiescent phase in upwelling activity observed at the end of March 2001. This prolonged period of weak across-shore pressure gradients and light variable winds was due to persistent west coast trough conditions. NCEP re-analysis 850 and 500 hPa geopotential height anomaly plots for March 2001 indicate a cyclonic anomaly south-west of South Africa, favourable for westerly wave development, and a stronger, southward shifted Angola heat low, conditions favourable for the development a west coast trough.

The simulated winds were validated against the limited observations available and the ability of the regional atmospheric model to simulate the response of synoptic flow to topography and thermal gradients was assessed. The spatial structure of the low-level wind fields simulated by the regional model over the 12-30 March 2001 case study period was examined and qualitatively compared to previous studies of the structure of the southern Benguela's low-level wind field. The regional model was capable of reproducing a qualitatively similar effect of topographic forcing on the equatorward flow. Local enhancement of low-level wind speed due to the interaction of the synoptic equatorward flow with both the Cape Peninsula and Cape Columbine was reproduced with associated bands of wind maxima, while lighter winds were seen in the lee of these capes.

SST forcing which more accurately resolved the cool SSTs resulting from coastal upwelling was found to enhance the effect of the coastal topography on synoptic flow due to a slightly greater slope in inversion layer towards the coast. A sloping ABL implies a strong horizontal across-shore temperature gradient between the cool ocean and warm land. Cooler SST due to coastal upwelling enhanced the land-sea thermal contrasts resulting in an increased slope in the inversion layer and a shallowing of the inversion towards the coast. The model was found to be capable of producing reasonable heat flux values, although latent, sensible and longwave estimates would have been improved by SST forcing which resolved individual upwelling events. In reality the SST field is not fixed as it was in the simulations undertaken. Adequately spatially and temporally resolved SST forcing appears to be important in improving the ability of the regional atmospheric model to simulate low-level winds and surface fluxes. Ultimately a coupled ocean-atmosphere model would be required

to capture feedbacks between the atmospheric simulation and the SST fields.

The presence of a low-level along-shore coastal jet structure in the model is similar to that found in California by Zemba and Friehe (1987) and near Cape Columbine and the Cape Peninsula by Jury (1984). The model was able to simulate the coastal wind jet to the west of Cape Columbine, the wind wake in its lee, and local seabreezes. The model appeared to do a good job of representing the mesoscale wind features which result from the interaction of synoptic flow with coastal topography and local thermal gradients in the greater St Helena Bay region.

Spatial variability in the low-level wind field north of Cape Columbine forced by topography and thermal land-sea gradients is suggested as being favourable for HAB development and on-shore advection in the greater St Helena Bay region. Wind stress and wind stress curl play an important role in determining ocean mixed layer characteristics and hence phytoplankton species dominance over the broad shelf region north of Cape Columbine. The Monin-Obukhov length scale compared well with observed mixed layer depth illustrating that variations in this depth may be primarily attributed to wind mixing and a positive buoyancy forcing. Slightly stratified conditions within the first few meters of the surface at stations inshore of station 8 during upwelling favourable winds may be attributed to the effect of strong solar heating and lower wind conditions in the sheltered wind wake which resides in the lee of Cape Columbine. Enhanced cyclonic curl at inshore stations due to land-sea contrasts in surface friction may be responsible for the gradual rise of the base of the thermocline inshore as Ekman pumping velocities increase inshore.

Increased uplift at the base of the thermocline due to enhanced Ekman pumping at inshore stations together with shallower average mixed layer depths at these stations, appears to be able to explain the resulting region of enhanced surface water stratification typically observed at these inshore station during upwelling favourable winds. These stratified surface waters together with the availability of nutrient rich sub-thermocline water near the surface in turn promote dinoflagellate growth during upwelling favourable winds, hence pre-conditioning the region prior to HAB events.

HAB events may develop during quiescent periods in upwelling, as dinoflagellate dominated surface waters become strongly stratified encouraging dinoflagellate growth and resulting in a high biomass bloom. A significant onshore wind stress component during quiescent phases in upwelling is needed to advect these high biomass blooms into the near-shore environment were they have the greatest impact upon coastal communities. Spatial variability in the

mean low-level wind field during periods of weak synoptic across-shore pressure gradient results in an enhanced on-shore component in wind stress north of Cape Columbine as the weak synoptic activity allows seabreezes to develop over the region. The influence of spatial and temporal variations in wind stress foricng on the mesoscale coastal circulation which acts to concentrate, dissipate and advect HABs requiers futher investigation using a numerical ocean model.

The implications of spatial variability in wind stress forcing over the southern Benguela on HAB development and advection is only one of a number of applications which may be investigated. The thesis has demonstrated the ability of a regional atmospheric model to simulate spatial variability in wind stress forcing over the southern Benguela, the implications of which have not been adequately considered to date. The impacts of mesoscale spatial variations in the low-level wind field on coastal ocean circulation in the southern Benguela may be significant. The coastal wind structure can significantly influence the along-shore current structure. Large cyclonic curl favours depth-averaged poleward currents through Sverdrup balance (although eddy Reynolds stress acts to further redistribute the wind-curl input). Wind stress curl may also result in Ekman pumping which influences the coastal upwelling temperature structure (Capet et al., 2004).

Inadequately resolved spatial variability in wind stress forcing may be the reason for discrepancies between the regional model outputs and observed data in the southern Benguela during summer (Penven, 2000a; Penven et al., 2000b). Simulated coastal SSTs were found to be significantly lower then those observed from satellites. This could be attributed to the use of poor spatially resolved wind data to force the model. Decreases in wind stress towards the coast are not resolved in the wind stress forcing and so greater wind stress magnitudes than those which occur at the real coast drive coastal Ekman divergence, resulting in greater upwelling velocities. This enhanced upwelling driven by coastal Ekman divergence may be the reason for cooler SSTs at the coast than those which occur in reality. In order to more accurately represent the upwelling structure and associated circulation, regional oceanic models need to be forced with higher resolution winds.

The significance of mesoscale spatial variability in wind stress forcing on coastal circulation and temperature structure needs to be evaluated in future work. Hydrodynamic modeling studies quantifying the impacts of spatial variability in wind stress forcing need to be conducted. Spatial variability in wind stress forcing appears to be an important physical mechanism in driving physical processes which control HAB development and advection. It is therefore necessary to resolve mesoscale variability in the wind forcing when predicting

HABs. Resolving mesoscale spatial variability in wind stress forcing may prove to be an important consideration when aiming to better understand and forecast physical processes operating in southern Benguela.

Bibliography

Andrews, W. R. H. and L. Hutchings. 1980. "Upwelling in the Southern Benguela current." *Progress in Oceanography* 9:1–81.

Austin, J. A. and S. J. Lentz. 2002. "The inner shelf response to wind-driven upwelling and downwelling." *J. Phys. Oceanogr.* 32:2171–2193.

Bakun, A. and C. S. Nelson. 1991. "The seasonal cycle of wind-stress curl in subtropical eastern boundary current regions." *J. Phys. Oceanogr.* 21:1815–1834.

Barker, E. H. 1992. "Design of the Navy's Multivariate Optimum Interpolation Analysis System." *Weather and Forecasting* 7:220–231.

Blanc, T. V. 1983. "Typical influences of moister on profile measurements in the marine atmospheric surface layer." *Boundary-Layer Meteorology* 25:411–415.

Blanke, B., S. Speich, A. Bentamy, C. Roy, and B. Sow. 2005. "Modeling the structure and variability of the southern Benguela upwelling using QuikSCAT wind forcing." *Journal of Geophysical Research* 110 C07018(doi10.1029/2004JC002529).

Boyd, A. J. and G. P. J. Oberholster. 1994. "Currents of the West and South coasts of Southern Africa." *SA Shipping News and Fishing Industry Review* pages 26–28.

Boyd, A. L., J. Taunton-Clark, and G. P. J. Oberholster. 1992. "Spatial features of the near-surface and midwater circulation patterns off western and southern South Africa and their role in the life histories of various commercially fished species." *S. Afr. J. Mar. Sci.* 12:189–206.

Boyer, L. D. and L. Tao. 1987. "On the motion of linearly stratified rotating fluids past capes." *Journal of Fluid Mechanics* 108:429–449.

Caldeira, R. M. A. and P. Marchesiello. 2002. "Oceanic responce to wind sheltering in the Southern Californian Bight." *Geophysical Research Letters* 29(13):10.1029/2001GL014563.

Capet, X. J., P. Marcheiello, and J.C McWilliams. 2004. "Upwelling response to coastal wind profiles." *Geophysical Research Letters* 31(L13311).

Chao, S-Y. 1985. "Coastal Jets in the Lower Atmosphere." *J. Phys. Oceanogr.* 15:361–371.

Chelton, D. B. 1982. "Large-scale response of the California Current to forcing by wind stress curl." *Calif. Coop. Oceanic Fish. Invest. Rep.* 23:130–148.

Chui, C. K. 1992. *An Introduction to Wavelets.* New York: Academic Press, 266pp.

Csanady, G. T. 1982. *Circulation in the Coastal Ocean.* Dordrecht: D. Reidel Publishing Company, 279pp.

Cullen, J. J. and J. MacIntyre. 1998. "Behaviour, physiology and the niche of depth-regulating phytoplankton." In *Physiological Ecology of Harmful Algal Blooms*, D.M. Anderson, A.D. Cembella, and G.M. Hallegraeff, eds., pages 559–579, NATO ASI Ser. 41., Berlin, Springer.

Daubechies, I. 1990. "The wavelet transform time-frequency localization and signal analysis." *IEEE Trans. Inform. Theory* 36:961–1004.

Daubechies, I. 1992. "Ten Lectures on Wavelets." *Society for industrial and Apllied mathematics* 357pp.

De Decker, A. H. B. 1970. "Notes on an oxygen-depleted subsurface current off the west coast of South Africa." *Investl. Rep. Div. Sea. Fish. S. Afr.* 76, 19pp.

Demarcq, H. and J. Citeau. 1995. "Sea Surface Temperature retrieval in tropical area with Meteosat: the case of the Senegalese coastal upwelling." *Int. J. Remote Sensing* 16(8):1371–1395.

Demarcq, H. and V. Faure. 2000. "Coastal upwelling and associated retention indices derived from satellite SST. Application to Octopus vulgaris recruitment." *Oceanol. Acta.* 23:391–408.

Dorman, C. E., T. Holt, D. P. Rogers, and K. Edwards. 2000. "Large-scale structure of the June-July 1996 marine boundary layer along California and Oregon." *Mon. Weather Rev.* 128:1632–1652.

Duncan, C. P. and J. H. Nell. 1969. "Surface currents off the Cape Coast." *Investl. Rep. Div. Sea Fish S. Afr.* 76:1–19.

Edwards, K. A., A. M. Rogerson, C. D. Winant, and D. P. Rogers. 2001. "Adjustment of the Marine Atmospheric Boundary Layer to a Coastal Cape." *Journal of Atmospheric Science* 58:1511–1528.

Ekman, V. W. 1905. "On the influence of the earth's rotation on ocean currents." *Ark. Mat. Astron. Fys.* 2:1–53.

Enriquez, A. G. and C. A. Friehe. 1995. "Effects of wind stress and wind stress curl variability on coastal upwelling." *J. Phys. Oceanogr.* 25:1651–1671.

Estrada, M. and E. Berdalet. 1998. "Effects of turbulence on phytoplankton." In *Physiological Ecology of Harmful Algal Blooms*, D.M. Anderson, A.D. Cembella, and G.M. Hallegraeff, eds., pages 601–618, NATO ASI Ser. 41., Berlin, Springer.

Farge, M. 1992. "Wavelet transforms and their applications to turbulence." *Annu. rev. fluid. Mech.* 24:395–457.

Fawcett, A. 2006. *Multi-sensor mooring development and its use to characterise physical processes relevant to Harmful Algal Bloom dynamics in the St Helena Bay area, South Africa.* Master's thesis, University of Cape Town, Cape Town.

Gan, J. P. and J. S. Allen. 2002a. "A modeling study of shelf circulation off northern California in the region of the Coastal Ocean Dynamics Experiment: Response to relaxation of upwelling winds." *Journal of Geophysical Research* 107(C9):3123.

Gan, J. P. and J. S. Allen. 2002b. "A modeling study of shelf circulation off northern California in the region of the Coastal Ocean Dynamics Experiment: Simulations and comparisons with observation." *Journal of Geophysical Research* 107(C11):3184.

Gan, J. P., J. S. Allen, and R. M. Samelson. 2005. "On open boundary conditions for a limited-area coastal model off Oregon. Part 2: Response to wind forcing from a regional mesoscale atmospheric model." *Ocean Modelling* 8:155–173.

Goerss, J. S. and P. A. Phoebus. 1992. "The Navy's Operational Atmospheric Analysis." *Weather and Forecasting* 7:232–249.

Graham, W. M. and J. L. Largier. 1997. "Upwelling shadows as near-shore retention sites: the example of the northern Monterey bay." *Cont. Shelf. Res.* 17(5):509–532.

Grell, G. A., J. Dudhia, and D. R. Stauffer. 1995. "A description ofthe fifth-generation Penn State/NCAR Mesoscale Model (MM5)." *National Center for Atmospheric Research Tech. Note* TN-398, 122 pp.

Guastella, L. A-M. 1992. "Sea Surface Heat Exchange at St Helena Bay and Implications for the Southern Benguela Upwelling System." *S. Afr. J. Mar. Sci.* 12:61–70.

Hardman-Mountford, N. J., A. J. Richardson, J. J. Agenbag, E. Hagen, L. Nykjaer, F. A. Shillington, and C. Villacastin. 2003. "Ocean Climate of the South East Atlantic observed from satellite data and wind models." *Progress in Oceanography* 59:181–221.

Hellerman, S. and M. Rosenstein. 1983. "Normal monthly wind stress over the world ocean with error estimates." *J. Phys. Oceanogr.* 13:1093–1104.

Hogan, T. F. and T. E. Rosmond. 1991. "The decription of Navy Opertational Global Atmospheric Prediction System's spectral forecat model." *Mon. Wea. Rev.* 119:1786–1815.

Holden, C. J. 1985. "Currents in St Helena Bay inferred from radio-tracked drifters." In *South African Ocean Colour and Upwelling Experiment*, L.V. Shannon, ed., pages 97–109, Cape Town: Sea Fisheries Research Institute.

Holden, C. J. 1987. "Observations of Low-Frequency Currents and Continental Shelf Waves Along the West Coast of South Africa." *S. Afr. J. Mar. Sci.* 5:163–169.

Holton, J. R. 1992. *An Introduction to Dynamic Meteorology*. San Diego California: Academic.

Hong, S-Y. and H-L. Pan. 1996. "Nonlocal Boundary Layer Vertical Diffusion in a Medium-Range Forecast Model." *Monthly Weather Review* 124:2322–2339.

Hortsman, D. A. 1981. "Reported red-water outbreaks and their effects on fauna of the west and south coasts of South Africa, 1959-1980." *fish. Bull. S. Afr* 15:71–88.

Jerlov, N. G. 1968. *Optical Oceanography.* Elsevier, 194pp.

Jury, M., C. Mac Arthur, and C. Reason. 1990b. "Observations of Trapped waves in the Atmosphere and Ocean along the coast of Southern Africa." *S. Afr. J. Sci.* 72:33–46.

Jury, M. R. 1988. "Case studies of the response and spatial distribution of wind driven upwelling of the coast of Africa: 29-34 south." *Cont. Shelf Res.* 8:1257–1271.

Jury, M. R., C. I. Mac Arthur, and G. B. Brundrit. 1990a. "Pulsing of the Benguela upwelling region: Large-scale atmospheric controls." *S. Afr. J. Sci.* 9:27–41.

Jury, M. R., F. Kamstra, and J. Taunton-Clark. 1985c. "Synoptic summer wind cycles and upwelling off the southern portion of the Cape Peninsula." *S. Afr. J. Mar. Sci.* 3(33-42).

Jury, M.R. 1980. *Characteristics of summer wind feilds and air-sea interactions over the Cape Peninsula upwelling region.* Master's thesis, University of Cape Town, 131pp.

Jury, M.R. 1984. *Wind shear and differential upwelling along the SW tip of Africa.* Ph.D. thesis, University of Cape Town, 51 pp.

Jury, M.R. 1985a. "Case studies of alongshore variations in wind-driven upwelling in the southern Benguela region." In *South African Ocean Colour and Upwelling Experiment*, L. V. Shannon, ed., pages 29–46, Cape Town: Sea Fisheries Research Institute.

Jury, M.R. 1985b. "Mesoscale variations in the summer winds over the Cape Columbine St Helena Bay region, South Africa." *S. Afr. J. Mar Sci.* 3(77-88).

Kalnay, E. and Coauthors. 1996. "The NCEP/NCAR 40-Year Reanalysis Project." *Bull. Amer. Meteor. Soc.* 77:437–471.

Kamstra, F. 1985. "Environmental features of the southern Benguela with special reference to the wind stress." In *In South African Ocean Colour and Upwelling Experiment*, L. V. Shannon, ed., pages 13–29, Cape Town: Sea Fisheries Research Institute.

Kamstra, F. 1987. "Interannual variability in the spectra of the daily surface pressureat four stations in the southern hemisphere." *Tellus* 39A:509–514.

Koracin, D. and C. E. Dorman. 2001. "Marine atmospheric boundary layer divergence and clouds along California in June 1996." *Mon. Weather Rev.* 129:2040–2056.

Kraus, E. B. 1972. *Atmosphere-Ocean Interaction.* Oxford, England: Clarendon Press, 275pp.

Lambeth, R. and G. Nelson. 1987. "Field and analytical drogue studies applicable to the St Helena Bay area off South Africa's west coast." *S. Afr. J. Mar. Sci.* 5:163–169.

Large, W. G., J. C. McWilliams, and S. C. Doney. 1994. "Oceanic vertical mixing: A review and a model with a nonlocal boundary layer parameterization." *Rev. of Geophys.* 32:363–403.

Large, W. G. and S. Pond. 1981. "Open Ocean Momentum Flux Measurments in Moderate to Strong Winds." *J. Phys. Oceanogr* 11:342–336.

Lau, K.-M. and H.-Y. Weng. 1995. "Climate signal detection using wavelet transform: How to make a time series sing." *Bull. Amer. Meteor. Soc* 76:61–78.

Lau, K.-M. and H.-Y Weng. 1999. "Interannual, Decadal-Interdecadal, and Global Warming Signals in Sea Surface Temperature during 1995-97." *Journal of Climate* 12:1257–1267.

Lutjeharms, J. R. E. and J. M. Meeuwis. 1987. "The extent and variability of south-east Atlantic upwelling." *S. Afr. J. Mar. Sci.* 5:51–62.

Marchesiello, P., J. C. McWilliams, and A. Shchepetkin. 2003. "Equilibrium Structure and Dynamics of the Californian Current System." *J. Phys. Oceanogr.* 33:753–783.

Margalef, R. 1978. "Life-forms of phytoplankton as survival alternatives in an unstable environment." *Oceanol. Acta.* 1:193–509.

Melice, J. L., A. Coron, and A. Berger. 2001. "Amplitude and frequency modulation of the Earth's obliquity for the last million years." *Journal of Climate* 14:1043–1054.

Nelson, C. S. 1977. "Wind stress curl over the California current." *NOAA Tech. Rep.* NMFS SSRF-714, 87pp.

Nelson, G. and L. Hutchings. 1983. "The Benguela upwelling area." *Progress in Oceanography* 12:333–356.

Paulson, C. A. and J. J. Simpson. 1977. "Irradiance measurements in the upper ocean." *J. Phys. Oceanogr.* 7:952–956.

Penven, P. 2000a. *A Numerical study of the southern Benguela circulation with application to fish recruitment.* Ph.D. thesis, Université de Bretagne Occidental, Brest.

Penven, P., C. Roy, J. R. E. Lutjeharms, A. Colin de Verdiere, A. Johnson, F. Shillington, P. Freon, and G. Brundrit. 2001. "A regional hydrodynamic model of the Southern Benguela." *S. Afr. J. Sci.* 97:472–476.

Penven, P., C. Roy, A. Colin de Verdiere, and J. Largier. 2000b. "Simulation of a coastal jet retention process using a barotropic model." *Oceanol. Acta.* 23:615–634.

Pickett, M. H. and J. D. Paduan. 2003. "Ekman transport and pumping in the Californian Current based on the U.S. Navy's high-resolution atmospheric model (COAMPS)." *Journal of Geophysical Research* 108(C10):3327.

Pitcher, G. C., J. Agenbag, D. Calder, D. Horstman, M. Jury, and J. Taunton Clark. 1995. "Red tides in relation to the meteorology of the southern Benguela upwelling system." In *Harmful Marine Algal Blooms*, P. Lassus, G. Arzul, E. Erard, P. Gentien, and C. Marcaillou, eds., pages 657–662, Lavoisier: Intercept Ltd.

Pitcher, G. C. and A. J. Boyd. 1996. "Across-shelf and alongshore dinoflagellate distributions and the mechanisms of red tide formation within the southern Benguela upwelling system." In *Harmful and Toxic Algal Blooms*, T. Yasumoto, Y. Oshima, and Y. Fukuyo, eds., pages 243–246, Paris: Intergovernmental Oceanographic Commission of UNESCO.

Pitcher, G. C., A. J. Boyd, D. A. Horstman, and B. A. Mitchell-Innes. 1998. "Subsurface dinoflagellate populations, frontal blooms and the formation of Red tide in the Southern Benguela upwelling system." *Marine Ecology Progress Series* 172::253–264.

Pitcher, G. C. and D. Calder. 2000. "Harmful Algal Blooms of the Southern Benguela Current: A Review and Appraisal of Monitoring from 1989 to 1997." *S. Afr. J. mar. Sci.* 22:255–271.

Pitcher, G. C. and G. Nelson. 2006. "The importance of surface boundary layer characteristics and advection in the development of red tide in the southern Benguela upwelling system." *Limnol. Oceanogr.* In press.

Pitcher, G. C. and S. J. Weeks. 2006. "The variability and potential for prediction of harmful algal blooms in the southern Benguela ecosystem." In *The Benguela: Predicting*

a large marine ecosystem, V. Shannon, G. Hempel, P. Malanotte-Rizzoli, C. Moloney, and J. Woods, eds., Elsevier.

Pomeroy, K. R. and T. R. Parish. 2001. "A Case study of the Interaction of the Summertime Coastal jet with the California topography." *Mon. Wea. Rev.* 129:530–539.

Preston-Whyte, R. A. and P. D. Tyson. 1973. "Note on pressure oscillations over South Africa." *Mon. Weath. Rev.* 101(8):650–653.

Preston-Whyte. R. A. and P. D. Tyson. 1988. *The Atmosphere and Weather of Southern Africa.* Cape Town: Oxford University Press, 374 pp.

Preston-Whyte, R. A. and P. D. Tyson. 2000. *The Weather and Climate of Southern Africa.* Cape Town: Oxford University Press.

Probyn, T. A., G. C. Pitcher, P. M. S. Monteiro, A. J. Boyd, and G. Nelson. 2000. "Physical processes contributing to harmful algal blooms in Saldanha Bay, South Africa." *S. Afr. J. Mar. Sci.* 22:285–297.

Reason, C. J. C. 1996. "Topography and the Dynamical Response of Easterly flow in Southern Hemisphere Subtropical West Coast Regions." *Meteorol. Atmos. Phys.* 61:187–199.

Reason, C. J. C., P. Florenchie, M. Rouault, and J. Veitch. 2006. "Influence of Large Scale Climate Modes and Agulhas System Variability on the BCLME Region." *Large Marine Ecosystems* 14:225–241.

Reason, C. J. C. and M. R. Jury. 1990. "On the generation and propagation of the Southern African coastal low." *Quart. J. R. Meteorol. Soc.* 116:1133–1151.

Risien, C. M. 2002. *Wind-Stress Variability Over The Benguela Upwelling System.* Master's thesis, University of Cape Town.

Risien, C. M., C. J. C. Reason, F. A. Shillington, and D. B. Chelton. 2004. "Variability in satellite winds over the Benguela upwelling system during 1999-2000." *Journal of Geophysical Research* 109(C3):C0301010.1029/2003JC001880.

Roughan, M., E. J. Terrill, J. L. Largier, and M. P. Otero. 2005. " Observations of divergence and upwelling around Point Loma, California." *Journal of Geophysical Research* 110(C04011).

Samelson, R., P. Barbour, J. Barth, S. Bielli, T. Boyd, D. Chelton, P. Kosro, M. Levine, E. Skyllingstad, and J. Wilczak. 2002. "Wind stress forcing of the Oregon coastal ocean during the 1999 upwelling season." *Journal of Geophysical Research* 107(C5):3034.

Schumann, E. H. and K. H. Brink. 1990. "Coastal-Trapped Waves off the Coast of South Africa: Generation, Propagation and Current Structures." *J. Phys. Oceanogr.* 20:1206–1218.

Shannon, L. V. 1985. "The Benguela ecosystem Part 1: Evolution of the Benguela, Physical features and processes." *Oceanogr. Mar. Biol. Ann. Rev.* 23:105–182.

Shannon, L. V. and G. Nelson. 1996. "The Benguela: Large scale features and processes and system variability." In *The South Atlantic: Past and Present Circulation*, G. Wefer, W. H. Berger, G. Siedler, and D.J. Webb, eds., pages 163–210, Berlin Heidelberg: Springer-Verlag.

Shillington, F. A., C. J. C. Reason, C. M. Duncombe Rae, P. Florenchie, and P. Penven. 2006. "Large Scale Physical Variability of the Benguela Current Large Marine Ecosystem (BCLME)." *Large Marine Ecosystems* 14(67-89).

Simpson, J. E. 1996. "Diurnal Changes in Sea-Breeze direction." *Journal of Applied Meteorology* 35:1166–1176.

Singleton, A. T. and C. J. C. Reason. 2006. "Variability in the characteristics of cut-off low pressure systems over subtropical southern Africa." *Int. J. Climatol.* accepted.

Smayda, T. J. 1997. "Harmful algal blooms: their ecophysiology and general relevanceto phytoplankton blooms in the sea." *Limnol. Oceanogr.* 42:1137–1153.

Smayda, T. J. and C. S. Reynolds. 2001. "Community assembly in marine phytoplankton: application of recent models to harmful dinoflagellate blooms." *J. Plankton Res.* 23:447–461.

Taunton-Clark, J. 1985. "The Formation, Growth and Decay of Upwelling Tongues in Response to the Mesoscale Wind Field during Summer." In *South African Ocean Colour and Upwelling Experiment*, L. V. Shannon, ed., Cape Town: Sea Fisheries Research Institute, 47-61.

Tilburg, C. E. 2003. "Across-shelf transport on a continental shelf: Do across-shelf winds matter?" *J. Phys. Oceanogr* 33:2675–2688.

Torrence, C. and G. P. Compo. 1998. "A practical guide to wavelet analysis." *Bull. Amer. Meteor. Soc.* 79:61–78.

Troen, I. and L. Mahrt. 1986. "A simple model of the atmospheric boundary layer: Sensitivity to surface evaporation." *Boundary Layer Meterology* 37:129–148.

Uppala, S.M. and Coauthors. 2005. "The ERA-40 re-analysis." *Quart. J. R. Meteorol. Soc* 131:2961–3012.

Weeks, S. J., G. C. Pitcher, and S. Bernard. 2004. "Satellite monitoring of the evolution of a coccolithophorid bloom in the southern Benguela ecosystem." *Oceanography* 17(1):83–89.

Yuan, X. and D. G. Martinson. 2000. "Antarctic sea ice extent variability and its global connectivity." *Journal of Climate* 13:1697–1717.

Zemba, J. and C. A. Friehe. 1987. "The marine atmospheric boundary layer jet in the coastal ocean dynamics experiment." *Journal of Geophysical Research* 92:1489–1496.

Appendix A

SAWS Synoptic Charts

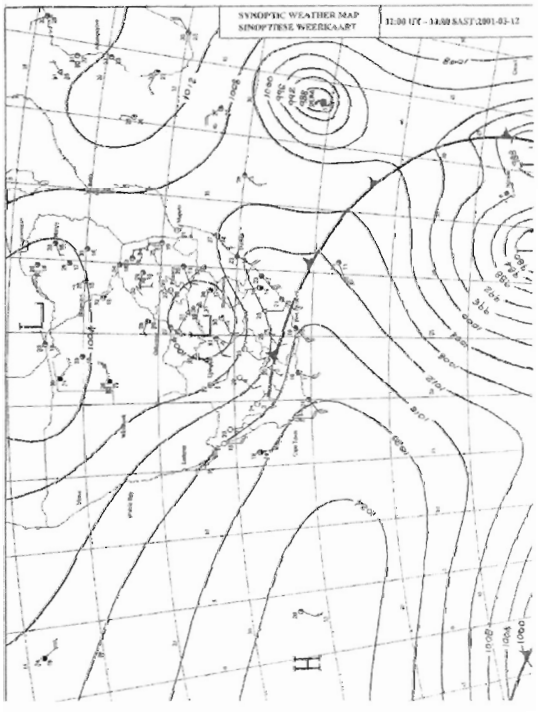

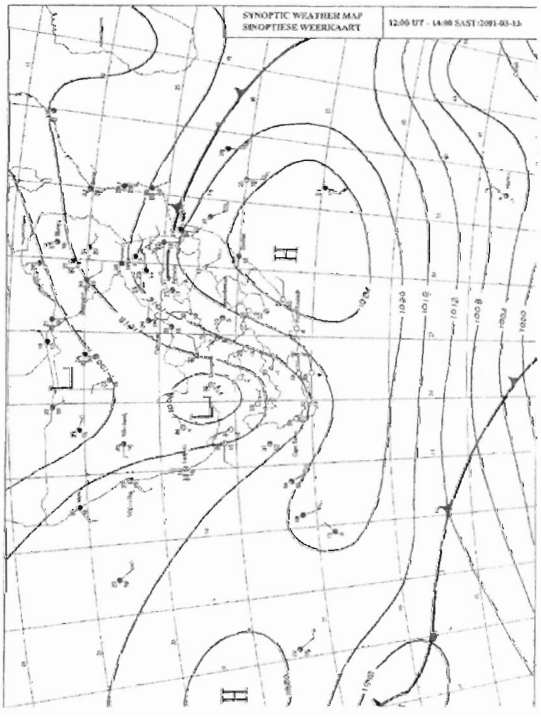

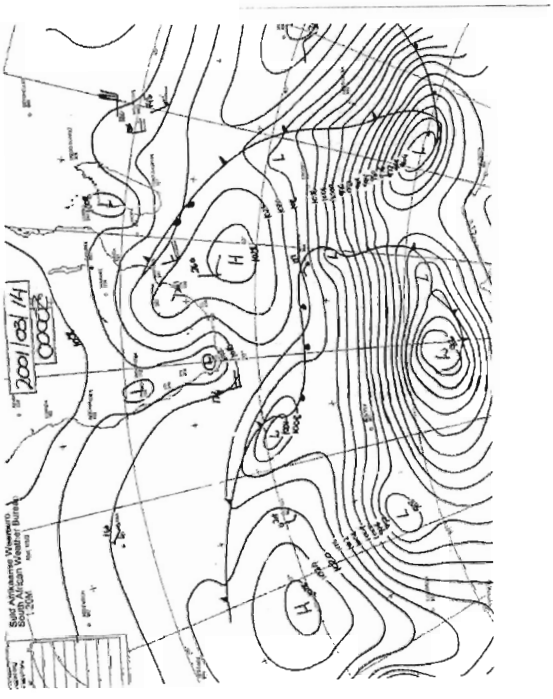
2001 03 14
South African Weather Service

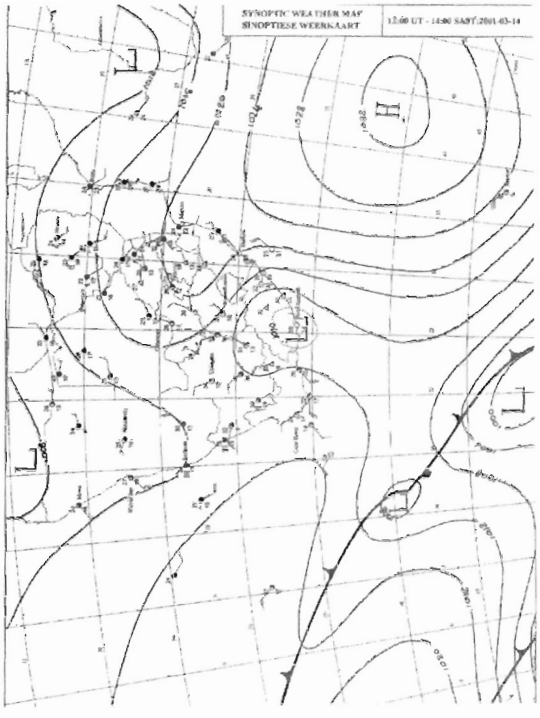
SYNOPTIC WEATHER MAP
SINOPTIESE WEERKAART
12:00 UT - 14:00 SAST 2001-03-14

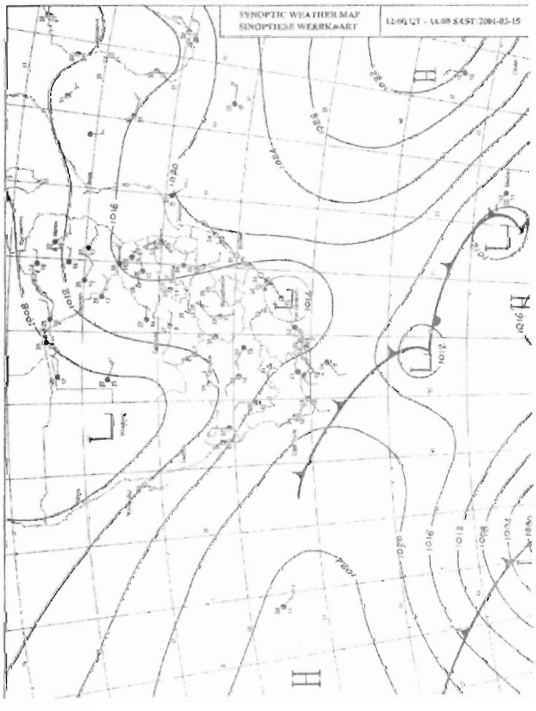
SYNOPTIC WEATHER MAP
SINOPTIESE WEERKAART
12:00 UT - 14:00 SAST 2001-03-15

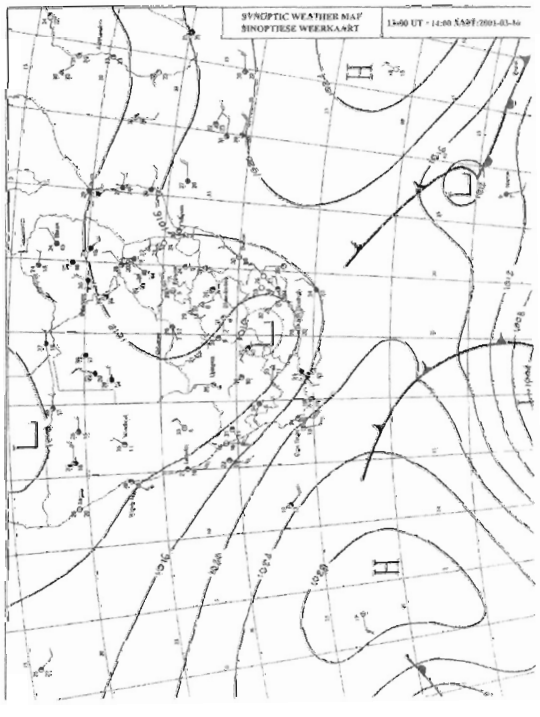
SYNOPTIC WEATHER MAP
SINOPTIESE WEERKAART

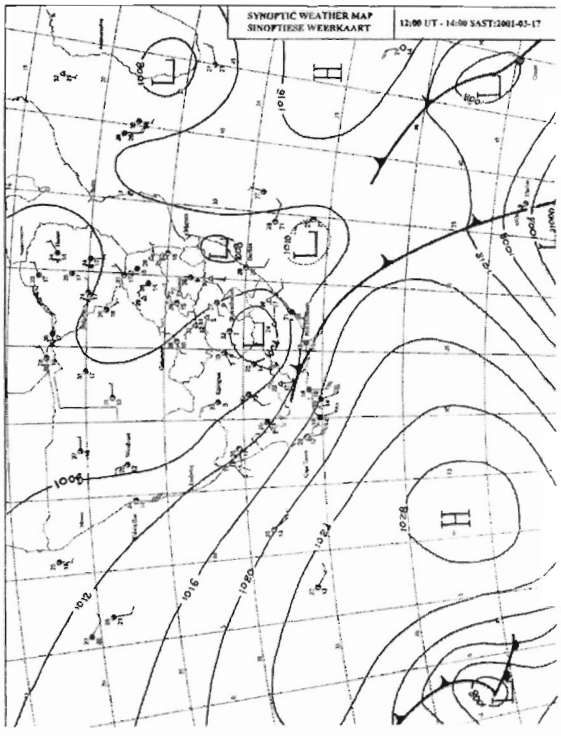
SYNOPTIC WEATHER MAP
SINOPTIESE WEERKAART
12:00 UT - 14:00 SAST:2001-03-17

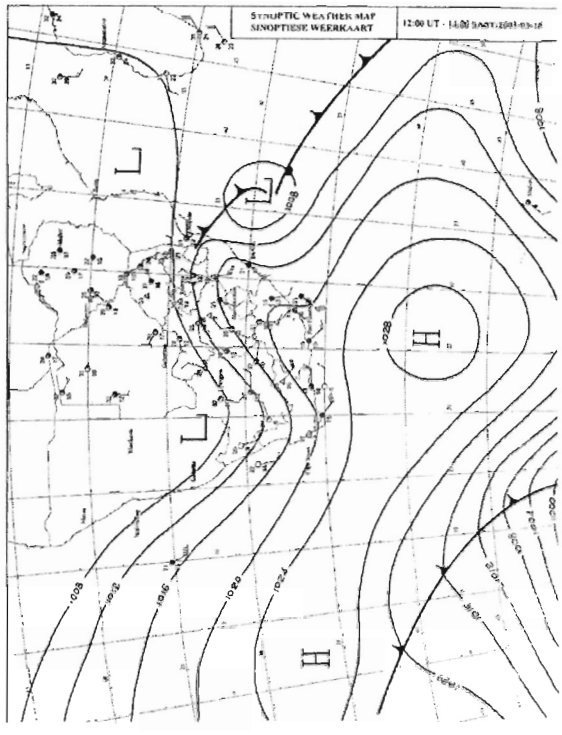
SYNOPTIC WEATHER MAP
SINOPTIESE WEERKAART

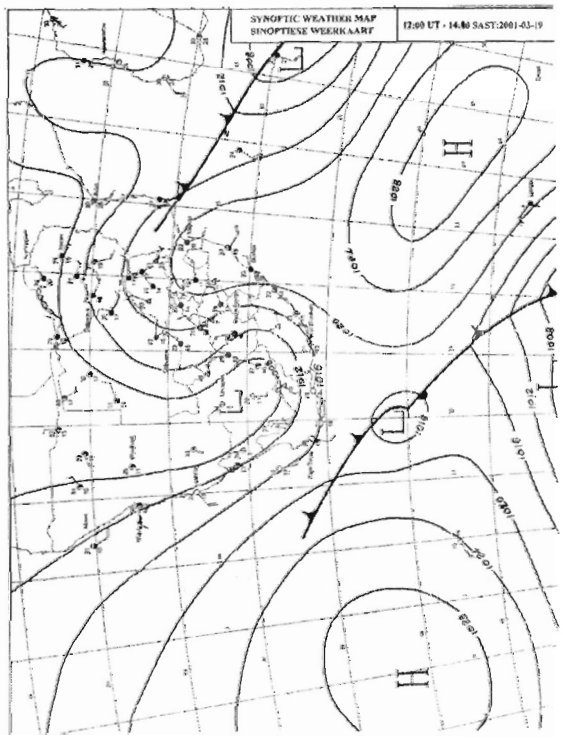
SYNOPTIC WEATHER MAP
SINOPTIESE WEERKAART
12:00 UT - 14:00 SAST:2001-03-19

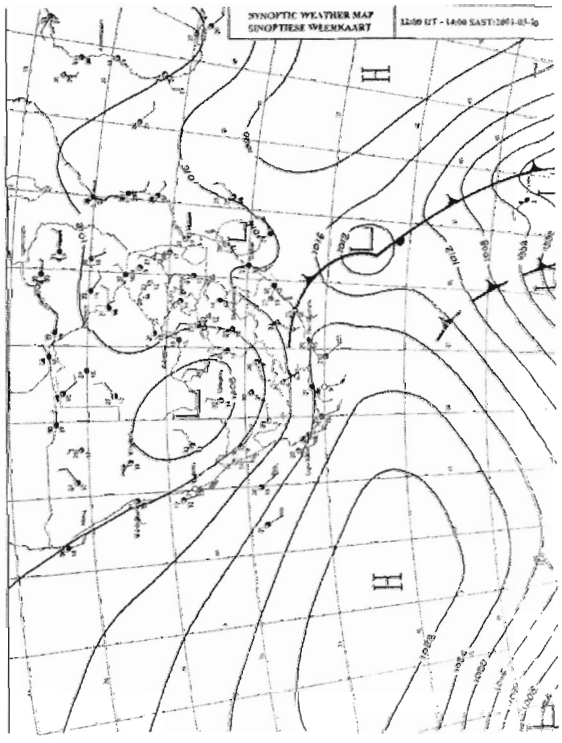
SYNOPTIC WEATHER MAP
SINOPTIESE WEERKAART

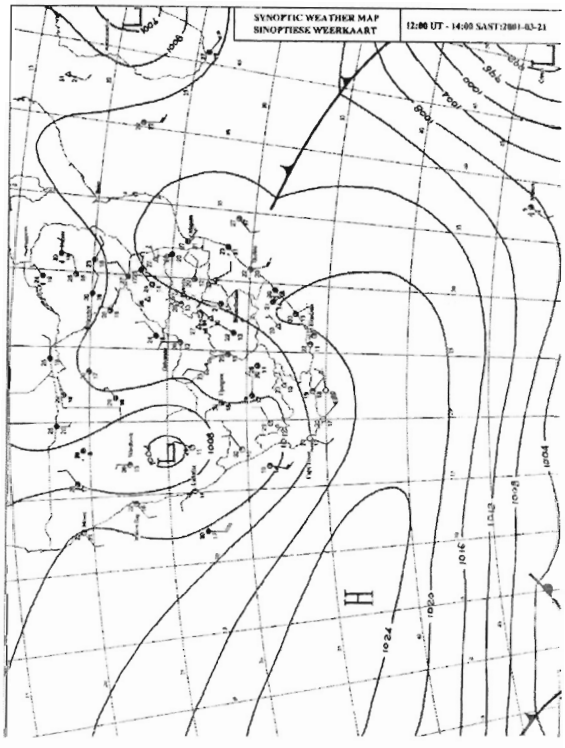
SYNOPTIC WEATHER MAP
SINOPTIESE WEERKAART
12:00 UT - 14:00 SAST:2001-03-21

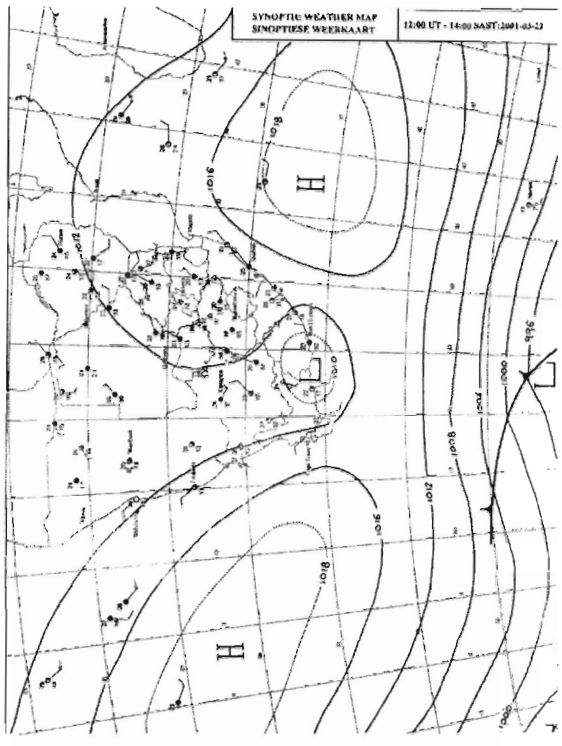
SYNOPTIC WEATHER MAP
SINOPTIESE WEERKAART
12:00 UT - 14:00 SAST:2001-03-22

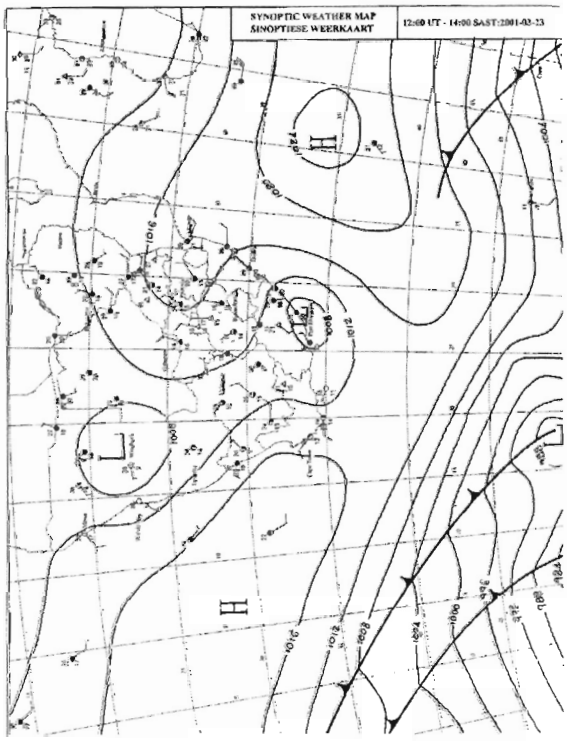
SYNOPTIC WEATHER MAP
SINOPTIESE WEERKAART
12:00 UT - 14:00 SAST:2001-03-23

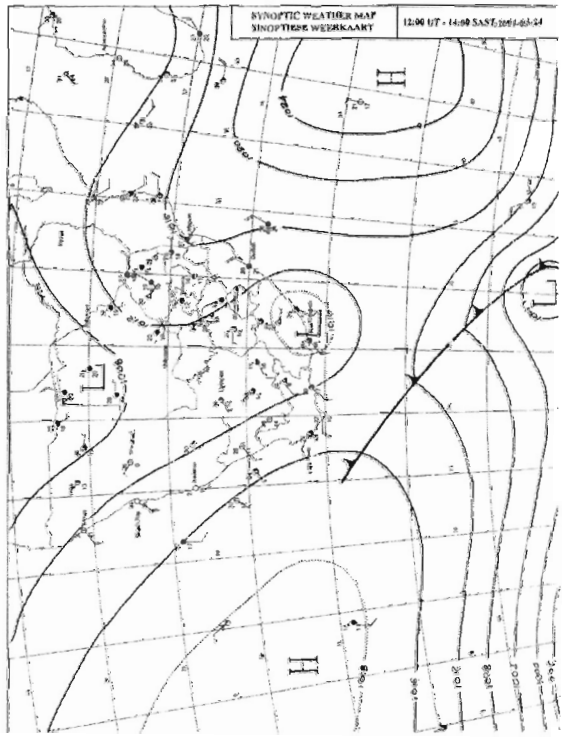
SYNOPTIC WEATHER MAP
SINOPTIESE WEERKAART
12:00 UT - 14:00 SAST:2001-03-24

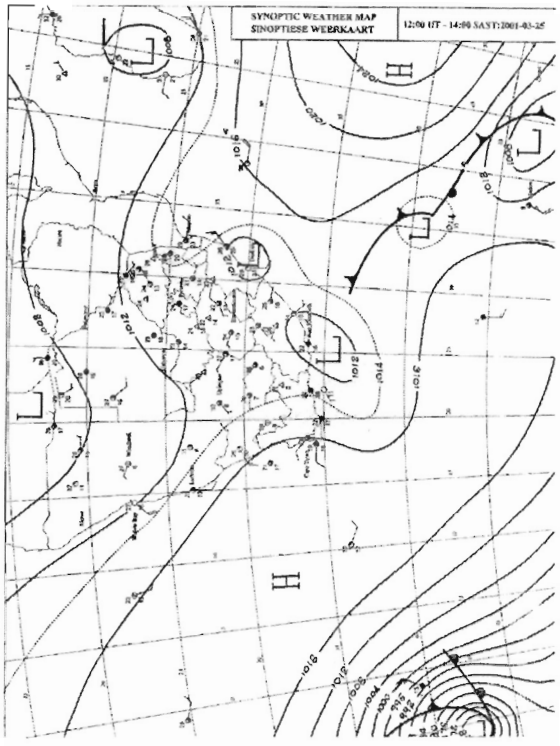
SYNOPTIC WEATHER MAP
SINOPTIESE WEERKAART
12:00 UT - 14:00 SAST:2001-03-25

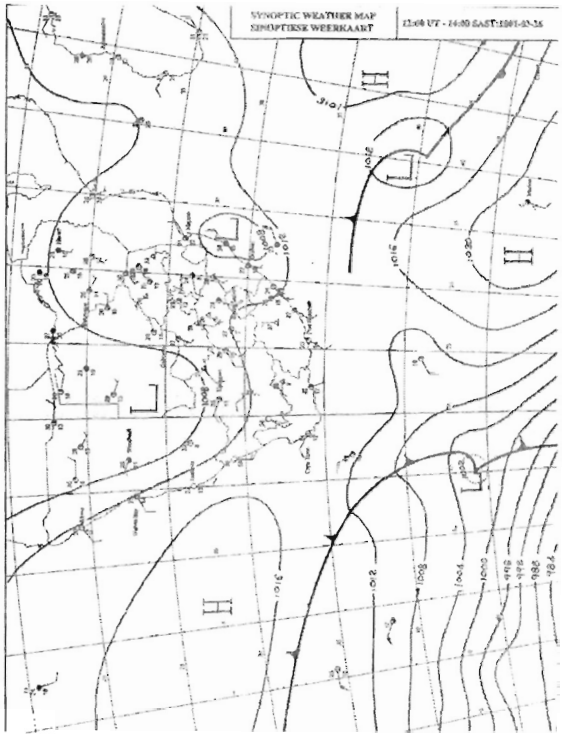
SYNOPTIC WEATHER MAP
SINOPTIESE WEERKAART

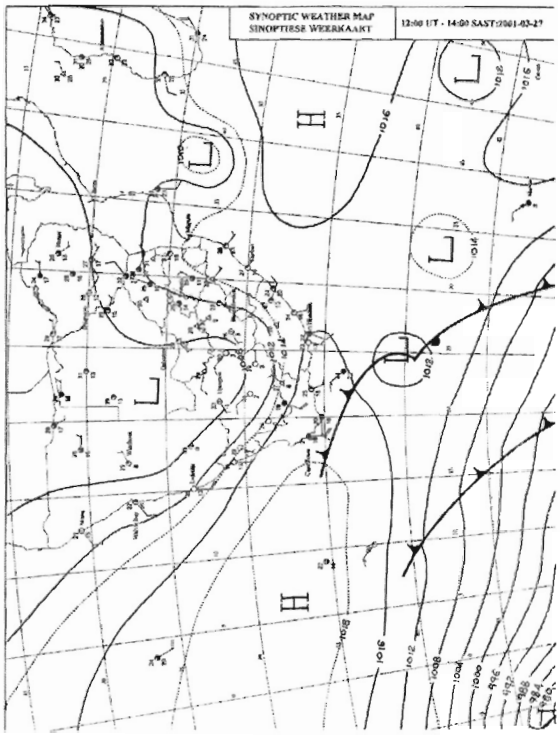
SYNOPTIC WEATHER MAP
SINOPTIESE WEERKAART
12:00 UT - 14:00 SAST:2001-03-27

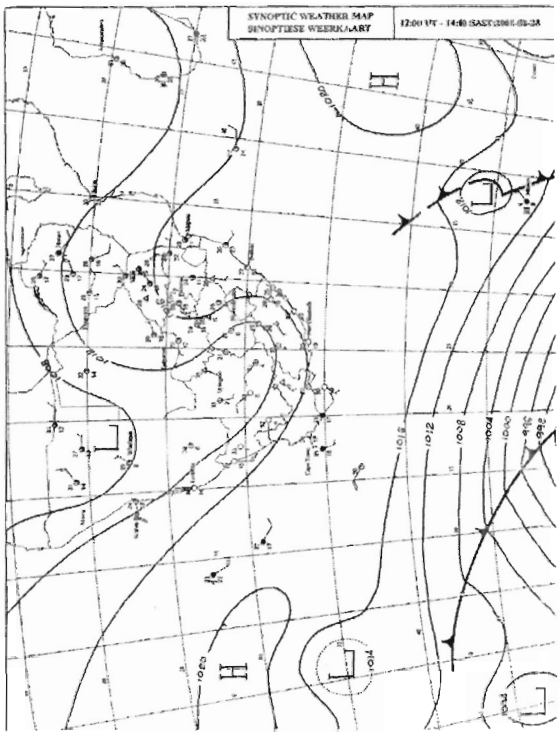
SYNOPTIC WEATHER MAP
SINOPTIESE WEERKAART

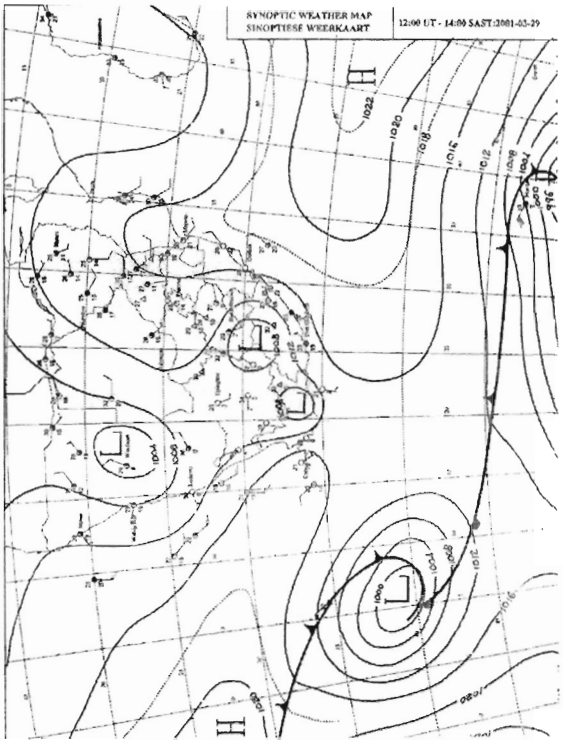
SYNOPTIC WEATHER MAP
SINOPTIESE WEERKAART
12:00 UT - 14:00 SAST:2001-03-29

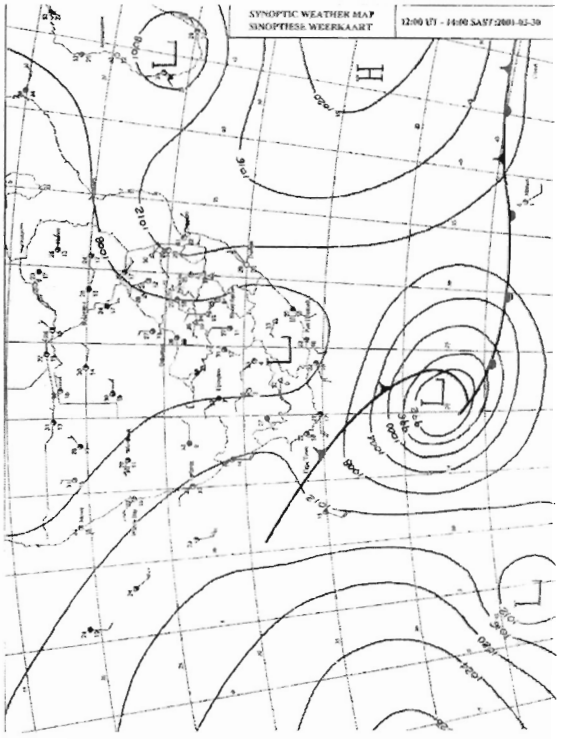
SYNOPTIC WEATHER MAP
SINOPTIESE WEERKAART

Appendix B

MM5 Programmes

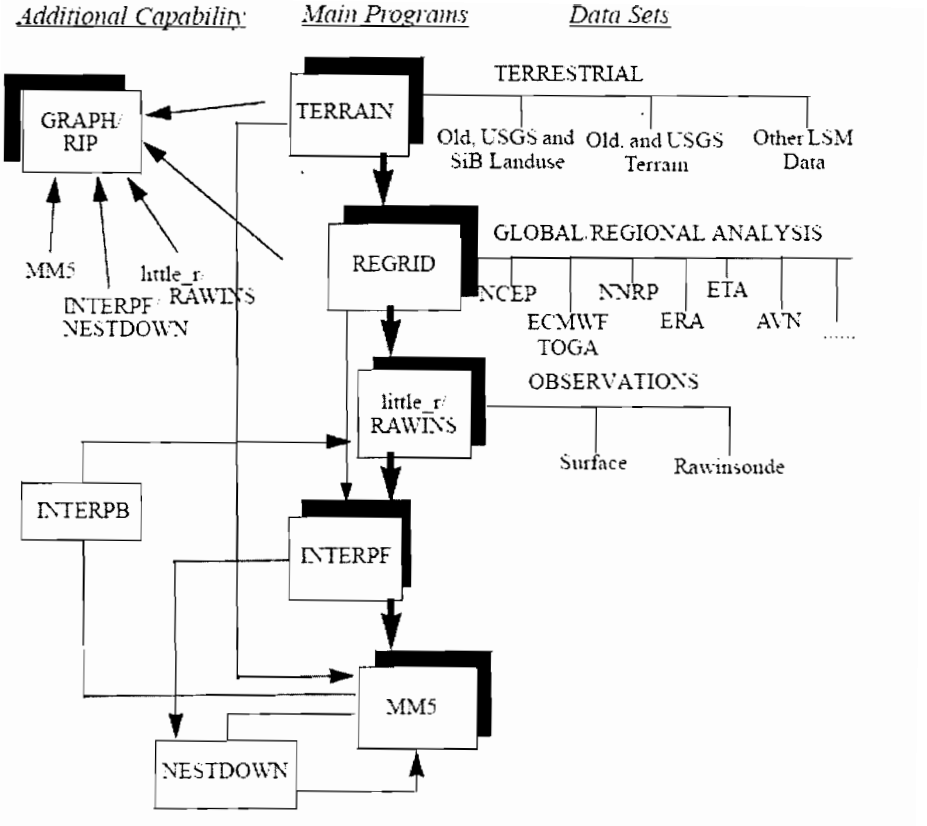

Figure B.1: Full suit of MM5 programmes available

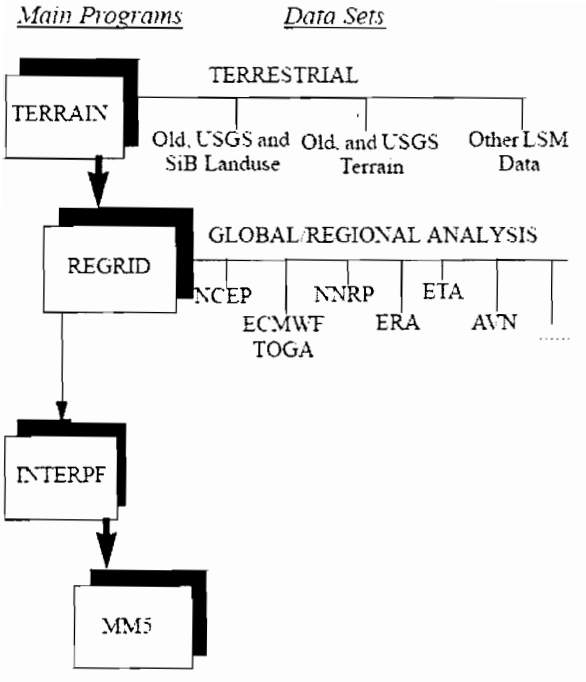

Figure B.2: Programmes used in simulations undertaken

Appendix C

Surface Fluxes

The buoyancy flux B per unit area of the sea surface is given by:

$$B = C_p^{-1}\rho_0^{-1}g\alpha Q + \rho_0^{-1}g\beta(E-P)s \tag{C.1}$$

$C_p$is the specific heat capacity of the surface sea water, $\rho_0$is the density of surface sea water, α and β are the thermodynamic expansion coefficients for the sea surface water all evaluated at surface values of temperature, salinity and pressure. Q is the net heat flux into the ocean, E is the evaporation rate and P is the rainfall rate. The buoyancy flux consists of two components, B = B_t+ B_S, $B_t = C_p^{-1}\rho_0^{-1}g\alpha Q$ is driven by the heat flux and $B_s = \rho_0^{-1}g\beta(E-P)s$ is driven by the fresh water flux.

C.0.1 The Heat Flux

The southern Benguela upwelling region is a region of positive net heat flux into the ocean (Guastella, 1992). The net heat flux between the atmosphere and the ocean is the sum of solar, longwave, sensible and latent heat fluxes. Guastella (1992) investigated air-sea heat exchange in St Helena Bay during 14-21 October 1986 by examining these different components of the heat budget. Guastella found the average heat flux into the ocean for this period to be 227Wm^{-2}. The daily average flux varied however from a minimum of 192Wm^{-2} on the 14th to maximum of 253Wm^{-2} on the 17th. Guastella's measurements showed that the two turbulent heat fluxes, the sensible and the latent heat fluxes were roughly equal and opposite, more or less cancelling each other out. On average over the eight day measurement period, the latent heat flux lost from the ocean was of the order

of 26Wm^{-2}, in contrast to an average sensible heat gain of 22Wm^{-2}. These two turbulent heat fluxes mirrored each other. On the 15th of October 1986, a maximum of the latent heat loss and sensible heat gain occurred in measurements taken over the survey period, due to high wind velocities with the heat transfer taking place in opposite directions over cold upwelled water. Magnitudes of the turbulent heat fluxes were small in comparison with a mean daily heat gain of 319Wm^{-2} due to insolation. Low SSTs in this region due to upwelling were found to result in a relatively low average heat loss due to longwave radiation of the order of 71Wm^{-2}. Clear skies were observed over the eight day survey period. The presence of cloud would have acted to reduce the loss of longwave radiation from the ocean surface, as well as reduce the insolation. While the daily net heat flux into the ocean is positive, the average diurnal cycle in the net heat flux exhibits a sinusoidal shape, with high heat gain during the day and a relatively small, consistent heat loss at the surface by night (Guastella, 1992). Variations in the net heat flux were found to be dominated by variations in solar radiation due the presence of cloud cover, with day to day variability in radiation capable of exceeding the seasonal variation in insolation (Guastella, 1992).

Guastella's finding can be compared with solar, longwave, sensible and latent heat fluxes derived for the transect stations (Figure 3.1), from run 2 of the model. Latent, sensible and solar fluxes were obtained directly from MM5 output. Net longwave radiation has been calculated as the sum of the longwave downwards radiation, obtained from the model and the upward grey-body longwave radiation, derived as a function of the SST used in the model. The station values for these fluxes have been horizontally interpolated from the 3km resolution model grid to the station positions. The flux values vary only slightly between transect stations 3-14. The radiative heat flux values derived for station 6 over the 13-30 March 2001 are depicted in Figure C.1. An average insolation of 251Wm^{-2} was received at station 6 between the 13-30 March 2001 which is consistent with typical insolation values for March derived from a long timeseries of observations at Cape Town international airport (Guastella, 1992). The average longwave heat flux at station six between 13-30 March 2001 is -39Wm^{-2}. This value is less than the 71Wm^{-2} that was observed by Guastella and may be attributed to the presence cloud of between the 13-30 March 2001 as opposed to the clear conditions during Guastella's survey period.

The turbulent heat flux values derived for station 6 over the 13-30 March 2001 are depicted in Figure C.2. Similar to Guastella (1992) the sensible and latent heat fluxes mirror each other and are small in comparison solar heat gain (Figure C.1). The average sensible heat

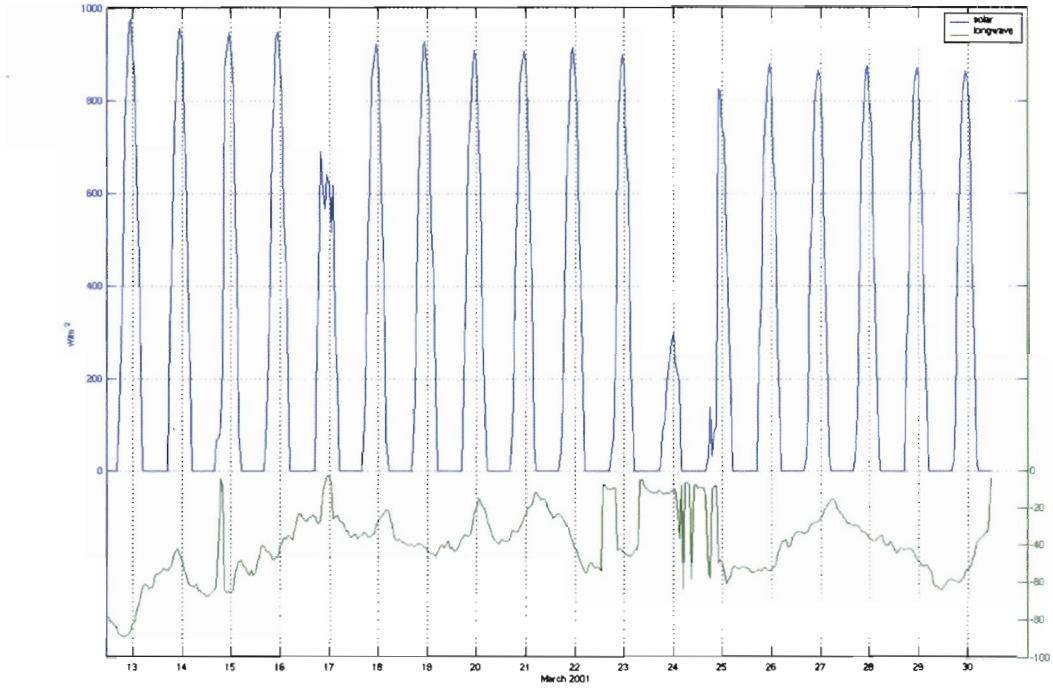

Figure C.1: Model run 2, longwave and solar radiative heat fluxes into the ocean at station 6 from the 13-30 March 2001.

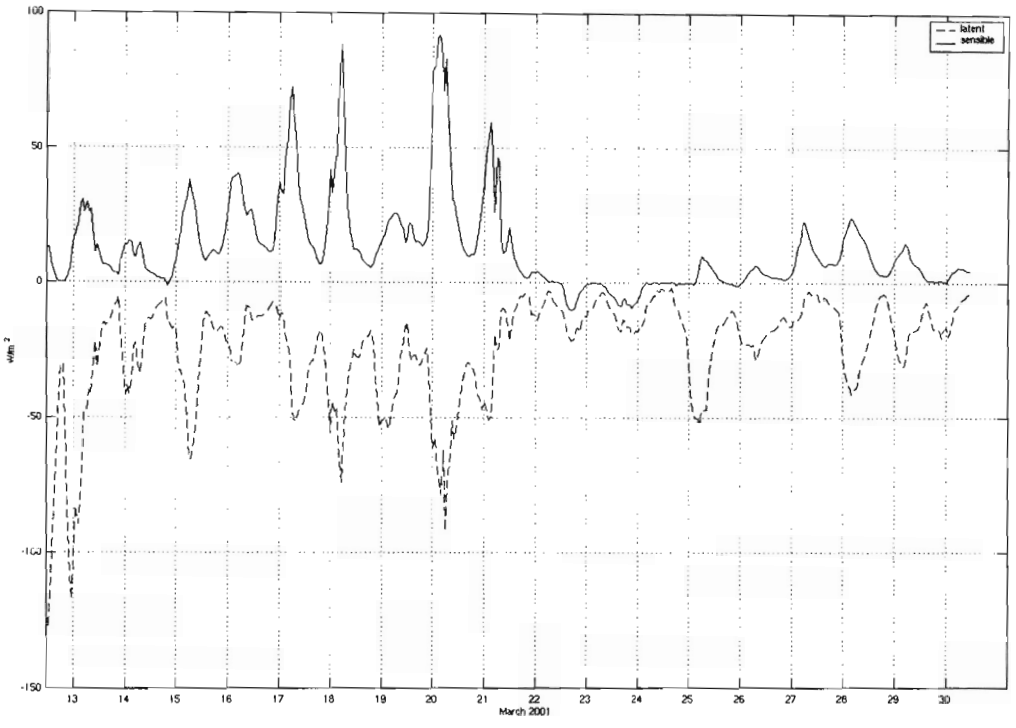

Figure C.2: Model run 2, latent and sensible turbulent heat fluxes into the ocean at station 6 from the 13-30 March 2001.

gain for station 6 from 13-30 march 2001 was 12Wm^{-2} and the average heat loss due to the latent heat flux was 25Wm^{-2}. The reason for the slightly lower average sensible heat flux gain than that recorded by Guastella is the difference in average SST. The average SST during Guastella's measurement programme was 14.9°C while the model SST at station 6 for the duration of the simulation was 16.6°C.

This result highlights a caveat in the simulated fluxes. The SST forcing was improved upon between the first and second model run so as to resolve the cooler coastal SSTs present in the southern Benguela due to upwelling. SST changes due to the individual upwelling events which took place during 13-30 March 2001 are not resolved in the second simulation. The impact of SST changes due to upwelling events during 13-30 March on longwave, latent and sensible fluxes is therefore not resolved by the model. Changes in SST would have particularly influenced these fluxes at the inshore stations 3 - 6 where SSTs drop significantly due to upwelling. The model longwave, latent and sensible fluxes

derived here therefore only represent changes due to atmospheric variability and do not resolve the influence of changes in SST. Decreased SSTs at these inshore station will have the greatest influence on the net heat flux in terms longwave heat loss as turbulent latent and sensible turbulent fluxes have been shown to be small and roughly cancel each other out for cool SSTs (Guastella, 1992). A decrease in SST of two degrees will result in a decreased longwave heat loss of the order of $10Wm^{-2}$.

The average net heat flux derived from the sum of the average sensible, latent, longwave and solar heat fluxes at station 6 from the 13-30 of March 2001 is $199Wm^{-2}$. This falls within the range of values observed by Guastella between 14-21 October 1986, yet is lower than the $227Wm^{-2}$ average. A lower average net heat flux would however be expected in March due to the fact that insolation, the primary contributor to the positive heat flux in this region, is $251Wm^{-2}$ during March in comparison to $319Wm^{-2}$ during October. Although the influence of SST changes on longwave, latent and sensible fluxes has not been not resolved in the calculated fluxes, the net heat flux derived from the model data appears to be consistent enough with previous observation for the purposes of the scale analysis used in Chapter 7.

C.0.2 The Fresh Water Flux

The fresh water flux (E-P) is a function of the evaporation rate E and the rainfall rate P. Minimal precipitation was received in the region between the 13-30 of March 2001 as is to be expected for this time of year and so P is taken as zero. The evaporation rate has been derived as a function of the latent heat flux and the latent heat of vaporisation ($L_v = 2.5^{*}10^{-6}\ J\,kg^{-1}$). The mean 13-30 March 2001 evaporation rate calculated for station 6 is $0.08\ cm\ day^{-1}$. Negligible precipitation and a low evaporation rate, results in the second term of the buoyancy flux B_S being an order of magnitude less then B_t. Therefor a positive heat flux, dominated by insolation, is the primary forcing for the surface buoyancy flux.